Distribution Agreement

In presenting this dissertation as a partial fulfillment of the requirements for an advanced degree from Emory University, I hereby grant to Emory University and its agents the non-exclusive license to archive, make accessible, and display my dissertation in whole or in part in all forms of media, now or hereafter known, including display on the world wide web. I understand that I may select some access restrictions as part of the online submission of this dissertation. I retain all ownership rights to the copyright of the dissertation. I also retain the right to use in future works (such as articles or books) all or part of this dissertation.

Signature:

_____ _____

Tesheka Stevenson Wortham **Date**

Molecular genetic analysis of *unc-94* and *unc-100*, two genes that are important for normal myofibril organization in *C. elegans*

By

Tesheka Stevenson Wortham
Doctor of Philosophy

Graduate Division of Biological and Biomedical Sciences
Genetics and Molecular Biology

_____
Guy Benian
Advisor

_____
Victor Faundez
Committee Member

_____
Judith Fridovich-Keil
Committee Member

_____
Steven L'Hernault
Committee Member

_____
Kenneth Moberg
Committee Member

Accepted:

_____
Lisa A. Tedesco, Ph.D.
Dean of the James T. Laney School of Graduate Studies

_____
Date

Molecular genetic analysis of *unc-94* and *unc-100*, two genes that are important for normal myofibril organization in *C. elegans*

By

Tesheka Stevenson Wortham
B.S., University of Georgia, 2002

Advisor: Guy Benian, M.D.

An abstract of
A dissertation submitted to the Faculty of the
James T. Laney School of Graduate Studies of Emory University
in partial fulfillment of the requirements for the degree of
Doctor of Philosophy
in Graduate Division of Biological and Biomedical Sciences
Genetics and Molecular Biology

2010

Abstract

Molecular genetic analysis of *unc-94* and *unc-100*, two genes that are important for normal myofibril organization in *C. elegans*

By Tesheka S. Wortham

Sarcomeres, highly ordered assemblages of several hundred proteins, perform the work of muscle contraction. Despite increasing knowledge of sarcomeric proteins and their functions, we lack a clear understanding about how sarcomeres are assembled and maintained. We study this question in the model organism, *C. elegans*. My studies focused on phenotypically characterizing and molecularly identifying two genes that are important for normal sarcomere assembly and maintenance*: unc-94* and *unc-100*.

Along with the original allele of *unc-94*, *su177*, I have recovered and characterized a new allele, *sf20*. In *unc-94* mutants, immunofluorescence microscopy shows that a number of known sarcomeric proteins are abnormal, but the most dramatic effect is in the localization of F-actin, with some, abnormally accumulated near muscle cell-to-cell boundaries. EM shows that *unc-94(sf20)* mutants have large accumulations of thin filaments near the boundaries of adjacent muscle cells. I have proven that *unc-94* encodes a tropomodulin, a conserved protein known to cap the pointed ends of thin filaments. *su177* is a splice site mutation specific to isoform *unc-94a*; *sf20*, has a stop codon, which is shared by both *unc-94a* and *unc-94b*. Promoter-GFP analysis revealed that *unc-94a* is expressed mainly in body wall muscle, whereas *unc-94b* is expressed mainly in pharyngeal muscle. Anti-UNC-94 antibodies detect polypeptides of expected size from wild type, wild type-sized proteins of reduced abundance from *unc-94(su177)*, and no detectable *unc-94* products from *unc-94(sf20)*. These antibodies localize UNC-94 to two closely spaced parallel lines, consistent with localization to the pointed ends of thin filaments. In addition, UNC-94 is localized near muscle cell to cell boundaries.

For *unc-100*, I characterized two alleles: *su115* and *su149*. By polarized light, myofibrils of *unc-100* animals are disorganized. EM shows missing M-lines, broken dense bodies, and a lack of defined A and I-bands. Staining of *su115* muscle with antibodies to a variety of known sarcomeric proteins revealed disruption of thick filaments, M-lines and dense bodies. We used three-factor and SNP mapping to place *unc-100* within a 500 kb region. After performing transgenic rescue, RNAi and/or sequencing many candidate genes within the given region, we have yet to determine the molecular identity of *unc-100*.

Molecular genetic analysis of *unc-94* and *unc-100*, two genes that are important for normal myofibril organization in *C. elegans*

By

Tesheka Stevenson Wortham
B.S., University of Georgia, 2002

Advisor: Guy Benian, M.D.

A dissertation submitted to the Faculty of the
James T. Laney School of Graduate Studies of Emory University
in partial fulfillment of the requirements for the degree of
Doctor of Philosophy
in Graduate Division of Biological and Biomedical Sciences
Genetics and Molecular Biology

2010

TABLE OF CONTENTS

Chapter 1: Introduction……1

Part 1: Purpose……2

Part 2: Muscle Structure and Function……....3

Part 3: *C. elegans* as a Model for Studying Muscle……....12

Part 4: Actin Filament Assembly……21

Part 5: The Roles of Actin Regulatory Proteins in Myofibril Assembly and Maintenance……....25

Part 6: Muscle Focal Adhesions……...32

Chapter 2: *unc-94* Encodes a Tropomodulin in *Caenorhabditis elegans*……45

Introduction……...46

Results……50

Figures……...58

Discussion……..72

Materials and Methods……78

Chapter 3: Genetic and Molecular Characterization of *unc-100,* a Gene Required for Normal Myofibril Maintenance or Growth, but not Initial Assembly, in *C. elegans*……86

Introduction……...87

Results and Discussion……88

Figures……...97

Materials and Methods……..114

Chapter 4: Conclusions and Future Directions……..120

Literature Cited……127

LIST OF TABLES

Table 3.1 **Candidate gene mapping of *unc-100*……104**

Table 3.2 **SNP mapping data for *dpy-5 unc-100* and *unc-29 unc-100* recombinants……...106**

Table 3.3 **Individual SNP data……107**

Table 3.4 ***unc-15* and *dcp-66* sequence comparison……..112**

Table 3.5 **RNAi (by feeding) of predicted genes on cosmids in set A (candidate gene mapping of *unc-100*)……113**

LIST OF FIGURES

Figure 1.1 **Structure of the skeletal muscle sarcomere……..8**

Figure 1.2 **The myosin head uses ATP to pull on an actin filament…….9**

Figure 1.3 **T tubules and the sarcoplasmic reticulum……..11**

Figure1.4 **The body-wall muscle of C. elegans……17**

Figure 1.5 **Polarized light images of wt, *unc-89* and alleles of *unc-96*……...19**

Figure 1.6 **Embryogenesis in wild-type and Pat mutants……...20**

Figure 1.7 **Polymerization of G-actin in vitro occurs in three phases……...24**

Figure 1.8 **Troponin and tropomyosin interact to control the attachment of crossbridges to actin……....30**

Figure 1.9 **Organization of accessory proteins in a sarcomere……..31**

Figure1.10 **Integrins mediate linkage between fibronectin in the extracellular matrix and the cytoskeleton…….40**

Figure1.11 **The costameric cytoskeleton of striated muscle……....42**

Figure 1.12 **Protein-protein interactions at M-lines and dense bodies…….. 43**

Figure 2.1 ***unc-94*** **mutants show disorganized muscle structure, decreased motility and low brood size…….58**

Figure 2.2 **Immunofluorescent localization of several known sarcomeric proteins in wild type and** ***unc-94*** **mutant muscle..60**

Figure 2.3 **Electron micrographs of body-wall muscle from wild type and from** ***unc-94(sf20)*** **……..61**

Figure 2.4 **Figure 2.4 Genetic and physical mapping of** ***unc-94*****, location of mutation sites for** ***su177*** **and** ***sf20,*** **and the sequences of UNC-94a and b……...62**

Figure 2.5 **Fluorescent images of GFP expression in transgenic animals that carry** ***unc-94*** **promoter elements……..64**

Figure 2.6 **By Northern blot,** ***unc-94*** **mutations result in decreased levels of** ***unc-94*** **mRNAs……..65**

Figure 2.7 **By Western blotting, UNC-94 polypeptides can be detected from wild-type, but are absent from or in reduced amounts in** ***unc-94*** **mutants or RNAi animals……..66**

Figure 2.8 **By immunofluorescence, UNC-94 localizes to the pointed ends of thin filaments and to muscle cell boundaries……..67**

Figure 2.1S **Electron micrographs of body-wall muscle from wild type and from** ***unc-94(sf20)*** **…….…69**

Figure 2.2S **Comparison of tropomodulin sequences from worms, flies and humans…….…70**

Figure 3.1 **Polarized light microscopy of body-wall muscle from** ***unc-100*** **adults…….…97**

Figure 3.2 **Liquid motility and brood size assays for** ***unc-100*** **animals...99**

Figure 3.3 **Immunofluorescent localization of several known sarcomeric proteins in wild type and** ***unc-100*** **adult body-wall muscle……....100**

Figure 3.4 **Electron micrographs of adult body-wall muscle from wild type and the two** ***unc-100*** **mutants…….….101**

Figure 3.5 **Immunofluorescent localization of MHC A in wild type and** ***unc-100*** **(*su149*) embryos…….....102**

Figure 3.6 **Deficiency mapping of *unc-100*……..103**

Figure 3.7 **Mapping of *unc-100*……105**

Figure 3.8 **Nomarski images of the gonad of *su115* and *su149* adult animals…….108**

Figure 3.9 **Transgenic Rescue of *unc-100*……...109**

Figure 3.10 **Predicted genes on cosmid C26C6…….110**

Figure 3.11 **Deficiency mapping of *unc-100*……..111**

Figure 4.1 **A model of synergistic regulation of sarcomeric actin organization by Tmod, ADF/cofilin, AIP1, and profilin….126**

Chapter 1

Introduction

Part 1: Purpose

Sarcomeres, specified versions of actin cytoskeleton, are the fundamental contractile units of muscle. Although it is well known that sarcomeres contain the major proteins actin and myosin, they are precise assemblages of hundreds of many other proteins. New components and functions of existing components are discovered every year. How these structures are assembled and maintained in the face of muscle contraction is not well understood. The purpose of my thesis is to discover new components of the sarcomere and understand their functions.

My studies, with the use of the model genetic organism *C. elegans*, take advantage of the highly conserved nature of sarcomere composition and structure throughout the animal kingdom. Work of this nature has both basic science and biomedical research significance. It is likely that the principles of sarcomere or myofibril assembly /function can be extrapolated to the assembly and function of many cellular organelles. Many human diseases of skeletal and cardiac muscle (e.g. muscular dystrophies, myopathies, cardiomyopathies) originate from malfunction (often mutation) of these sarcomeric proteins and their attachment structures at the cell membrane (costameres). Therefore, learning the roles of individual sarcomeric and associated proteins is crucial for understanding the pathogenesis of these muscle diseases and in designing future therapeutics.

Part 2: Muscle Structure and Function

Muscle is an important tissue for both vertebrates and invertebrates. Derived from the mesoderm of embryonic germ cells, muscle is the contractile tissue of an organism. Muscle cells can be classified as smooth, cardiac or skeletal and their common function is to produce force and cause motion. Muscles are used for voluntary actions such as locomotion and eating/chewing food. They can also be used for involuntary actions such as the pumping of the heart or breathing.

Although skeletal muscle is voluntary and cardiac muscle is involuntary, they both differ from smooth muscle in the fact that they share a similar cellular composition and structure. Skeletal muscle cells, also referred to as muscle fibers, are very large multinucleated cells that contain many cylindrically shaped organelles called myofibrils. Myofibrils are a type of actin cytoskeleton that are arranged within muscle cells as parallel bundles of filaments that span from one end of the cell to the other and are attached to the cell surface membrane at each end. Myofibrils are highly ordered and have a precise structure that allows for coordinated muscle contraction. Each myofibril is a very long chain of the most fundamental repeating unit called the sarcomere. Because sarcomeres of adjacent myofibrils are in register, vertical stripes or striations are created (Fig. 1.1). Extending from one Z-disk to the next, the sarcomere has a precisely ordered array of parallel and partially overlapping myofilaments; these filaments are called thin filaments and thick filaments. Thin filaments consist primarily of F-actin, coiled with nebulin filaments; thick filaments consist mainly of the protein myosin.

There are regions of the sarcomere that consist of actin filaments, but no thick filaments and a region where there are myosin filaments. The area where there are actin filaments, but no thick filaments, is called the I-band and the region containing thick filaments is called the A-band. In the I-band regions of the sarcomere, the plus ends of actin filaments are attached to Z disks. In the A-band, the M line, or midline, is where proteins can be found that link adjacent thick filaments to one another (Fig 1.1). When the muscle cells are viewed by polarized light, the I and A-bands appear as alternating dark and bright bands, respectively. This difference in reflected light intensity is due to the isotropic nature of the actin filaments and the anisotropic nature of thick filaments. In contrast, when the filaments are stained with hematoxylin or eosin and visualized by light microscopy, the opposite occurs; I-bands appear light and A-band appear dark (Fig 1.1). By electron microscopy, I-bands are light and A-bands are dark, also.

Sarcomere shortening, technically termed as muscle contraction, results from actin filaments sliding past myosin filaments, with no change in length of either filament (Huxley and Hansen, 1954). As mentioned earlier, thick filaments are made of myosin molecules which in turn are composed of a rod portion and hinge region, accompanied by two globular heads. Being bipolar in nature, the thick filaments move toward the plus end of thin filaments, driven by the force of many independent myosin heads (reviewed in Warrick and Spudich, 1987). The myosin heads bind to the actin filaments at myosin binding sites. Upon strong binding, myosin and actin undergo isomerization, which then causes and extension in the hinge region of the myosin molecule. Shortening of the sarcomere occurs when the extensible hinge region pulls the filaments across each other. In the presence of ATP, myosin heads are released from the actin filaments. While

detached, the ATP may be hydrolyzed, which then "recharges" the myosin heads (Huxley, 1969; Lymn and Taylor, 1971). The heads now have a greater affinity for actin and can bind to actin filaments where there are available binding sites. Because there is a lack of coordination in movement amongst the myosin heads, it is necessary that the heads operate with a low processivity. The heads are bound to each actin filament for only a short period of each ATPase cycle, so that one does not slow down the progression of the others. It is through the collective and repeated binding and releasing of myosin heads from actin filaments that muscle contraction and relaxation is achieved (Fig 1.2).

New molecular interactions between myosin heads and actin filaments only occur when an action potential, carried by a motor nerve arrives at a skeletal muscle cell (Constantin, 1970). This leads to an increase in the concentration of free Ca^{2+} within the muscle cell (Jöbsis and O'Connor, 1966; Taylor et al., 1975). First, the signal leaves the nerve and triggers and action potential in the muscle cell membrane. This electrical excitation then spreads to membranous folds called transverse tubules, or T-tubules, which extend inward from the plasma membrane to surround each myofibril (Constantin, 1970). The signal then moves through a small opening to the sarcoplasmic reticulum, a modified sheath of endoplasmic reticulum that surrounds each myofibril like a mesh stocking (Franzini-Armstrong , 1971; Franzini-Armstrong, 1975) (Fig 1.3). Voltage sensitive proteins within the T-tubules are then activated by the incoming action potential, triggering the opening of Ca^{2+}- release channels in the sarcoplasmic reticulum (Schneider and Chandler, 1973). The cytosol is then flooded with Ca^{2+} and initiates myofibrillar contraction (Ebashi et al., 1969). Because the signal from the muscle cell membrane is passed to every sarcomere in the cell, there is synchronized contraction of all of the

myofibrils in the cell. There is only a transient increase in the concentration of Ca^{2+} because it is speedily pumped back into the sarcoplasmic reticulum by an ATP-dependent Ca^{2+} pump. Normally, there is restoration of the Ca^{2+} concentration to resting levels within a time period of 30 msec; during this brief period, the myofibrils are able to relax. Thus, efficient muscle contraction depends on two processes that both consume large amounts of ATP: filament sliding, which is powered by the ATPase of the myosin motor domain and Ca^{2+} pumping, driven by the Ca^{2+} pump. Typically, cytosolic free [Ca^{2+}] of 10^{-5} M leads to contraction, while [Ca^{2+}] of 10^{-8} M leads to relaxation.

The free Ca^{2+} concentration activates the myosin head/actin filament interaction by one of two mechanisms, depending on muscle type. In skeletal muscle, and to some extent in cardiac muscle, Ca^{2+} acts through thin filaments, or is actin based; whereas, in smooth muscle or non-muscle cells, Ca^{2+} acts through thick filaments, or is myosin based. Thin filaments contain not only F-actin and nebulin; they also contain tropomyosin and the troponins. Tropomyosin is a rod-like, 2-stranded, α-helical coiled-coil protein; one tropomyosin interacts with 7 actin monomers in the groove of F-actin. There are three subunits of troponins-I, T, and C (reviewed in Phillips et al., 1986). In thin filament based Ca^{2+} regulation, which occurs in striated muscle, when the Ca^{2+} concentration is elevated, Ca^{2+} binding to troponin-C partially activates the filament by moving tropomyosin away from its lateral position in relaxed muscle, where it blocks the myosin-binding sites of actin. Myosin head binding to the "partially activated" filament moves tropomyosin further out of the way in the active position (reviewed in Phillips et al., 1986). In thick filament based Ca^{2+} regulation, which occurs in smooth muscle, Ca^{2+} binds to calmodulin and Ca^{2+}-calmodulin binds to the normally inactive protein kinase

called “myosin light chain kinase” (MLCK), thereby activating it. MLCK’s phosphorylation of one of the two myosin light chains (“regulatory myosin light chains,” rMLCs), in some still mysterious way, makes myosin heads “active” or more likely to interact with actin thin filaments.

Sarcomeres are not merely composed of overlapping myosin thick and actin thin filaments, but probably contain several hundred different proteins, organized in a highly ordered fashion. New components of sarcomeres are being discovered each year. The sarcomere contains many proteins that are found in multiple locations within the muscle cell, some of which are able to move from one place to another. For example, some proteins of the Z-disk and M-line translocate to the nucleus and may affect sarcomere gene expression. Exactly how all of these components are assembled and maintained is poorly understood and is the subject of ongoing research.

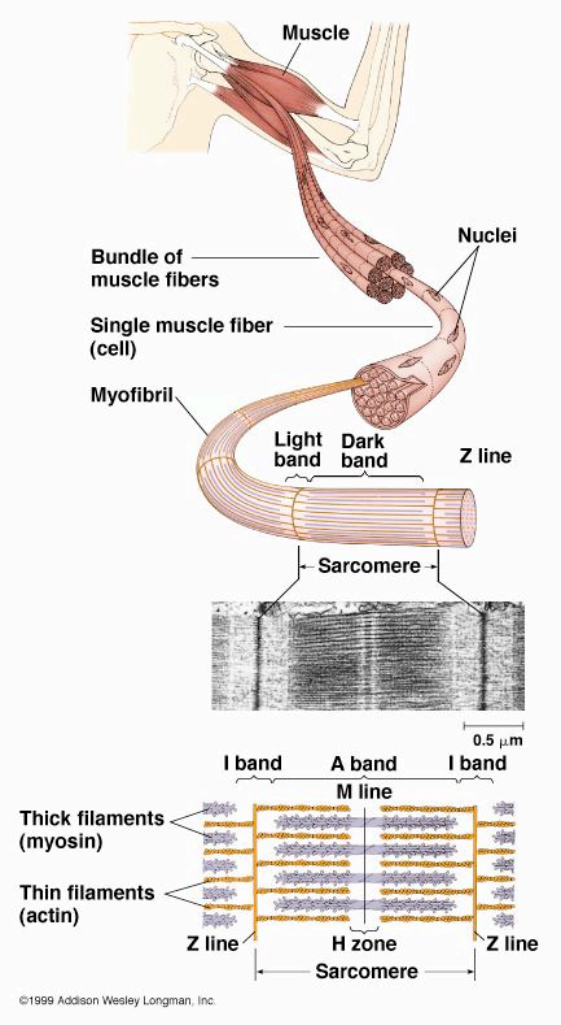

Figure 1.1 Structure of the skeletal muscle sarcomere. Skeletal muscles consist of muscle fibers made of bundles of multinucleated cells. Each cell contains a bundle of myofibrils, which consist of thousands of repeating contractile structures called sarcomeres. (b) Electron micrograph of mouse striated muscle in longitudinal section, showing one sarcomere. On either side of the Z disks are the lightly stained I bands, composed entirely of actin thin filaments. These thin filaments extend from both sides of the Z disk to interdigitate with the dark-stained myosin thick filaments in the A band. (c) Diagram of the arrangement of myosin and actin filaments in a sarcomere. (Figure taken from Alberts, Bruce et al. Molecular Biology of the Cell, 2002.)

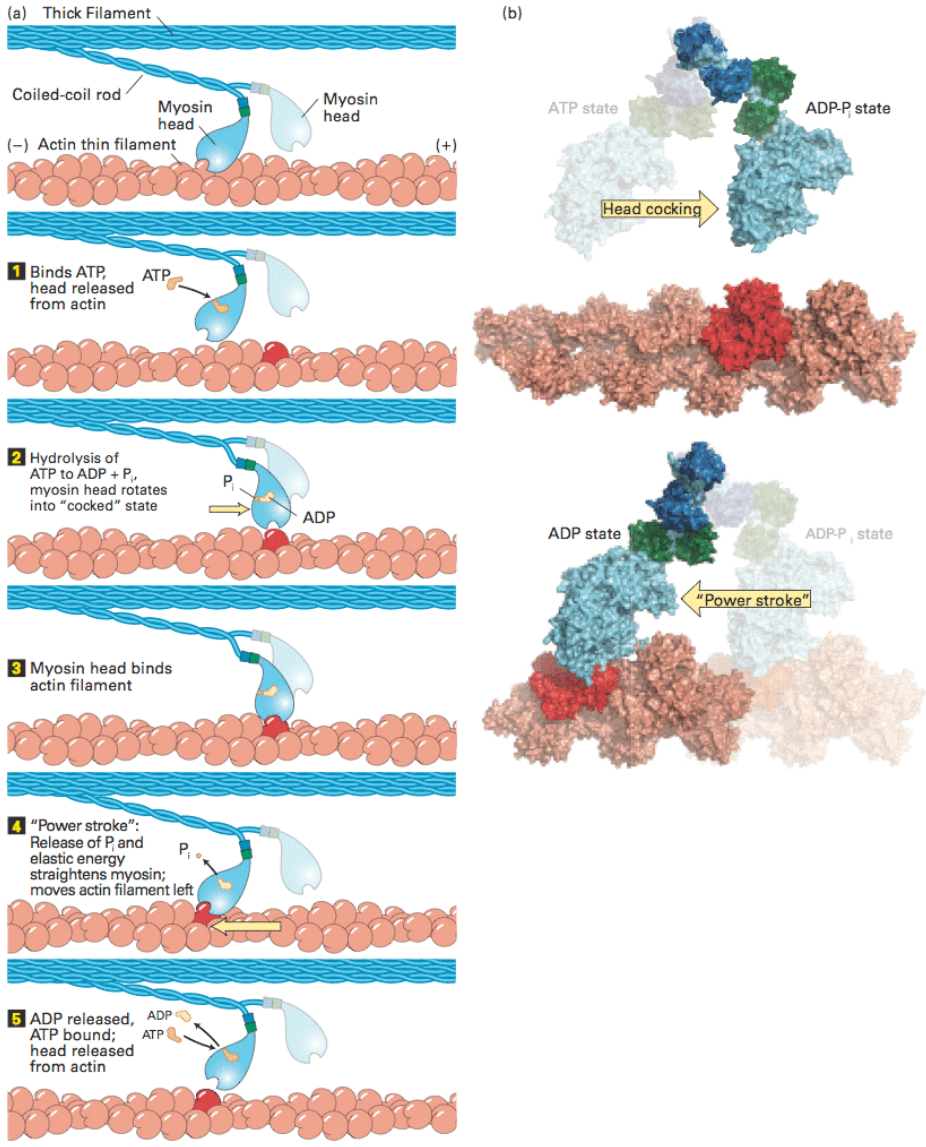

Figure 1.2 The myosin head uses ATP to pull on an actin filament.

(a) In the absence of ATP, the myosin head is firmly attached to the actin filament. Although this state is very short-lived in living muscle, it is the state responsible for muscle stiffness in death (rigor mortis). Step (1): On binding ATP, the myosin head releases from the actin filament. Step (2): The head hydrolyzes the ATP to ADP and Pi which induces a rotation in the head with respect to the neck. This "cocked state" stores

the energy released by ATP hydrolysis as elastic energy, like a stretched spring. Step (3): Myosin in the “cocked” state binds actin. Step (4): When bound to actin the myosin head couples release of Pi with release of the elastic energy to move the actin filament. This is known as the “power stroke” as it involves moving the actin filament with respect to the end of the myosin neck domain. Step (5): The head remains tightly bound to the filament as ADP is released and before fresh ATP is bound by the head. (b) Molecular models of the conformational changes in the myosin head involved in “cocking” the head (upper panel) and during the power stroke (lower panel). The myosin light chains are shown in dark blue and green; the rest of the myosin head and neck are colored in light blue, and actin is red. (Figure taken from Alberts, Bruce et al., Molecular Biology of the Cell, 2002.)

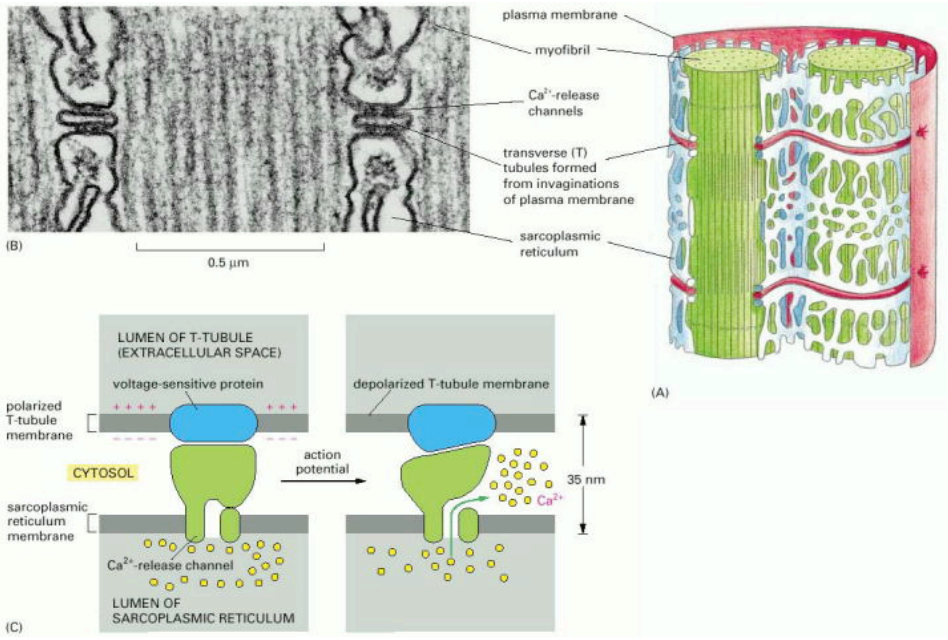

Figure 1.3 T tubules and the sarcoplasmic reticulum. (A) Drawing of the two membrane systems that relay the signal to contract from the muscle cell plasma membrane to all of the myofibrils in the cell. (B) Electron micrograph showing two T tubules. Note the position of the large Ca2+-release channels in the sarcoplasmic reticulum membrane; they look like square-shaped "feet" that connect to the adjacent T-tubule membrane. (C) Schematic diagram showing how a Ca2+-release channel in the sarcoplasmic reticulum membrane is thought to be opened by a voltage-sensitive transmembrane protein in the adjacent T-tubule membrane. (Figure taken from Alberts, Bruce et al., Molecular Biology of the Cell, 2002.)

Part 3: *C. elegans* as a Model for Studying Muscle

The nematode *C. elegans* is a popular model organism for studying muscle lattice assembly and function since its muscle structure and muscle proteins have been highly conserved throughout evolution (Satoko et al., 2000). Much of the insight gained from *C. elegans* has been helpful in studying other animals, including humans (Maduro et al., 2000). There is a need to learn and understand the mechanisms responsible for myofibrillar assembly and maintenance because of the clinical significance of degenerative muscular atrophies, myopathies and cardiomyopathies. *C. elegans* is a desirable model genetic organism because it is non-pathogenic, easily maintained and cost efficient, which is mainly due to its small size (1 mm as an adult) and simple nutritional requirements (*E. coli* bacteria). Other key features of the nematode that make it an attractive model system to study muscle include: a short life cycle (from fertilized egg to adult takes ~ 3.5 days at a growth temperature of 25ºC), large brood size (200-300 progeny per worm), and the ability to store frozen strains for prolonged periods of time. What ultimately sets *C. elegans* apart from other model genetic systems is that its genome has been completely sequenced and its entire developmental cellular lineage has been traced and documented.

Specific characteristics that make *C. elegans* an excellent candidate to study muscle include: its ability to self-fertilize (hermaphrodites produce both oocytes and sperm), and the optical transparency of its outermost layer, the cuticle. Although *C. elegans* comes in two sexes, male (XO) and hermaphrodite (XX), the appearance of males is very infrequent because they only occur naturally by non-disjunction of the X

chromosome during meiosis. The ability of hermaphrodites to self-fertilize is also important for the propagation of uncoordinated and paralyzed animals that are not able to move around to find a mate. The nematode's optically transparent cuticle allows for the visualization of muscle cells in live animals. The striations of the myofilament lattice (A and I-bands) can be easily viewed by polarized light microscopy and the localization of GFP-tagged proteins in the sarcomere can also be visualized.

C. elegans is made up of various muscle types which include: pharyngeal, vulval, enteric and body-wall. The body-wall muscle, used by the animal for locomotion, is comprised of 95 spindle –shaped cells that lie just underneath and parallel to the basement membrane and are arranged into four quadrants of the body-wall (Fig 1.4). Each quadrant contains 24 mononucleate cells, except for the ventral left quadrant, which contains 23 cells. The cells are arranged into interlocking pairs in the anterior half of the animal, with progressively less pairing and overlap in the anterior half. There are three parts of each muscle cell that can easily be distinguished: (1) the cell body, which contains the single nucleus and cytoplasmic organelles, (2) the arm, which is a process that extends from the cell body to the dorsal or ventral nerve cord to receive signals from motor neurons, and (3) the spindle, the region that contains the contractile myofilaments.

Although *C. elegans* is used as a model to study vertebrate muscle, there are a few distinct differences between vertebrate striated muscle and *C. elegans* body-wall muscle. The first and most obvious difference between the two is that *C. elegans* muscle cells are mononucleated, while skeletal muscle cells of vertebrates are multinucleated. While myofibrils of vertebrate striated muscle fill the entire cross sectional area of the cell, they only occupy a space 1-2 μm deep, just underneath the hypodermis in *C. elegans.* In

vertebrate striated muscle, only the outer layer of myofibrils are attached, by costameres, to the sarcolemma; whereas, in *C. elegans* the close proximity of the body-wall muscle to the hypodermis allows for all of the myofibrils to be anchored to the sarcolemma by both dense bodies (analogous to Z-disks) and M-lines (Fig 1.4). Another key difference between the two is that nematode muscle is obliquely striated rather than cross striated as in vertebrates. While the filaments are oriented longitudinally, adjacent structural components are offset relative to one another, causing the striations in *C. elegans* muscle to be at an angle of 5-7° to the longitudinal axis of the filaments and the animal itself.

C. elegans has been used to obtain mutants defective in the formation, function or structure of muscle. There are two major classes of muscle-affecting mutations. In the uncoordinated or "Unc" class, comprising about 40 genes, the worms develop into adults but are slow moving or paralyzed (Brenner, 1974; Waterston et al., 1980; Zengel and Epstein, 1980) (Fig 1.5). The second class, the "Pat" class of mutants (*p*aralyzed *a*rrested at *t*wo-fold), display a characteristic embryonic lethality in which embryos do not move within the eggshell and stop development at the twofold stage (Williams and Waterston, 1994) (Fig 1.6). There are about 16 genes that when mutant display this phenotype. A few genes have hypomorphic Unc and null Pat phenotypes; examples include *unc-112* (Rogalski et al., 2000) and *unc-45* (Barral et al., 1998). To date, nearly all the muscle Unc and many of the Pat genes have been cloned and studied at the molecular level. The encoded proteins include both previously known and novel components of the thick and thin filaments and their organizing and membrane attachment structures (M-lines and dense bodies). The cloning of M-line and dense body components has revealed a number of familiar components of focal adhesions (perlecan, integrins, vinculin, integrin linked

kinase, PINCH), but has also revealed new components of these structures (UNC-112, UNC-98, UNC-96 and UNC-89) (reviewed in Moerman and Williams, 2006; Mercer et al., 2006). This analysis is consistent with a model in which myofibril assembly is directed by signals first laid down in the ECM and the muscle cell membrane. This model is supported by a study of the first appearance and localization of these components during normal embryonic development (Hresko, Williams & Waterston, 1994). In addition, most of the components of dense bodies and M-lines are shared, except for the proteins involved in the later stages of assembly; for example, for the dense bodies, vinculin and α-actinin, and for the M-lines, UNC-89 (For more details see Part 5 on muscle focal adhesions.).

For *C. elegans* thick filaments, the genes for the myosins and paramyosin were among the first identified. New and evolutionarily conserved components of thick filaments were first revealed by many genetic analyses. One example is twitchin (Moerman et al., 1988; Benian et al., 1989; Benian et al., 1993), the founding member of the giant kinases which include mammalian titin and insect projectin. Another example is UNC-45, which is a conserved chaperone for myosin head folding and for the assembly of myosin into thick filaments (Barral et al., 1998; Barral et al., 2002). For thin filaments, genes encoding the actins and the troponin-tropomyosin complex have been found. In addition, novel components have been found (e.g. UNC-87; Goetinck and Waterston, 1994), and the roles in myofibril assembly were first revealed for several previously known proteins. There are many actin binding proteins, which regulate actin filament dynamics in all eukaryotic cells. This includes proteins that promote actin polymerization (e.g. profilin), sever (e.g. gelsolins, ADF/cofilin) or stabilize (e.g. tropomyosin) existing

filaments, promote loss of subunits from the pointed end (e.g. ADF/cofilin), or cap the barbed end (e.g. CapZ) or pointed end (e.g. tropomodulin) to prevent gain or loss of actin subunits. Molecular genetic analysis of UNC-60B (an ADF/cofilin protein; McKim et al., 1994; Ono et al., 1999), tropomyosin (Ono and Ono, 2002), and UNC-78 (Ono, 2001; Mohri & Ono, 2003), have clearly demonstrated the requirement for regulating actin filament dynamics to ensure proper assembly and maintenance of muscle thin filaments.

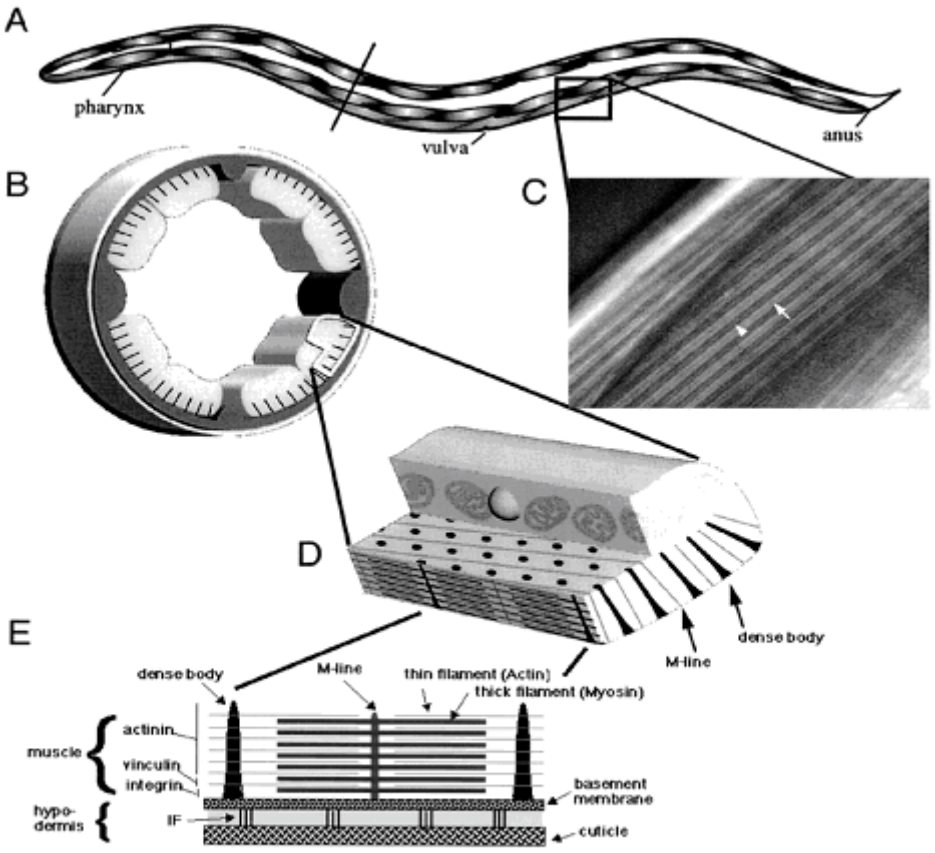

Figure 1.4 The body-wall muscle of C. elegans.

(A) Depiction of the 95 spindle shaped mononuclear muscle cells of the body-wall. Two of the four quadrants are depicted. Each quadrant has interlocking pairs of cells (23 or 24 per quadrant). (B) Cross section at the level given by the diagonal line in (A), showing the cuticle, hypodermis, basement membrane and muscle cells. The myofilament lattice is located close to the basement membrane. (C) Polarized light image of parts of several muscle cells. Bright A-bands alternate with dark I-bands that contain bright cross sections of dense bodies. Arrowhead, dense body; arrow, center of A-band. (D) Enlargement of part of a muscle cell. Notice that all the M-lines and dense bodies are anchored to the cell

membrane. (E) Enlargement of one sarcomere with “classical” components labeled. (Hobert et al.1999; modified by D. Moerman)

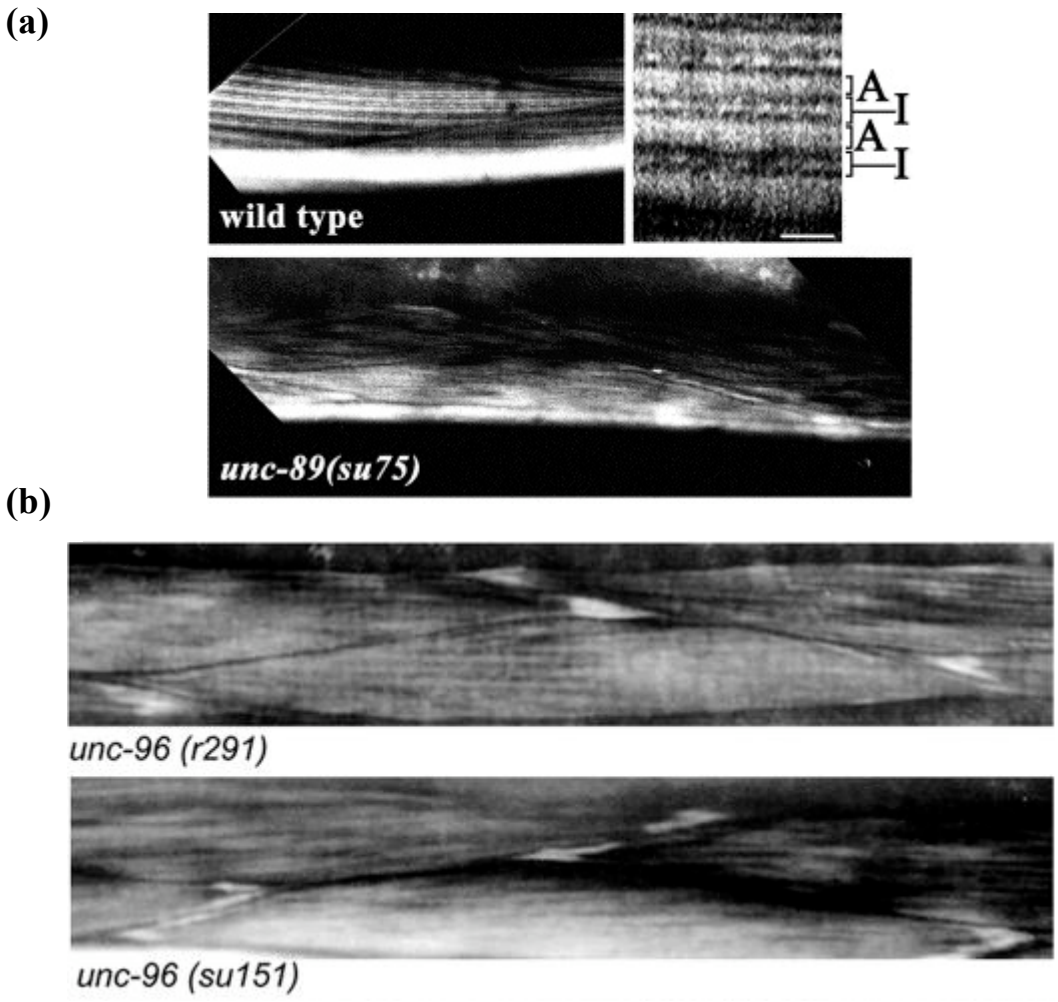

Figure 1.5 Polarized light images of wt, *unc-89* and alleles of *unc-96*.

(a) The inset to the right of the wild-type image shows an enlarged view; note the birefringent A-bands alternating with the darker I-bands, each containing a row of birefringent dense bodies (Z-disc analogs). *unc-89 (su75)* shows the appearance of a typical *unc-89* mutant allele: less organized myofilament lattice with an almost "basketweave" pattern. *unc-96* mutants are also defective in muscle structure. (b) In muscle from the two *unc-96* mutants note the reduced level of organization and appearance of birefringent needles at the ends of the muscle cells. (Part (a) is modified from Small et al., 2004. Part (b) is modified from Mercer et al., 2006.)

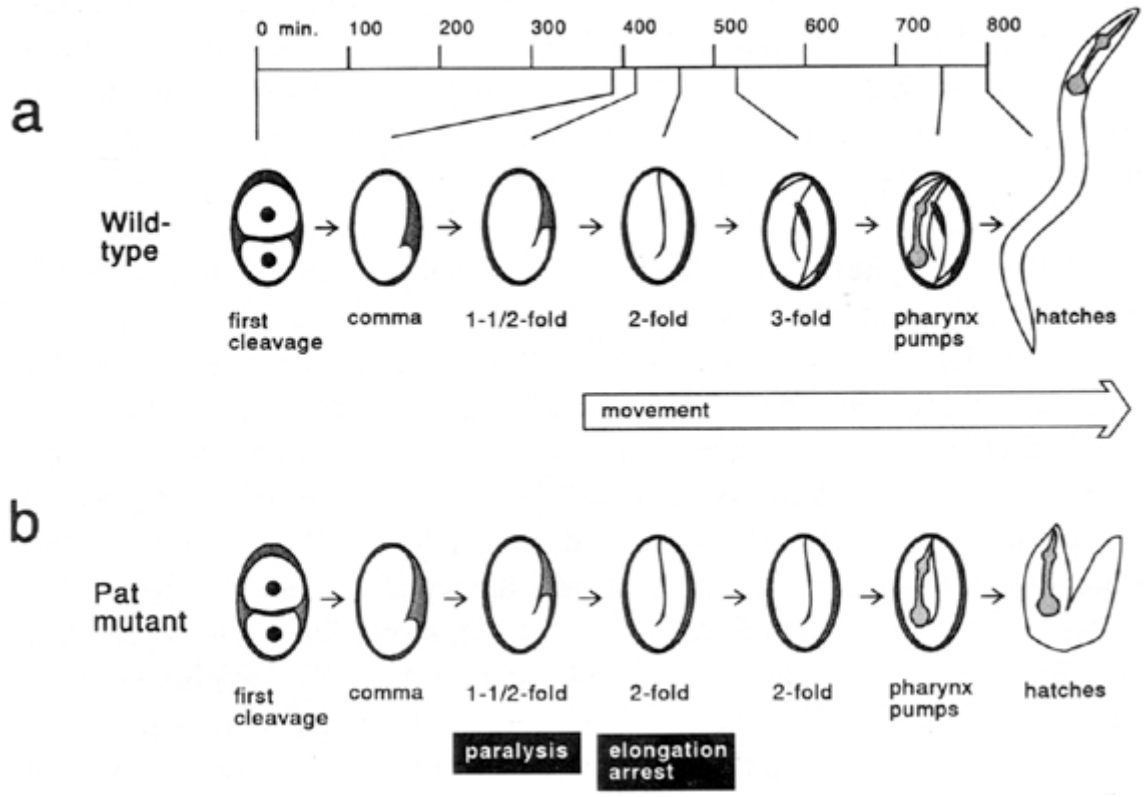

Figure 1.6 Embryogenesis in wild-type and Pat mutants. (*a*) Wild type. The first contractions of body-wall muscles occur as the embryos reach the 1.5-fold length. By twofold, embryos roll vigorously within the egg. (*b*) Pat mutants. 1.5-fold embryos fail to start moving and remain severely paralyzed. Elongation continues until the embryos are twofold, but then stops. Pharyngeal morphogenesis occurs. Embryos often hatch near the normal time as misshapen, inviable larvae. (Figure from Williams and Waterston, 1994)

Part 4: Actin Filament Assembly

Making up 1-5 % of cellular protein in eukaryotic cells, actin is the basic building block of microfilaments in non-muscle cells and thin filaments in muscle (Korn, 1982). Actin has the ability to reversibly assemble into polarized filaments with ends that have distinct functions. These filaments form many different structures due to interactions with a huge number of actin-binding proteins and actin polymerization can be used to do work or to form tracks for myosin motors (Tuxworth and Titus, 2000).

Actin exists freely in the cell as a globular monomer called G-actin. X-ray crystallography shows that G-actin is divided into two lobes by a deep cleft, which is the ATPase fold where ATP and Mg^{2+} are bound. When G-actin monomers link up to form a linear chain, the result is a filamentous polymer called F-actin. Each actin molecule in the polymer contains a Mg^{2+} ion that forms a complex with either ATP or ADP. When either ATP or ADP is bound to G-actin, the conformation of the molecule changes; without a bound nucleotide, G-actin rapidly denatures. The addition of cations to a solution of G-actin causes the monomers to assemble, or polymerize, into F-actin filaments. As mentioned earlier, this process is reversible; when the ionic strength of the solution containing F-actin filaments is lowered, the filaments depolymerize, resulting in a solution of G-actin monomers.

The actin subunits in a filament are all oriented in the same direction, giving the filament structure and polarity. One end of the filament is designated as the (+) end; it is this end that is favored for the addition of actin monomers. Conversely, the opposite end is designated as the (-) end of the filament and is favored for the dissociation of actin

subunits. At the (+) end of the filament, the ATP binding cleft of the terminal actin subunit contacts the adjacent subunit, whereas on the (-) end, the cleft is exposed to surrounding solution.

The polarity of actin filaments was determined by the use of electron microscopy in "decoration" experiments (Brown and Spudich, 1979). This type of experiment capitalizes on the ability of myosin head domains (myosin S1) to bind to actin subunits in a particular orientation. When myosin S1 is bound to all the subunits of the filament, S1 coats the filament in a spiral-like fashion and produces a series of arrowhead-like decorations that all point toward one end of the filament. The arrowhead points toward the (-) end of the filament and is therefore called the "pointed" end; the (+) end is called the "barbed" end. Because myosin binds to actin filaments and does not bind to either microtubules or intermediate filaments, arrowhead decoration is a criterion by which actin filaments can be definitively identified when viewed amongst other cytoskeletal structures.

The rate at which G-actin polymerizes depends on the starting concentration of ATP-G-actin. Its polymerization in vitro proceeds in three sequential steps (Fig 1.7). The first step, called the nucleation phase, is marked by a lag period in which G-actin monomers combine to form short, unstable oligomers. When the oligomers reach three subunits in length, it can then act as a stable seed, or nucleus, for the rapid increase in filament length during the elongation phase; during the elongation phase actin monomers are added to both ends of the filament. As the F-actin filaments grow, the concentration of free G-actin begins to decline until equilibrium is achieved between filaments and monomers. In the third phase of the process, the steady-state phase, G-actin monomers

exchange with subunits at the ends of the filament, without a net change in the total mass of the filaments. At steady state, ATP-G-actin subunits are preferentially added to the (+) end, while ADP-actin subunits disassemble from the (-) end, causing a "treadmilling" effect of actin monomers.

Treadmilling enhancement and the conversion of ADP-actin to ATP-actin are achieved by the proteins profilin and cofilin. Profilin is a small protein that binds to G-actin on the side opposite the nucleotide-binding cleft. When profilin is attached to the ADP-G-actin complex, it opens the cleft and tremendously enhances the loss of ADP, which is replaced by the more abundant cellular ATP, creating a profilin-ATP-G-actin complex. The (-) end of the actin filament cannot be bound by this complex because profilin blocks the sites on G-actin for (-) end assembly. However, this complex binds very efficiently to the (+) end and after the new subunit is bound, profilin dissociates. While this does not enhance the rate of treadmilling, it provides a supply of ATP-G-actin from released ADP-G-actin. Thus, almost a large fraction of G-actin in the cell is bound by ATP. Unlike profilin, cofilin specifically binds to F-actin. In F-actin, the subunits are older going toward the (-) end and are bound by ADP. Cofilin binds the actin polymer by bridging two actin monomers and producing a small change in the twist of the filament, which destabilizes and breaks the filament into short pieces. By severing the filament into many short pieces, cofilin generates many more (-) ends, enhancing the disassembly of the (-) end of each filament. When the ADP-actin subunits are released, they are then recharged by profilin and added to the (+) ends of filaments.

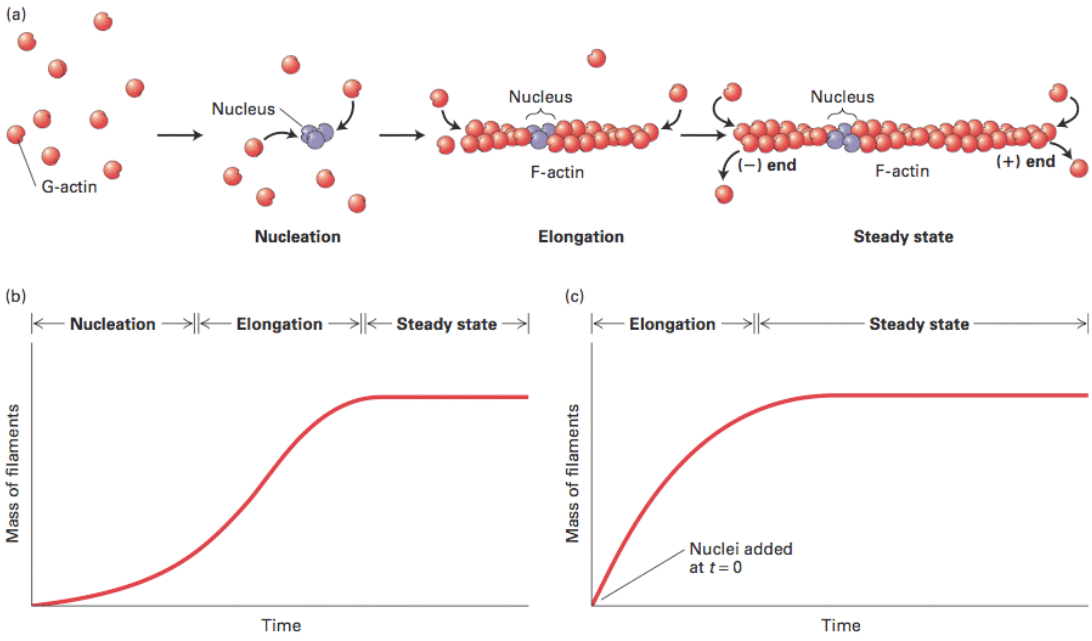

Figure 1.7 Polymerization of G-actin in vitro occurs in three phases. (a) In the initial nucleation phase, ATP–G-actin monomers (red) slowly form stable complexes of actin (purple). These nuclei are rapidly elongated in the second phase by the addition of subunits to both ends of the filament. In the third phase, the ends of actin filaments are in a steady state with monomeric G-actin. (b) Time course of the in vitro polymerization reaction reveals the initial lag period associated with nucleation, the elongation phase, and steady state. (c) If some short stable actin filament fragments are added at the start of the reaction to act as nuclei, elongation proceeds immediately without any lag period. (Figure taken from Alberts, Bruce et al. Molecular Biology of the Cell, 2002.)

Part 5: The Roles of Actin Regulatory Proteins in Myofibril Assembly and Maintenance

Myofibril maintenance and assembly is regulated by several well characterized actin binding proteins, two of which were discussed in the previous section (profilin and cofilin). While profilin and cofilin aid in the polymerization and severing of actin filaments, respectively, many other actin binding proteins can stabilize filaments, or cap the ends to prevent gain or loss of actin subunits (Didry et al., 1998). These proteins include: tropomyosin, troponin, nebulin, CapZ and tropomodulin.

Tropomyosin (TM) is a 40 nm alpha-helical protein that forms a coiled-coil dimer structure of two parallel helices containing 2 sets of 7 alternating actin binding sites. TM molecules are linked head to tail and form a continuous chain along both sides of the actin thin filament (Seymour and O'Brien, 1980). Associated with each tropomyosin molecule is a protein complex called troponin (TN). Troponin is composed of three subunits; TN-T is the tropomyosin binding troponin, TN-I is the inhibitory troponin and TN-C is the calcium binding troponin. It is TN-C that controls the position of TM on the surface of an actin filament through the TN-I and TN-T subunits (Pirani et al., 2006).

In resting muscle, when $[Ca^{2+}]$ is around 10^{-8} M, tropomyosin overlays myosin binding sites on actin thin filaments and is "locked" down in this position by troponin T and troponin I (Seymour and O'Brien, 1980). Upon release of calcium from the sarcoplasmic reticulum, calcium binds to troponin C; this causes a conformational change in troponin C and the entire troponin-tropomyosin complex move slightly, "unlocking" tropomyosin from F-actin, exposing the myosin binding sites on the actin filament.

Myosin heads can now access the binding sites (Fig. 1.8). Once one myosin head binds, this fully displaces tropomyosin and allows additional myosin heads to bind, initiating muscle contraction. Once calcium is pumped out of the cytoplasm, back into the sarcoplasmic reticulum, calcium levels return to 10^{-8} M. Troponin C and the entire troponin-tropomodulin complex move in the direction such that the myosin binding sites on F-actin are again blocked.

Nebulin, which has isoforms ranging from 600-900 kDa, binds as many as 200 actin monomers in a filament. Nebulin consists of many tandem, ~35 residue domains mostly arranged into 7 domain "super-repeats" (Kruger et al., 1991). It is likely that a single domain interacts with a single actin monomer in F-actin and each super-repeat interacts with one turn of the F-actin helix (7 actin monomers) and one troponin-tropomyosin complex. It is believed that the number of actin binding repeats, and therefore the length of nebulin, determines the length of the thin filaments; in other words, it is thought that nebulin acts as a "ruler," regulating thin filament length during sarcomere assembly (McElhinny et al., 2005) (Fig. 1.9).

Actin filament dynamics and treadmilling are largely regulated by "capping" proteins that specifically interact with the ends of the filaments. There are two classes of capping proteins: a class that binds to the (+) ends of actin thin filaments and a class that binds to the (-) ends (Pope et al., 1994). If actin filaments were not regulated by such proteins, they would constantly grow and disassemble in an uncontrolled manner. Thus, having the F-actin capped in thin filaments is essential to maintain a stable sarcomere.

Localized to the Z-disk of the sarcomere, CapZ binds to the barbed, or (+) end of actin thin filaments (Hug et al., 1992) (Fig. 1.9). CapZ is a heterodimer consisting of an

alpha and beta subunit; it regulates actin assembly by inhibiting the addition or loss of actin monomers to the (+) ends. The concentration of CapZ in muscle cells is generally sufficient to rapidly cap the (+) ends of all newly formed thin filaments. There are at least two mechanisms that regulate the capping activity of CapZ. The capping activity of CapZ is inhibited by a regulatory lipid in the plasma membrane called PI (4, 5) P2 (Heiss and Cooper, 1991). The activity of CapZ is also regulated by a number of regulatory proteins that bind to the (+) end, protecting the end from the binding of CapZ; therefore, allowing assembly there. Thus, it appears that muscle cells have evolved an elaborate scheme to block the assembly of actin thin filaments at their (+) ends, except when it is necessary not to do so.

Tropomodulin (Tmod) is one of the few capping proteins for the (-) ends of actin thin filaments (Fowler et al., 1993) (Fig. 1.9). Localized closer to the M-line of the sarcomere, tropomodulin is an elongated molecule that has a molecular mass of about 40 kDa. Tmod acts by inhibiting polymerization and depolymerization of actin monomers. Unlike proteins that cap actin filament (+) ends, tropomodulin also binds tropomyosin and requires tropomyosin for optimal function. The N-terminal half of tropomodulin has two tropomyosin binding sites as well as a tropomyosin–dependent actin-binding site; the tropomyosin-independent actin binding site is located at the C-terminal end. One tropomodulin molecule binds two tropomyosin molecules, thus it has been shown that only one molecule of tropomodulin is necessary and sufficient for capping the (-) ends of actin filaments (Kostyukova et al, 2006). Because tropomyosin/tropomodulin interactions are isoform specific, differences in tropomyosin affinity for the two binding sites within tropomodulin may regulate its correct positioning as well as its effectiveness at capping.

When the sequence for tropomodulin was initially determined, there was no homology found with other known proteins. Presently, there are four tropomodulin genes in humans. Tmod1, previously called E (erythrocyte)-Tmod, was found in many tissues, but mainly in erythrocytes and cardiac and skeletal muscle. Tmod2, also known as N (neuron)-Tmod, was detected in brain cells. Tmod3, also known as U (ubiquitous)-Tmod, was found in many tissues. Tmod4, Sk (skeletal)-Tmod, was found in skeletal muscle cells, where it is known to replace Tmod1 during development. These four isoforms share ~70% sequence identity.

In *C. elegans* there are two Tmod genes, namely *unc-94* (*tmd-1*) (the subject of Chapter 2 of this dissertation) and *tmd-2*. Each gene encodes two different isoforms by using different promoters and by alternative splicing, a process that is not used with vertebrate Tmod genes. I have shown that *unc-94*a is primarily expressed in body-wall, uterine and vulval muscle, but not in pharyngeal muscle. *unc-94b* is highly expressed in the pharynx and anal depressor muscles and can also be detected in the muscles of the vulva and uterus as well as in the spermatheca and intestinal epithelial cells. SAGE data suggests that *tmd-2* is also expressed in muscle, but because TMD-2 may lack a tropomyosin-binding region, it might have a different function and localization in the sarcomere than *unc-94*(*tmd-1*) (caps actin filaments at their (-) ends).

Because tropomodulin plays such an important role in actin dynamics, many studies have been performed *in vivo* and *in vitro* to determine what happens when Tmod is absent or is in excess in muscle cells. Tmod over-expression in mice cardiac myocytes causes myofibril degeneration, which leads to dilated cardiomyopathy (Sussman et al., 1998). Reduced Tmod expression results in the formation of abnormally long actin

filaments and muscle which cannot contract. Over-expression of GFP-Tmod in cardiac myocytes results in shorter thin filaments. In Tmod1 knockout mice, several heart defects were reported, including aborted development of the myocardium and the inability to pump blood, which leads to embryonic lethality (Fritz-Six et al., 2003).

There are many other actin binding proteins that work (individually or cooperatively) to ensure proper assembly and maintenance of actin filaments. Of the 160 that are currently known, only a small portion of them are well characterized. It is for this reason that studies such as the ones mentioned above are an important aspect of muscle research.

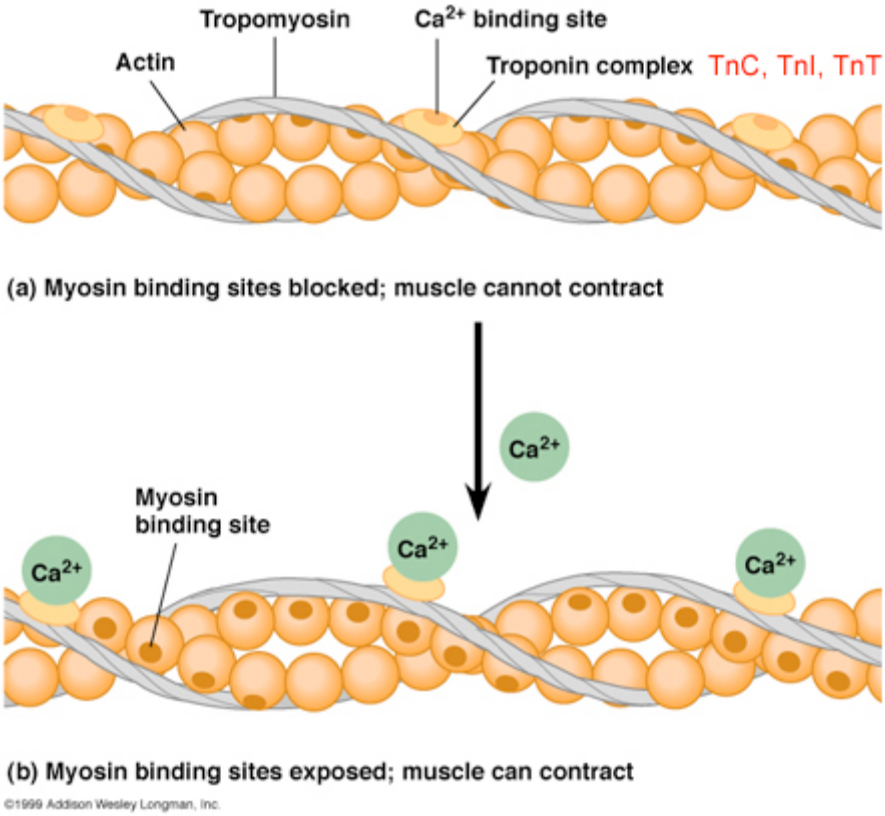

Figure 1.8 Troponin and tropomyosin interact to control the attachment of crossbridges to actin. When intracellular calcium is low ($<10^{-8}$M), tropomyosin blocks all actin sites along one turn of the actin helix. However when intracellular calcium is elevated ($>10^{-7}$M), calcium binds to troponin which then alters the position of tropomyosin on the actin filament. Once tropomyosin has moved, the actin sites are exposed allowing crossbridges to attach. (Figure taken from Alberts, Bruce et al. Molecular Biology of the Cell, 2002.)

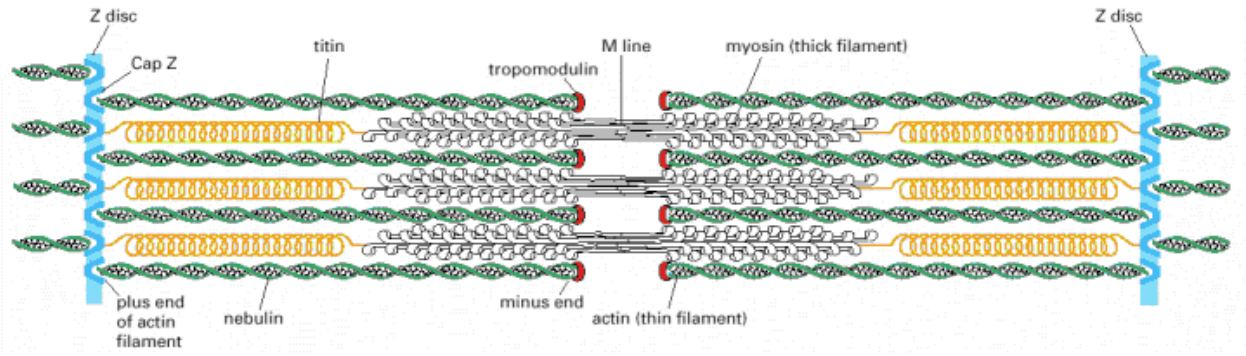

Figure 1.9 Organization of accessory proteins in a sarcomere. Each giant titin molecule extends from the Z disc to the M line—a distance of over 1 μm. Part of each titin molecule is closely associated with a myosin thick filament (which switches polarity at the M line); the rest of the titin molecule is elastic and changes length as the sarcomere contracts and relaxes. Each nebulin molecule is exactly the length of a thin filament. The actin filaments are also coated with tropomyosin and troponin and are capped at both ends. Tropomodulin caps the minus end of the actin filaments, and CapZ anchors the plus end at the Z disc, which also contains α-actinin. (Figure taken from Alberts, Bruce et al. Molecular Biology of the Cell, 2002.)

r.

Part 6: Muscle Focal Adhesions

One way in which cells of multicellular organisms communicate with their environment is thorough cell-extracellular matrix (ECM) adhesion. Cells adhere through the binding of adhesion receptors in the plasma membrane to components of the surrounding extracellular matrix, a complex of interdigitating meshwork of proteins and polysaccharides secreted by cells into the spaces between them. Cell-ECM adhesion is essential for many processes, such as organogenesis during embryonic development and maintaining tissue integrity and organ function in adults. Therefore, disruption of cell-ECM adhesion is commonly associated with human disease including neuromuscular and skeletal disorders as well as cancer (Schwock et al., 2010). Because of this association, it is important to understand how cell-ECM adhesion is mediated, regulated and how it influences cell function.

There are many subcellular structures that mediate cell-ECM adhesion. These structures greatly vary from one another in size, shape, distribution, dynamics and molecular components. This heterogeneity gives morphological plasticity to cell-ECM adhesions, allowing cells to sense, adapt and respond to a variety of extracellular environments. Despite the heterogeneity of ECM adhesion structures, they do share certain common features which include connecting cell surface integrins to the actin cytoskeleton (Fig. 1.10).

One of the earliest described and best-characterized cell-ECM adhesion structures are focal adhesions. Focal adhesions are specific types of macromolecular assemblies through which both mechanical force and regulatory signals are transmitted. They serve

as the mechanical linkages to the ECM and act as a biochemical signaling hub to concentrate and direct numerous signaling proteins at sites of integrin binding and clustering. Focal adhesions are very strong ECM adhesion structures that are often found in adherent cells (such as fibroblasts) cultured on rigid ECM substrata. Although cultured mammalian cells are often used as a model system for studying focal adhesions, cell-ECM adhesions similar to focal adhesions have been found in vivo, in both invertebrate (*C. elegans* body-wall muscle attachment structures) and vertebrate organisms.

In vertebrate striated muscle cells, the components that are structurally and compositionally similar to focal adhesions are called costameres (Fig. 1.11). Costameres are subsarcolemmal protein assemblies that circumferentially align in register with the Z-disk, and possibly the M-line, of peripheral myofibrils and physically couple force-generating sarcomeres with the sarcolemma. Focal adhesion proteins have not only been located beneath the Z-disks of peripheral myofibrils, but have also been found at peripheral M-lines. In the cases of both focal adhesions and Z-disk costameres, integrins are coupled to cytoskeletal actin filaments and myofibrillar thin filaments, respectively.

As mentioned earlier, the nematode *C. elegans* has body-wall attachment structures that are very similar to focal adhesions. *C. elegans* body-wall muscle is organized such that actin thin filaments are attached to Z-disk analogues called dense bodies and myosin thick filaments are organized around M-lines (Moerman and Williams, 2006). While being attached to myofibril components, all the dense bodies and M-lines of a muscle cell appear to be anchored to the cell membrane, thus serving the same function as vertebrate costameres. The physical linkage between myofibrillar components and the

muscle cell membrane is critical in allowing myofilament contraction for locomotion of the animal.

Through analysis of mutants and staining of various muscle components during embryonic muscle development, muscle development in *C. elegans* occurs from the outside in at future M-lines and dense bodies (Z-disk analogs) (see summary in Moerman and Williams, 2006). First to accumulate at these sites is the ECM protein UNC-52 (perlecan) and its associated transmembrane heterodimeric protein integrin. Associating with the cytoplasmic tail of β -integrin is a complex of four conserved proteins, UNC-112 (Mig-2 or Kindlin), PAT-4 (integrin linked kinase), PAT-6 (actopaxin) and UNC-97 (PINCH) (Norman et al., 2007) (Fig. 1.12). Our lab is learning about which proteins associate with UNC-97 at the M-line, the site at which thick filaments are cross-linked. Thus, in Mercer et al. 2003, we reported that the first two of the five total LIM domains of UNC-97 associate with the 4 C2H2 Zn fingers of UNC-98. In Miller et al. (2006) we show that the N-terminal 110 residues of UNC-98 interact with the C-terminal portion of a myosin heavy chain, MHC A, which resides in the middle of thick filaments in the proximity of M-lines. Through a combination of genetic, cell biologic and biochemical evidence we support a model in which *UNC-98 links integrin-associated proteins to myosin in thick filaments at M-lines.* Because in *C. elegans* body-wall muscle all the M-lines and dense bodies are anchored to the muscle cell membrane, they serve the same function as vertebrate muscle costameres, which are focal adhesion structures for peripheral myofibrils. Although costameres are usually regarded to reside at the level of Z-disks, some components of focal adhesions, including α v integrin have also been found at M-lines (McDonald et al., 1995). Thus, our results in *C. elegans* muscle suggest

the possibility of a similar mechanism of linkage between integrins and myosin thick filaments at the M-lines of peripheral myofibrils of vertebrate muscle.

In Qadota et al. (2007), we demonstrate another mechanism by which this linkage from muscle cell membrane to myosin occurs. We identified three novel UNC-97 (PINCH) interactors: LIM-8, LIM-9 and UNC-95. We show that these proteins are involved in three additional mechanisms by which linkage from UNC-97 to myosin occurs: from UNC-97 through LIM-8 to myosin, or from UNC-97 through LIM-9/UNC-96 to myosin, or from UNC-97 through UNC-95/LIM-8 to myosin (Fig. 1.12a). Previously, it was reported that *unc-95* mutants are slow moving and have disorganized muscle structure, including a lack of M-lines (Broday et al., 2004). LIM-8 and LIM-9 are novel LIM domain containing proteins, and LIM-9's mammalian homolog is FHL (four and a half LIM domain protein). In humans, FHL1 has been associated with myopathies: missense mutations in FHL1 result in either X-linked dominant (Quinzii et al., 2008) or recessive scapuloperoneal myopathies (Windpassinger et al., 2008). All three new UNC-97 interactors contain LIM domains that we have shown are required for binding. Among the three interactors, LIM-8 and LIM-9 also bind to UNC-96, a protein that we previously described as a component of M-lines (Mercer et al., 2006). UNC-96 and LIM-8 also bind to the C-terminal portion of MHC A (to a slightly different portion of MHC A that binds to UNC-98). All interactions were first identified by yeast 2-hybrid and then confirmed by in vitro binding assays using purified proteins. All three novel UNC-97 interactors are expressed in body-wall muscle and by antibodies localize to M-lines. Either a decreased (by loss of function mutation) or an increased level (by a heat shock promoter in adult muscle) of UNC-96 results in disorganization of thick filaments.

In Miller et al. (2009) we demonstrate that both UNC-98 and UNC-96 interact with CSN-5. Interactions were identified by a yeast 2-hybrid screen and confirmed by biochemical methods. CSN-5 is a member of the highly conserved "COP-9 signalosome complex" which has been found in multiple organisms to regulate protein stability, usually through SCF ubiquitin ligases. Anti-CSN-5 antibody co-localizes with paramyosin at A-bands in wild type, and co-localizes with abnormal accumulations of paramyosin found in *unc-98*, *unc-96*, and *unc-15* (encodes paramyosin) mutants. Knock down of *csn-5* results in a great increase in the level of UNC-98 protein and a slight reduction in the level of UNC-96 protein, suggesting that CSN-5 promotes the degradation of UNC-98 and that CSN-5 stabilizes UNC-96. In *unc-15* and *unc-96* mutants, CSN-5 protein is reduced, implying the existence of feed back regulation from myofibril proteins to CSN-5 protein levels. Our results are the first to implicate CSN-5 or the COP9 signalosome in myofibrillar organization or function. Nevertheless, the report is consistent with the growing recognition that the ubiquitin proteasome system is required for muscle protein turnover in vertebrate muscle, and mediated by the muscle specific ubiquitin ligase Atrogin-1, and the MuRF family (Muscle specific RING Finger proteins) (Gomes et al., 2001; Bodine et al., 2001). Indeed, for C. elegans muscle, the RING finger protein, RNF-5 is localized to dense bodies and regulates the levels of UNC-95 (Broday et al., 2004): RNF-5 and UNC-95 interact by yeast 2-hybrid (Didier et al., 2003); heat shock induced overexpression of RNF-5 results in a reduction in UNC-95::GFP, and this reduction depends on the presence of an active RING finger domain in RNF-5; in contrast, RNAi knockdown of rnf-5 results in an increase in UNC-95::GFP (Broday et al., 2004).

Like UNC-98 and UNC-96, UNC-89 (mammalian homolog is called "obscurin") is also an M-line protein in *C. elegans* muscle. It is a giant (up to 900 kDa) multi-domain protein consisting primarily of Ig domains, SH3, DH and PH domains, and two protein kinase domains (Benian et al., 1996; Small et al., 2004; Ferrara et al., 2005). We have discovered that a portion of UNC-89 (containing the kinase domains) interacts with a member of the UNC-98/UNC-96 complex, namely LIM-9 (FHL), and we reported this finding in Xiong et al. (2009). Indeed, we can now incorporate all the known *C. elegans* M-line proteins into our M-line protein interaction matrix; the interactions were first identified through our 2-hybrid analysis and later confirmed by both in vitro binding using purified proteins and immuno-colocalization (Fig. 1.12a).

As indicated in Fig. 1.12a and 1.12b, UNC-52 (perlecan), integrins (PAT-2/PAT-3) and the four-protein complex are found at the base of both M-lines and dense bodies. At the dense bodies, there are additional dense body-specific proteins such as DEB-1 (vinculin) (Barstead and Waterston, 1989), ATN-1 (α-actinin) (Barstead et al., 1991), UIG-1 (Cdc42 GEF) (Hikita et al., 2005), ALP-1 (ALP/Enigma) (McKeown et al., 2006), DYC-1 (Lecroisey et al., 2008), and ELP-1 (EMAP-like protein) (Hueston and Suprenant, 2009). The only known nematode M-line-specific protein is UNC-89 (obscurin) (Benian et al., 1996; Small et al., 2004); as mentioned below, UNC-98 and UNC-96 are most prominent at M-lines. For the structure and molecular components of dense bodies see the recent review by Lecroisey et al. (2007). Through collaboration with Don Moerman's lab at Univ. of British Columbia, our lab is making similar progress in defining a dense body protein interaction matrix that explains linkage of the muscle cell membrane to thin filaments (Fig. 1.12b).

In recent years, there has been growing recognition that in mammalian striated muscle, a number of Z-disk and M-line proteins translocate to the nucleus in response to mechanical stimuli or extracellular signals, and once inside the nucleus, influence gene transcription (Lange et al., 2006; Gautel, 2008). A similar situation appears to exist for nematode muscle, but at this time, the mechanisms of nuclear translocation and the functional significance of M-line and dense body proteins in the nucleus is less understood than it is for mammalian muscle. But given the power of worm genetics and its advantages for imaging live muscle cells, this area holds much promise for future insights. Here is what we know for proteins that are at least partly localized to M-lines: In transgenic worms, translational GFP fusions of full-length UNC-97 (Hobert et al., 1999), UNC-98 (Mercer et al., 2003), UNC-95 (Broday et al., 2004), and ZYX-1 (zyxin) (Lecroisey et al., 2008) show localization to M-lines, dense bodies and nuclei. However, antibodies that we have developed to UNC-98 (Mercer et al., 2003), to UNC-97 (Miller et al., 2006), and to UNC-95 (Qadota et al., 2007), when used in immunofluorescent experiments, failed to localize to nuclei under normal conditions. There are no reports of antibodies having been generated or localized for ZYX-1. Nevertheless, anti-UNC-98 reacted to nuclei, when a non-standard fixation method was used on wild type nematodes, or when UNC-98 was overexpressed (Mercer et al., 2003). Additional support that endogenous UNC-98 and UNC-97 reside in nuclei was obtained during our purification of native thick filaments reported in Miller et al. (2006): nuclear-enriched fractions from wild type worms contain western blot detectable UNC-98 and UNC-97. In the 2-hybrid system, when either UNC-98 (Mercer et al., 2003), or UNC-97 (H. Qadota, K. Norman and D. Moerman, unpub. data) are fused to the GAL4 DNA binding domain, they can

activate transcription, suggesting that UNC-98 and UNC-97 may activate transcription in vivo. By testing deletion derivatives of UNC-98::GFP, we have shown that the N-terminal 110 residues of UNC-98 are sufficient for nuclear localization (Mercer et al., 2003). A similar approach by Norman et al. (2007) indicates that LIM2 and LIM3 are required for nuclear localization of UNC-97 (PINCH).

In addition to nuclear localization of proteins that are localized to M-lines and dense bodies, nuclear localization has also been found for the dense-body specific protein ALP-1 (McKeown et al., 2006). The *alp-1* gene encodes 4 different isoforms, one is ALP-like (ALP-1A), and three are Enigma-like (ALP-1B, -1C, -1D). Use of GFP translational fusions demonstrates a complex pattern of expression of these proteins in embryos and adults, and localization to muscle cell dense bodies, and nuclei of muscle and hypodermal (epithelial) cells. In fact, ALP-1 is one of the few muscle focal adhesion proteins showing strong localization to embryonic muscle (ALP-1A) and hypodermal cell (ALP-1B,C,D) nuclei.

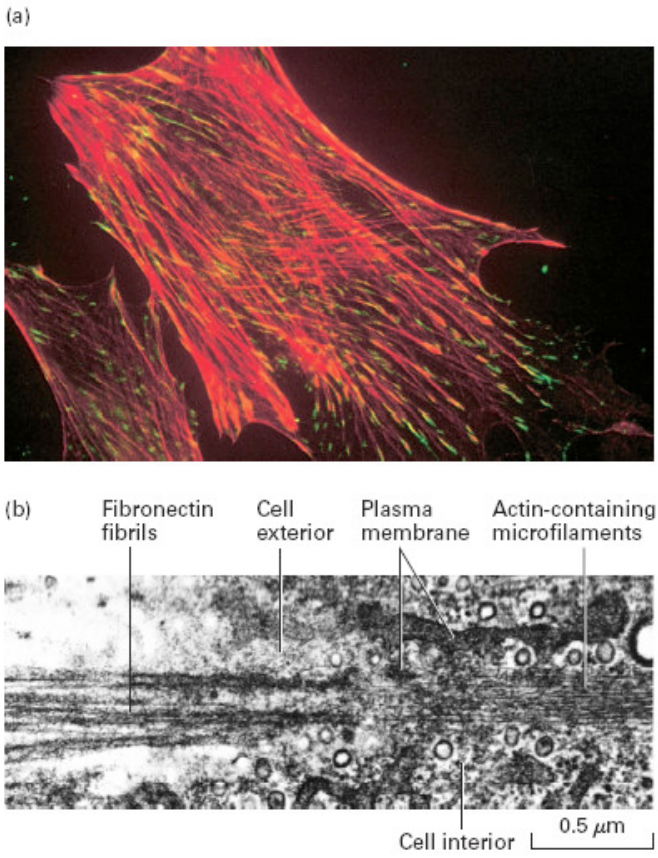

Figure 1.10 Integrins mediate linkage between fibronectin in the extracellular matrix and the cytoskeleton. (a) Immunofluorescent micrograph of a fixed cultured fibroblast showing co-localization of the α5β1 integrin (green) and actin-containing stress fibers (red). The cell was incubated with two types of monoclonal antibody: an integrin-specific antibody linked to a green fluorescing dye and an actin-specific antibody linked to a red fluorescing dye. Stress fibers are long bundles of actin microfilaments that radiate inward from points where the cell contacts a substratum. At the distal end of these fibers, near the plasma membrane, the coincidence of actin (red) and fibronectin-binding integrin (green) produces a yellow fluorescence. (b) Electron micrograph of the junction of fibronectin and actin fibers in a cultured fibroblast. Individual actin-containing 7-nm

microfilaments, components of a stress fiber, end at the obliquely sectioned cell membrane. The microfilaments appear aligned in close proximity to the thicker, densely stained fibronectin fibrils on the outside of the cell. (Part (a) from J. Duband et al., 1988, Part (b) from I. J. Singer, 1979)

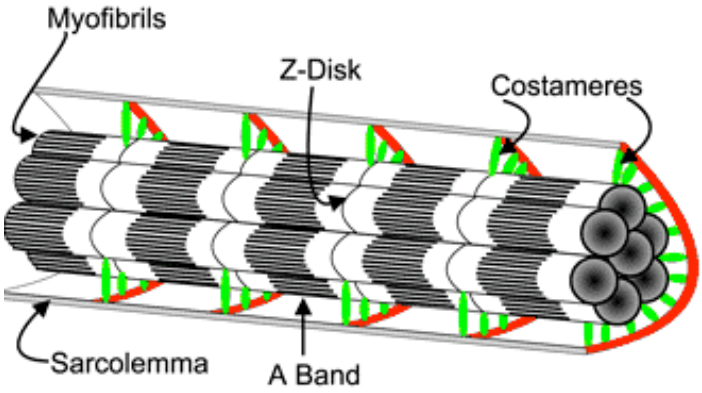

Figure 1.11 The costameric cytoskeleton of striated muscle. In mammalian striated muscle, myofibrils fill the entire cell, but peripherally located myofibrils are linked to the sarcolemma. Linkage occurs at costameres, which are structurally & compositionally similar to focal adhesions. (Figure from J.M. Ervasti, 2003)

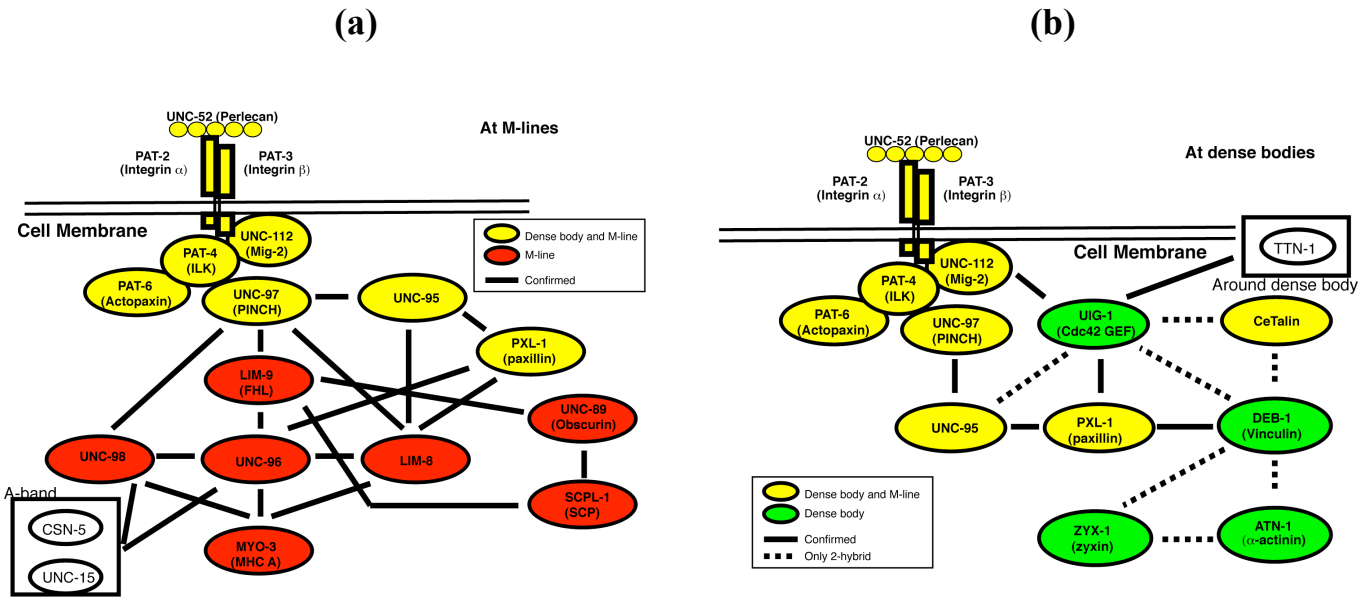

Fig. 1.12 Protein-protein interactions at M-lines and dense bodies (a) Protein complexes at M-lines in *C. elegans* body-wall muscle. Myofilaments are located close to the surface and anchored by M-lines and dense bodies to the muscle cell membrane. At these attachment structures, UNC-52 (perlecan) is located in the ECM. Inside the muscle cell, the cytoplasmic tail of PAT-3 (β integrin) is associated with a 4 protein complex [UNC-112 (kindlin), PAT-4 (ILK), PAT-6 (actopaxin), UNC-97 (PINCH)]. At M-lines, additional proteins link UNC-97 (PINCH) to MHC A (myosin heavy chain); these are UNC-98, LIM-9 (FHL) / UNC-96, LIM-8, and UNC-95 / LIM-8. In addition, LIM-9 (FHL) links to UNC-89 (obscurin), and UNC-98 and UNC-96 link to UNC-15 (paramyosin), and CSN-5. (b) Protein complexes at dense bodies in *C. elegans* body-wall muscle. The same 4 protein complex [UNC-112, PAT-4, PAT-6, UNC-97] is associated with the cytoplasmic tail of PAT-3. Two proteins, UIG-1 (a Cdc42 GEF) and PXL-1

(paxillin) link the 4 protein complex and UNC-95 to two dense body structural proteins, Ce Talin and DEB-1 (vinculin) which presumably link to actin thin filaments (H. Qadota and G. Benian, unpub. data; A. Warner and D. Moerman, pers. comm.). Additionally, UIG-1 links to and is phosphorylated by the kinase domain of the giant protein TTN-1 (D. Greene, H. Qadota, G. Benian, unpub. data).

Chapter 2

unc-94 Encodes a Tropomodulin in *Caenorhabditis elegans*

The contents of this chapter were published in Stevenson et al., J of Mol. Biol., 374: October, 10 2007.

Introduction

Sarcomeres are specialized actin cytoskeletal structures that perform the work of muscle contraction. Sarcomeres are molecular or "nano"-machines consisting of a highly ordered assemblage of many proteins. Despite ever increasing knowledge of the components and functions of sarcomeric proteins, we still do not have a clear picture about how sarcomeres are assembled, and how sarcomeres are maintained in the face of repeated muscle activity. The ability to analyze mutants in the nematode *C. elegans* is being exploited to obtain insights into these questions (Waterston, 1988; Moerman and Fire, 1997; Moerman and Williams, 2006). Molecular genetic experiments using *C. elegans* complement the typical biochemical analyses that are carried out in mammalian systems. The major striated muscle in the worm lies in the body-wall and is used for locomotion. In adults, there are 95 spindle shaped cells that are divided among four quadrants, which lie just underneath a basement membrane, hypodermis and cuticle. Due to the optical transparency of the worm, the myofibrils can be viewed by polarized light, which reveals obvious striations. Bright A-bands alternate with dark I-bands, and each I-band contains a row of dense bodies, which are the analogs of Z-disks of vertebrate striated muscle. Because the striations lie at a slightly oblique angle with respect to the long axis of the worm, this muscle is "obliquely striated." Rather than filling the entire cell as is the case for vertebrate striated muscle, in *C. elegans* body-wall muscle, the myofibrils are restricted to a narrow zone of ~1.5 microns along one side of the cell. All the M-lines and Z-disks are attached to the muscle cell membrane, making these

structures good models for studying muscle costameres (Miller et al., 2006) and focal adhesions of non-muscle cells (Moerman and Williams, 2006).

C. elegans has been used profitably to obtain mutants defective in the formation, function and/or structure of muscle. There are two major classes of muscle-affecting mutations. In one class, the uncoordinated or "Unc" class, the worms develop into adults but are slow moving or paralyzed (Brenner, 1974; Waterston et al., 1980; Zengel and Epstein, 1980) (The second class, the "Pat" class of mutants (*p*aralyzed *a*rrested at *t*wo-fold) display a characteristic embryonic lethality in which embryos do not move within the eggshell and stop development at the twofold stage (Williams and Waterston, 1994). A few genes have both hypomorphic Unc and null Pat phenotypes; examples include *unc-112* (Rogalski et al., 200) and *unc-45* (Barral et al., 1998). To date, nearly all the muscle Unc and many of the Pat genes have been cloned and studied at the molecular level. The encoded proteins include both previously known and novel components of the thick and thin filaments and their organizing and membrane attachment structures (M-lines and dense bodies). The cloning of M-line and dense body components has revealed a number of familiar components of focal adhesions (perlecan, integrins, vinculin, integrin linked kinase, PINCH), but has also revealed new components of these structures (UNC-112, UNC-98, UNC-96 and UNC-89) (Moerman and Williams, 2006; Mercer et al., 2006). This analysis is consistent with a model in which myofibril assembly is directed by signals first laid down in the ECM and the muscle cell membrane. In addition, most of the components of dense bodies and M-lines are shared, except for the proteins involved in the later stages of assembly; for example, for the dense bodies, vinculin and α-actinin, and for the M-lines, UNC-89.

For thick filaments, the expected genes for the myosins and paramyosin were among the first worm muscle genes identified. New and evolutionarily conserved components of thick filaments were first revealed by this genetic analysis. One example is twitchin, the founding member of the giant kinases which include mammalian titin and insect projectin (Moerman et al., 1988; Benian et al., 1989; Benian et al., 1993). Another example is UNC-45, which is a conserved chaperone for myosin head folding and for the assembly of myosin into thick filaments (Barral et al., 1998; Barral et al., 2002). For thin filaments, genes encoding the actins and the troponin-tropomyosin complex have been found. In addition, novel components have been identified (e.g. UNC-87) (Goetinck and Waterston, 1994), and roles in myofibril assembly were first revealed for several previously known proteins. There are many actin binding proteins, many of which regulate actin filament dynamics in many eukaryotic cells. This includes proteins that promote actin polymerization (e.g. profilin), severing (e.g. gelsolins, ADF/cofilin), stability (e.g. tropomyosin), depolymerization (e.g. ADF/cofilin), barbed end capping (e.g. capZ) or pointed end capping (e.g. tropomodulin). Molecular genetic analysis of UNC-60B (an ADF/cofilin protein) (McKim et al., 1994; Ono et al., 1999), tropomyosin (Ono and Ono, 2002) and UNC-78 (Ono, 2001; Mohri and Ono, 2003), has clearly demonstrated the requirement for regulating actin filament dynamics to ensure proper assembly and maintenance of muscle thin filaments.

In 1980, Zengel and Epstein reported results of a screen for mutants with altered body-wall muscle structure (Zengel and Epstein, 1980). Their screen involved enrichment for slow moving worms, followed by assessment by polarized light microscopy. Mutants represented new alleles of 10 previously identified genes (Brenner, 1974; Waterston et al.,

1980) and 7 new genes. Among them was a single mutant allele for a new gene, *unc-94*. *unc-94 (su177)* was described as slow moving and by polarized light to have "irregular birefringent areas". EM showed large collections of thin filaments interspersed with possible intermediate filaments and patches of thick filaments. Here, we report that *unc-94* encodes a tropomodulin, an F-actin pointed-end capping protein. Our results show the expected localization of a tropomodulin in the sarcomere of another animal, its in vivo importance, and point to a new role for tropomodulin in regulating F-actin at muscle cell-cell boundaries.

Results

As is the case for most muscle Unc mutants, *unc-94(su177)* displays a less organized myofilament lattice as compared to wild type (Fig. 2.1a). There is alternation between normal and increased width of individual birefringent bands. To gain further understanding about the *unc-94* mutant phenotype, we sought to identify additional *unc-94* mutant alleles. By an F1 non-complementation screen, we recovered a new allele, *sf20*. As shown in Fig. 1a, *sf20* has the same polarized light phenotype as *su177*. Neither allele shows any obvious defects by polarized light in the organization of pharyngeal muscle (data not shown). There were no marked differences in pharyngeal pumping on plates seeded with bacteria between wild type and either of the two mutant alleles (data not shown).

Each *unc-94* allele moves more slowly than wild type when viewed by the dissecting microscope. To quantitate this difference, we placed a worm in liquid and counted the number of times the "head" moved away from and returned to an imaginary starting point. This swimming assay was conducted on both L4 larvae and adults because for many muscle Uncs, motility is most compromised in adults. As shown in Fig. 2.1b, both *su177* and *sf20* animals have significantly reduced motility as compared to wild type. A worsening in adults was not observed. Because many components of body-wall muscle are also expressed in muscles required for egg laying (e.g. vulval and uterine muscles), we hypothesized that egg laying ability might be affected in *unc-94* animals. This indeed is the case. Brood size measurements (Fig. 2.1c) show that both *su177* and *sf20* lay many fewer eggs as compared to wild type. In fact, *sf20* is more severe than *su177* by this assay,

consistent with the fact that Western blot analysis of *sf20* worm extracts failed to detect UNC-94 gene products (Figure 2.7).

To further characterize the structural defect in adult *unc-94* mutant muscle, immunofluorescence microscopy was used to visualize the localization of a number of known sarcomeric proteins. These proteins included F-actin, myosin heavy chain A (MHC A), UNC-89 as a marker for M-lines, and α-actinin as a marker for dense bodies. As shown in Fig. 2.2, each of these proteins shows some degree of mislocalization. The severity of the mislocalization appears similar in the two mutant alleles, *su177* and *sf20*. As revealed by MHC A staining, the thick filaments appear discontinuous and at places perhaps broken. UNC-89 staining suggests that M-lines are also somewhat disorganized; the M-lines appear rather wavy and of variable width. α-actinin staining shows that the dense bodies are not as well defined and not arranged in as regular a pattern of rows as in wild type. However, the most dramatic effect is on the localization of F-actin as revealed by phalloidin staining. In either *unc-94 (su177)* or *sf20*, there is abnormal accumulation of F-actin near muscle cell-to-cell boundaries, and yet in most other areas of the myofilament lattice, F-actin localization and I-band organization appear normal. Significantly, in both *unc-94* mutants, including the stronger allele *sf20* (which has no detectable UNC-94 proteins by Western blot), there are still gaps (H-zones) between the I bands.

As an additional approach for understanding the role of *unc-94* in myofibril organization, we examined the new *unc-94* mutant allele *sf20* by electron microscopy. Figure 2.3 shows cross sections of wild type and *unc-94(sf20)* body-wall muscle, in each case, showing the broad part of one muscle cell, and an adjacent thin process of a

neighboring cell (indicated with brackets). In wild type, the individual sarcomeres have well organized A-bands of thick filaments centered about M-lines, and I-bands of thin filaments centered about dense bodies. In *unc-94(sf20)*, the sarcomeres are clearly disorganized, especially having irregular (short, thin and jagged) dense bodies and a lack of M-lines; the muscle cell process is dilated and contains a higher ratio of thin to thick filaments than wild type. In other sections of *sf20* muscle, near cell-cell boundaries, there are large accumulations of what appear to be thin filaments without associated thick filaments (see Supplementary Figure 2.1).

After having characterized the phenotype of *unc-94* mutants, a combination of deficiency and SNP mapping was used to determine where in the *C. elegans* genome *unc-94* resides (Fig. 2.4). Initial studies[7] of *unc-94* mapped the gene to a location on chromosome I, between *dpy-5* and *unc-13* (2.03 map units and 2MB apart). Therefore, this region of the genetic map was inspected for deficiencies, but only one deficiency was available, *qDf16*. When animals containing this deficiency were mated with *su177* animals, all of the out-crossed F1 progeny showed wild-type organization of body-wall muscle by polarized light. From this result, it was concluded that the area which is deleted in this particular deficiency does not uncover the location of *unc-94*. SNP mapping was employed to limit *unc-94*'s position to a 500kb region, between (and including) cosmids F26B1 and C06A5, which contains a set of twelve overlapping cosmids. The left and right boundaries of this region agree with the results of the deficiency mapping, because this 500kb region was not deleted in *qDf16*. After scanning the 500 kb region for muscle expressed genes, a gene encoding a tropomodulin was identified, *tmd-1*(C06A5.7*)*. Inspection of WormBase revealed that there are two

predicted isoforms for C06A5.7 called a and b, each one containing 10 coding exons. Sequencing of cDNA clones confirms these predicted splicing patterns. Conceptual translation indicates that TMD-1a is 392 residues (calculated molecular weight of 44,399) and TMD-1b is 401 residues (molecular weight of 45,536). Isoforms *a* and *b* differ in their first and third exons: exon 1 of *tmd-1a* encodes 7 amino acids, and exon 1 of *tmd-1b* encodes 19 amino acids, with no obvious sequence similarity. Exon 3 of isoform *a* encodes an extra 3 residues at its 5' end, which is not present in isoform *b*. The only notable feature of the N-terminal 19 residues of TMD-1b is that it contains a segment of 4 consecutive prolines.

To determine if *unc-94* was truly *tmd-1*, several experiments were performed. First, RNAi by feeding was used to knock down *tmd-1* (C06A5.7) in wild type animals. As shown in Figure 2.1, C06A5.7 RNAi phenocopies Unc-94 by polarized light. Next, we injected *su177* animals with C06A5 cosmid DNA to test whether the cosmid could rescue the Unc-94 phenotype when it is carried by the animals as an extrachromosomal array. The last panel of Figure 2.1a shows that CO6A5 rescues the unorganized patterning of A and I-bands to that of wild type. To gain additional evidence that *unc-94* is *tmd-1,* we sequenced *tmd-1* protein coding regions from genomic DNA of *su177* and *sf20*. The *su177* allele is a G-to-A transition in the splice donor site of the first intron, specific for isoform a (Figure 2.4). In contrast, the *sf20* allele is a nonsense mutation in exon 5 which is shared by both *tmd-1* isoforms; it is a C-to-T transition which converts glutamine 184 of isoform a and glutamine 193 of isoform b to the stop codon UAA. Since *unc-94* mutants were isolated before the sequence-based identification of *tmd-1*, we refer to the gene, henceforth, as *unc-94*.

Given that there are two predicted isoforms for *unc-94*, which differ primarily in their first exons, we sought to determine whether their expression patterns were different. Promoter-GFP plasmids were created that contained the putative promoter regions and first exons fused in-frame to GFP (Figure 2.5). Animals carrying transgenic arrays of these plasmids were examined to determine where the promoters were expressed by the presence of GFP signal. As shown in Figure 2.5, *unc-94a* is expressed in body-wall muscle (Figure 2.5 a and c), but not in pharyngeal muscle (Figure 2.5b), and is also expressed in vulval and uterine muscles (Figure 2.5d). *unc-94b* is not expressed in body-wall muscle (Figure 2.5e), but is expressed in pharyngeal muscle (Figure 2.5f) and the vulval and uterine muscles (Figure 2.5g; arrowhead). In addition, *unc-94b* is expressed in a number of other tissues including spermatheca (Figure 2.5g, arrows), gut epithelial cells (Figure 2.5g, asterisks), and anal depressor muscle (Figure 2.5h; arrow). In summary, *unc-94a* but not *unc-94b* is expressed in body-wall muscle, whereas b but not a is expressed in pharyngeal and anal depressor muscles. Both isoforms are expressed in vulval and uterine muscles.

To gain further understanding into how the mutations in *su177* and *sf20* result in phenotypes, we performed Northern analysis. Equal amounts of total RNA from wild type and the two *unc-94* mutants were separated on a gel, transferred to a membrane and hybridized with: (1) a probe consisting of most of exons 2 through 4 and expected to detect both unc-94a and unc-94b transcripts; (2) a probe consisting of the unc-94a-specific first exon (mostly 5' UTR); and (3) a probe for detecting the *unc-15* (paramyosin) mRNA to verify that equal amounts of RNA were indeed loaded. (The short unc-94b-specific sequence (mostly 5'UTR of 90 bp) precluded preparation of a

convenient isoform b-specific probe.) As shown in Figure 2.6, each *unc-94* probe detects from wild type and the mutants a fairly broad band measured to be approximately 2 kb. cDNA analysis indicates that unc-94a transcript is 2, 135 nucleotides, and that the unc-94b transcript is 1,927 nucleotides. Since the sizes of these mRNAs may be too close to be resolvable on a gel, the observed 2 kb broad band is close to what was expected. Significantly, both *unc-94* mutant alleles show decreased levels of unc-94a transcripts. The decreased level of unc-94a mRNA in *su177* might result from reduced efficiency of splicing of the entire unc-94a transcript, since the *su177* mutation lies in the splice donor site of the first intron. In *sf20,* the decreased level of unc-94a and possibly unc-94b transcripts likely results from the premature stop codon in *sf20* targeting the messages for degradation by the nonsense mediated decay system (Pulak and Anderson, 1993).

Affinity-purified rabbit antibodies generated to residues 144-401 of UNC-94b/TMD-1b (Cox et al., 2007) were used in immunoblot and immunofluorescent experiments. As shown in Figure 2.7, these antibodies react primarily to a band of ~45 kD and two faint bands just slightly above and below it; there are also two moderate intensity bands of ~60 and ~75 kD. Based on the absence of these ~45 kD bands in *unc-94(sf20)* and *unc-94(RNAi)* animals, it is very likely that these proteins are the products of *unc-94*. These bands are also consistent with the predicted sizes of UNC-94 isoforms from sequence analysis. Even after an overnight exposure of the Western blot, no detectable ~45 kD bands could be detected from *sf20*. *unc-94(su177)* shows decreased intensity of the 45 kD bands: the faint upper band (presumably isoform b, predicted to be 45,536 Da) is missing, and the main band (presumably isoform a, predicted to be 44,399 Da) is reduced. This result is unexpected given the fact that the mutation in *su177* lies in

an isoform a-specific exon. Perhaps the a and b isoforms run anomalously on a gel, or isoform a is post-translationally modified, causing it to migrate at a higher than expected position. At present, the identity of the 60 and 75 kD bands are unknown. The *C. elegans* genome has a second tropomodulin encoding gene called *tmd-2*. The region of TMD-1b used as immunogen does have some similarity (32% identity, 55% similarity) to both TMD-2a (35.5 kD) and TMD-2b (73 kD) so there is the potential for cross-reactivity. Thus, the band detected on the Western at ~75 kD is possibly TMD-2b. We performed RNAi for *tmd-2* using the Ahringer library feeding clone, but we did not detect a phenotype or a change in the Western blot pattern using this anti-UNC-94 antibody as compared to wild type (data not shown).

The same antibodies were used to localize UNC-94 in worm body-wall muscle. Separate batches of adult wild type worms were fixed using either the Nonet method (Nonet et al., 1993) (Figure 2.8a, b) or the Finney and Ruvkun method (Finney and Ruvkun, 1990) (Figure 2.8c, d, e). Anti-UNC-94 was co-incubated with either marker antibodies to dense bodies (α-actinin) or M-lines (UNC-89). As shown in Figure 2.8a, using the Nonet method of fixation, UNC-94 localizes as two closely spaced parallel lines flanking the M-lines. This localization is in the I-bands, but not within the row of dense bodies where the barbed ends of the thin filaments are located (Figure 2.8b). Thus, our localization is consistent with the known localization of tropomodulins in striated muscle of other animals, in which tropomodulins are located at the pointed or minus ends of thin filaments (see model of worm body-wall muscle and UNC-94 localization in Figure 2.8f). Figure 2.8c shows anti-UNC-94 staining of worms fixed by the most commonly used method of fixation (Finney and Ruvkun, 1990). These images reveal broad I-band

localization with no hint of the two closely spaced bands as seen in Figure 2.8a and b. A possible explanation is that the structures to which UNC-94 is associated (pointed ends of thin filaments) are fragile and may require rapid fixation not achievable by the Finney and Ruvkun procedure.

Because of the possible cross reactivity between the anti-UNC-94 antibodies and the related protein, TMD-2 (see Figure 2.7), we wondered if some of the staining of these antibodies in body-wall muscle was due to the presence of TMD-2. However, as shown in Figure 2.8d, this is likely not the case since *unc-94 (sf20),* which shows no detectable UNC-94 proteins by Western blot, also does not show any detectable staining with the antibody. Thus, this suggests that all the protein detected in body-wall muscle is due to UNC-94, and given results of our promoter analysis, specifically, UNC-94a. A lower magnification view (Figure 2.8e) of UNC-94 and α-actinin staining reveals that UNC-94 extends beyond the rows of dense bodies (white arrows), probably at muscle cell to cell boundaries. This enrichment of UNC-94 near cell to cell boundaries might explain the accumulation of actin filaments near cell boundaries in *unc-94* loss of function mutants as revealed by phalloidin staining and EM (Figures 2.2 and 2.3, respectively).

Figures

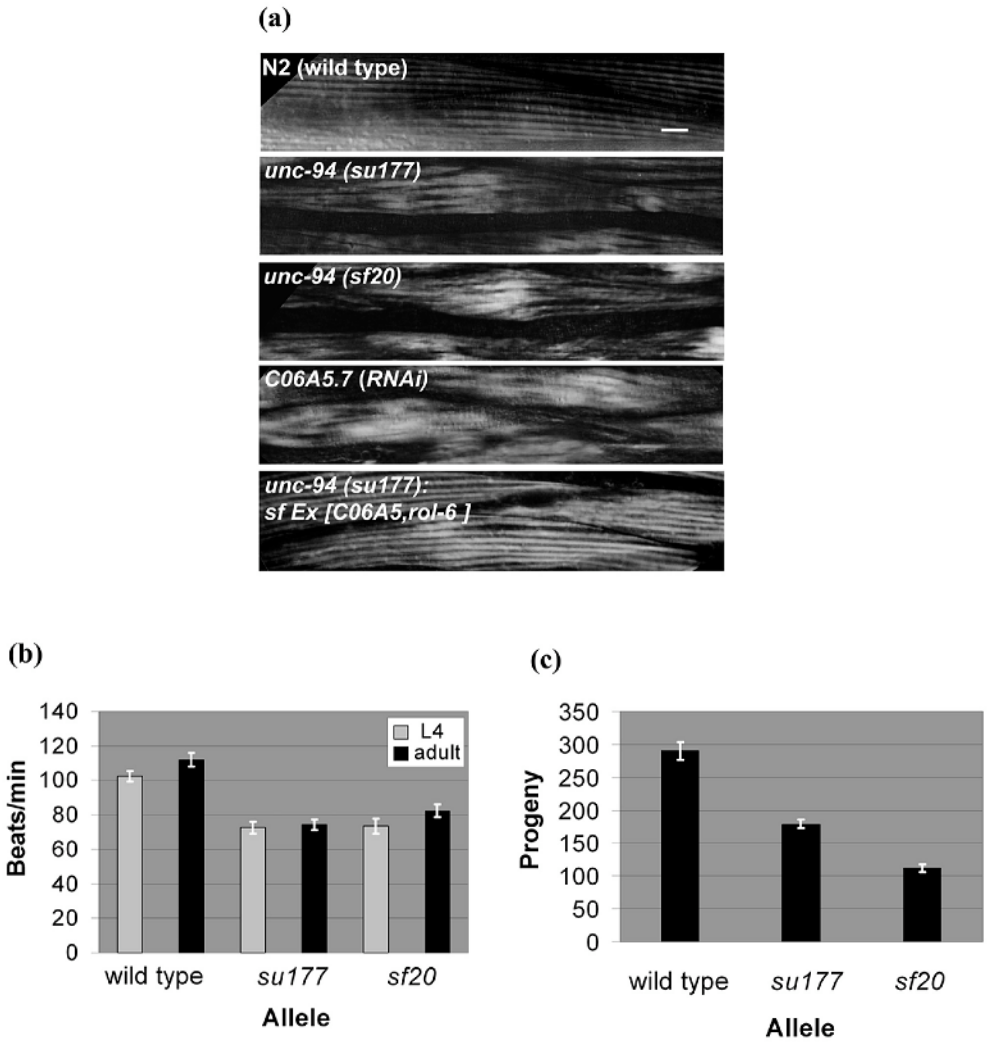

Figure 2.1. ***unc-94*** **mutants show disorganized muscle structure, decreased motility and low brood size**. (a) Polarized light microscopy of body-wall muscle in adult worms. In wild type muscle there is a normal arrangement of alternating birefringent A-bands with dark I-bands that run parallel to the long axis of the worm. In the muscle of worms expressing the two mutant alleles and C06A5.7 (RNAi) animals, there is reduced

organization with alternation between normal and increased width of individual birefringent bands. The mutant phenotype can be rescued in *unc-94* transgenic animals that carry an extrachromosomal array of the cosmid C06A5. Scale bar represents 10 μm. (b) Liquid motility assays of wild type and *unc-94* animals at the 4th larval (L4) and adult stages of development. Data are shown as means and SEMs, with n=30. Both mutant alleles show reduced motility as compared to wild type. (c) Brood size assay comparing the amount of eggs laid by wild type animals and the *unc-94* mutants. As shown, a normal N2 animal can lay between 200-300 eggs. Both *unc-94* mutants show a significant decrease in their brood sizes, with *su177* laying about 40% fewer eggs and *sf20* laying 60% fewer eggs than wild type animals.

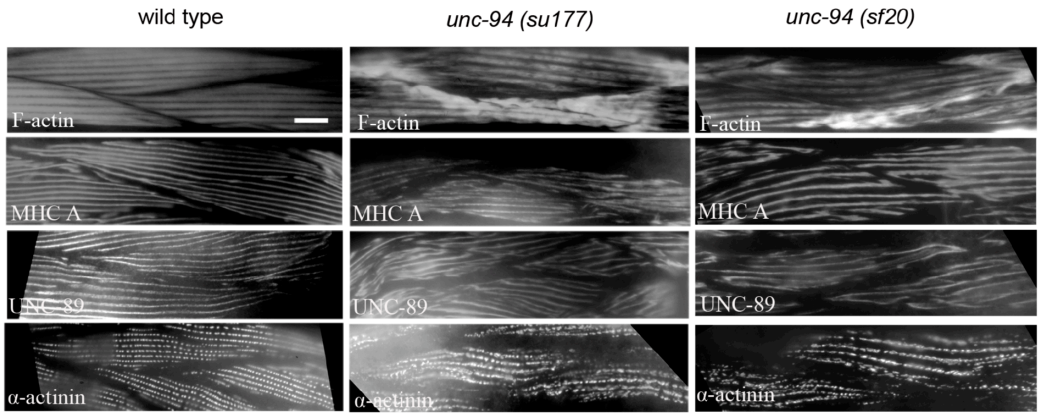

Figure 2.2 Immunofluorescent localization of several known sarcomeric proteins in wild type and *unc-94* mutant muscle. Antibodies were used to detect MHC A (thick filaments), F-actin (thin filaments), UNC-89 (M-lines), and α-actinin (dense bodies). Each of these proteins shows some degree of mislocalization, in a similar way for both mutant alleles. The most dramatic effect is on the localization of F-actin, with abnormal accumulation near muscle cell-to-cell boundaries; in most other areas of the cell, I-band organization appears normal. Scale bar represents 10 μm.

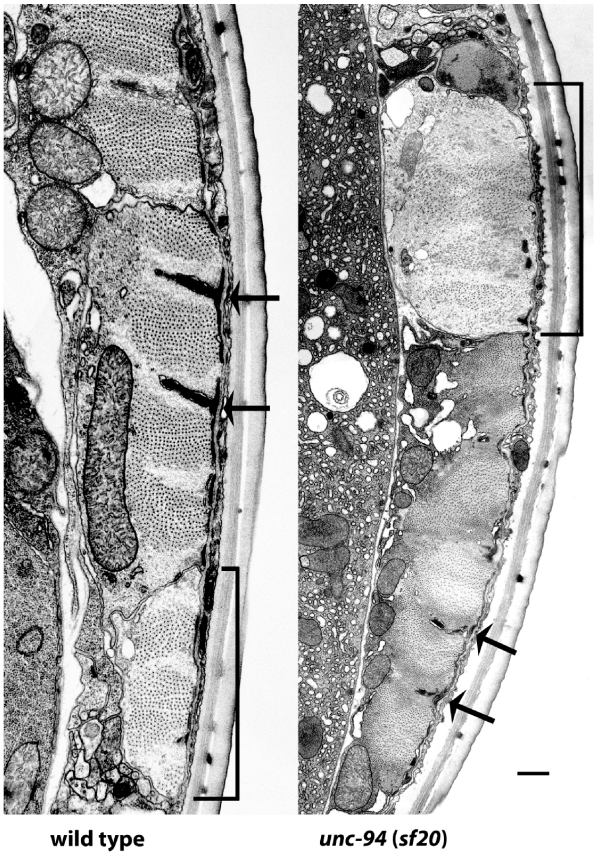

Figure 2.3 E**lectron micrographs of body-wall muscle from wild type and from *unc-94(sf20)***. These low power electron micrographs show most of one muscle cell next to a muscle cell process (indicated with a bracket), cut in transverse section. Thick filaments appear as large dots; thin filaments appear as barely discernible thin dots, most prominent around dense bodies. Dense bodies are indicated with arrows. In wild type highly ordered sarcomeres are present, with thin filaments in normal positions, either in I-bands, surrounding dense bodies, or in A-bands associated with thick filaments. Note that in *sf20*, the muscle cell process is dilated and contains a higher ratio of thin to thick filaments than wild type; also, a small amount of dense body material is found close to the cell membrane. In the adjacent muscle cell, sarcomere organization is better, but dense bodies are irregular. Scale bar, 500 nm.

(a)

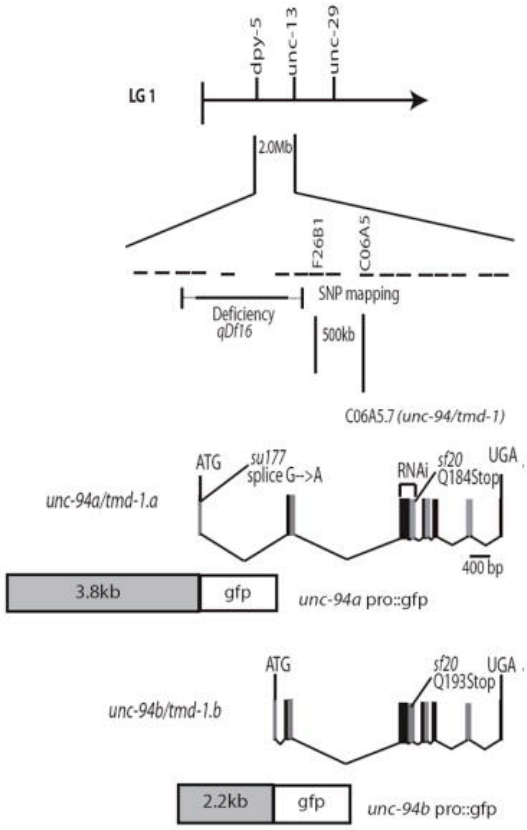
dpy-5
unc-13
unc-29
LG 1
2.0Mb
F26B1
C06A5
SNP mapping
Deficiency
qDf16
500kb
C06A5.7 (unc-94/tmd-1)
ATG
su177
splice G-->A
RNAi
sf20
Q184Stop
UGA
unc-94a/tmd-1.a
400 bp
3.8kb
gfp
unc-94a pro::gfp
ATG
sf20
Q193Stop
UGA
unc-94b/tmd-1.b
2.2kb
gfp
unc-94b pro::gfp

(b)


stop
(sf20)

Figure 2.4 Genetic **and physical mapping of *unc-94*, location of mutation sites for *su177* and *sf20,* and the sequences of UNC-94a and b**. (a) By using a combination of deficiency and SNP mapping, *unc-94* was placed within a 500 kb region between/within cosmids F26B1 and C06A5. (Each dashed line represents the span of one cosmid insert.) After scanning the region for candidate genes, cosmid C06A5 was injected into *unc-94* (*su177*) animals and was able to rescue the Unc-94 mutant phenotype. When *rrf-3* animals were fed dsRNA for C06A5.7, their progeny showed a polarized light phenotype similar to that of *unc-94* (*su177 and sf20*). As shown, WormBase predicts two isoforms for C06A5.7, a and b. In the figure, for clarity consecutive exons are represented as black or grey boxes. After having sequenced both *unc-94* alleles, it was noted that *su177* contains a splice site mutation in the first intron for isoform a, while *sf20* contains a nonsense mutation in the fifth exon, which is shared among the two isoforms. Putative promoter regions plus the first exon of each isoform were used to create promoter-gfp fusions in order to analyze expression patterns. (b) Alignment of UNC-94 a and b protein sequences. The UNC-94 proteins are identical except in two places: (1) at their N-termini because of different first exons, and (2) beginning at residue 39 of UNC-94a which has an additional 3 residues (DLE) not found in UNC-94b because the 5' end of exon 3 in UNC-94a is 9 bp earlier than in UNC-94b. Indicated is the mutation site of *sf20*: it is a C-to-T transition which converts glutamine 184 of isoform a (and glutamine 193 of isoform b) to a stop codon (CAA to TAA). The horizontal black lines indicate a putative tropomyosin-binding domain in the amino-terminal half, and a putative actin-binding domain in the carboxy-terminal half of each protein.

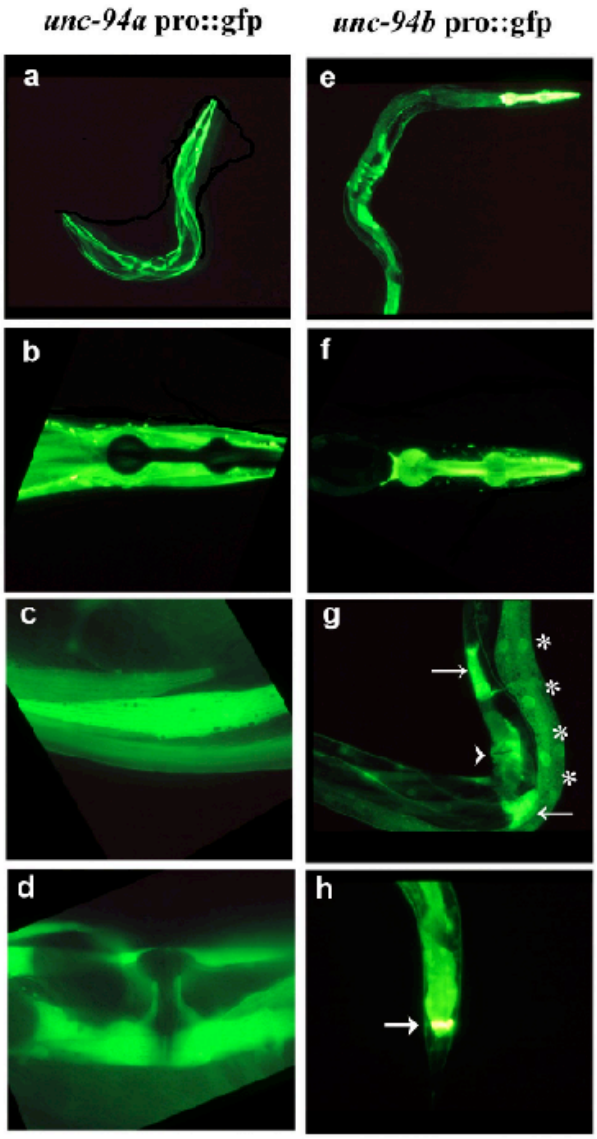

Figure 2.5 Fluorescent images of GFP expression in transgenic animals that carry *unc-94* promoter elements. (a-d) Isoform a is primarily expressed in body-wall (a and c), uterine and vulva muscle (d). As shown in (b), isoform a is not expressed in pharyngeal muscle. (e-h) Isoform b is highly expressed in the pharynx (e and f) and anal depressor muscles (h) and can also be detected in the muscle of the vulva and uterus (arrowhead), spermatheca (arrows), and intestinal epithelial cells (asterisks) (g).

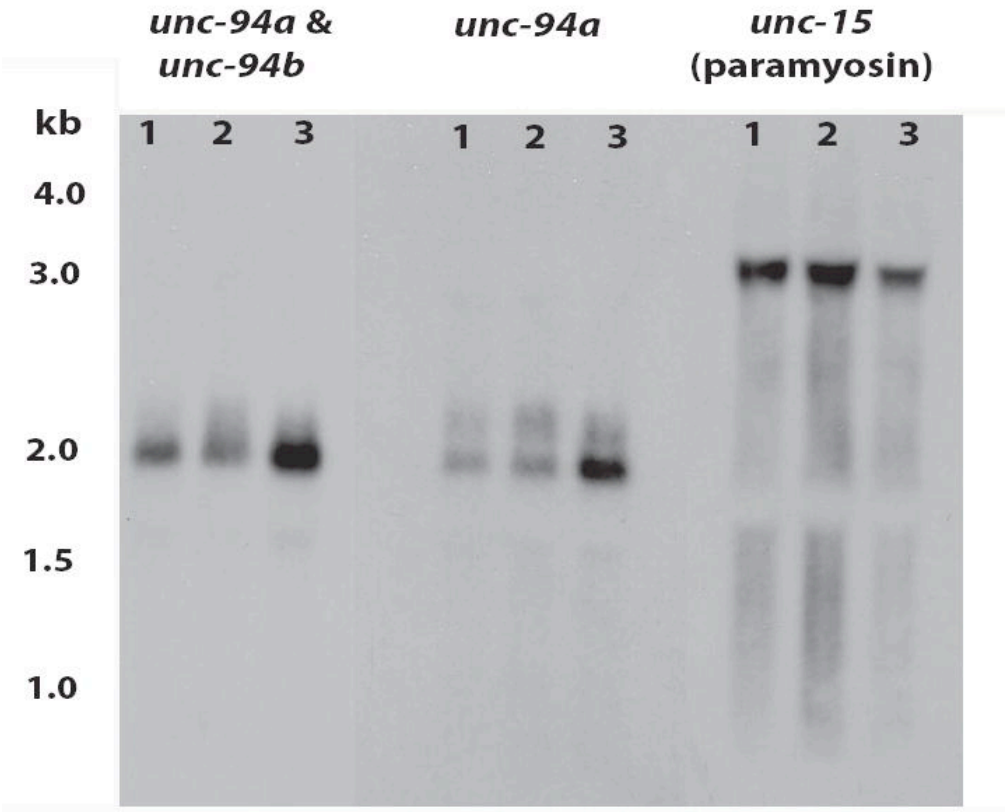

Figure 2.6 By Northern blot, *unc-94* mutations result in decreased levels of *unc-94* mRNAs. Total RNA from wild type (3), *unc-94(sf20)* (2)*, and unc-94(su177)* (1) mutant worms were separated on a gel, transferred to a membrane and hybridized with probes that were expected to detect both *unc-94a* and *unc-94b*, *unc-94a* alone, or *unc-15* transcripts (as loading control). Each *unc-94* probe detects a broad band of approximately 2 kb, close to the size expected for *unc-94a* (2,135 nucleotides) and *unc-94b* (1,927 nucleotides) by cDNA analysis. Note that the *unc-94a* mRNA is decreased in both *su177* and *sf20*. The numbers denote the sizes, in kilobase pairs, of the RNA markers.

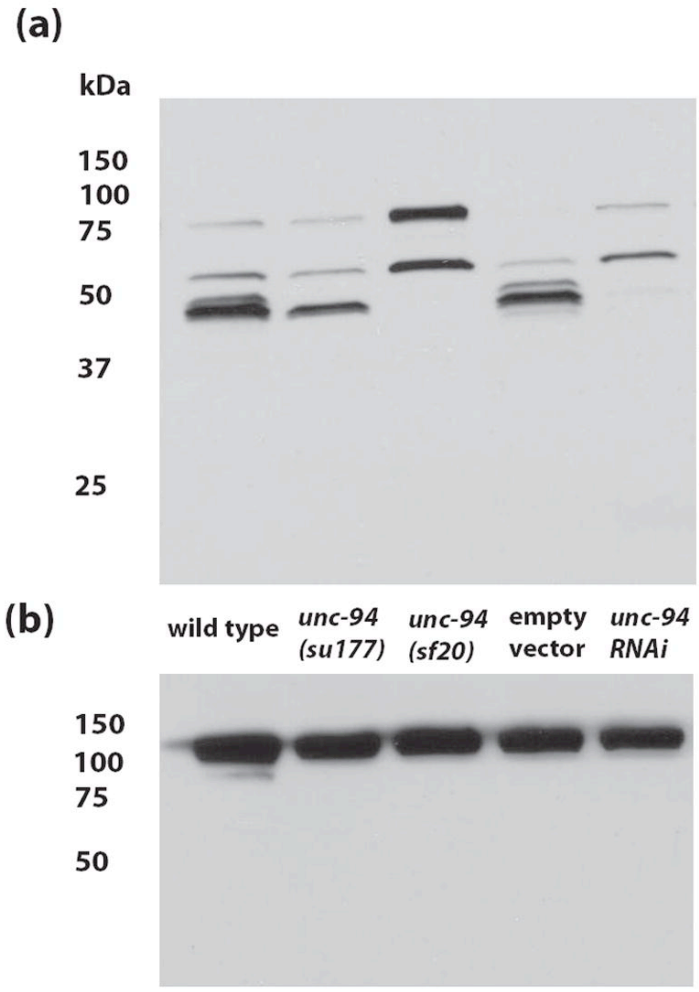

Figure 2.7 By Western blotting, UNC-94 polypeptides can be detected from wild-type, but are absent from or in reduced amounts in *unc-94* mutants or RNAi animals. (a) Affinity-purified anti-UNC-94 antibodies detect proteins of the expected size (~45 kDa) for the products of the *unc-94* gene from wild type *C. elegans*. Note that these bands are absent from *unc-94(sf20)* and *unc-94(RNAi)* animals ("empty vector" refers to the use of the RNAi feeding vector without insert). (b) The same blot was washed and then reacted with anti-paramyosin to demonstrate equal loading of total protein in each lane. The columns of numbers and their positions represent molecular mass markers in kilodaltons.

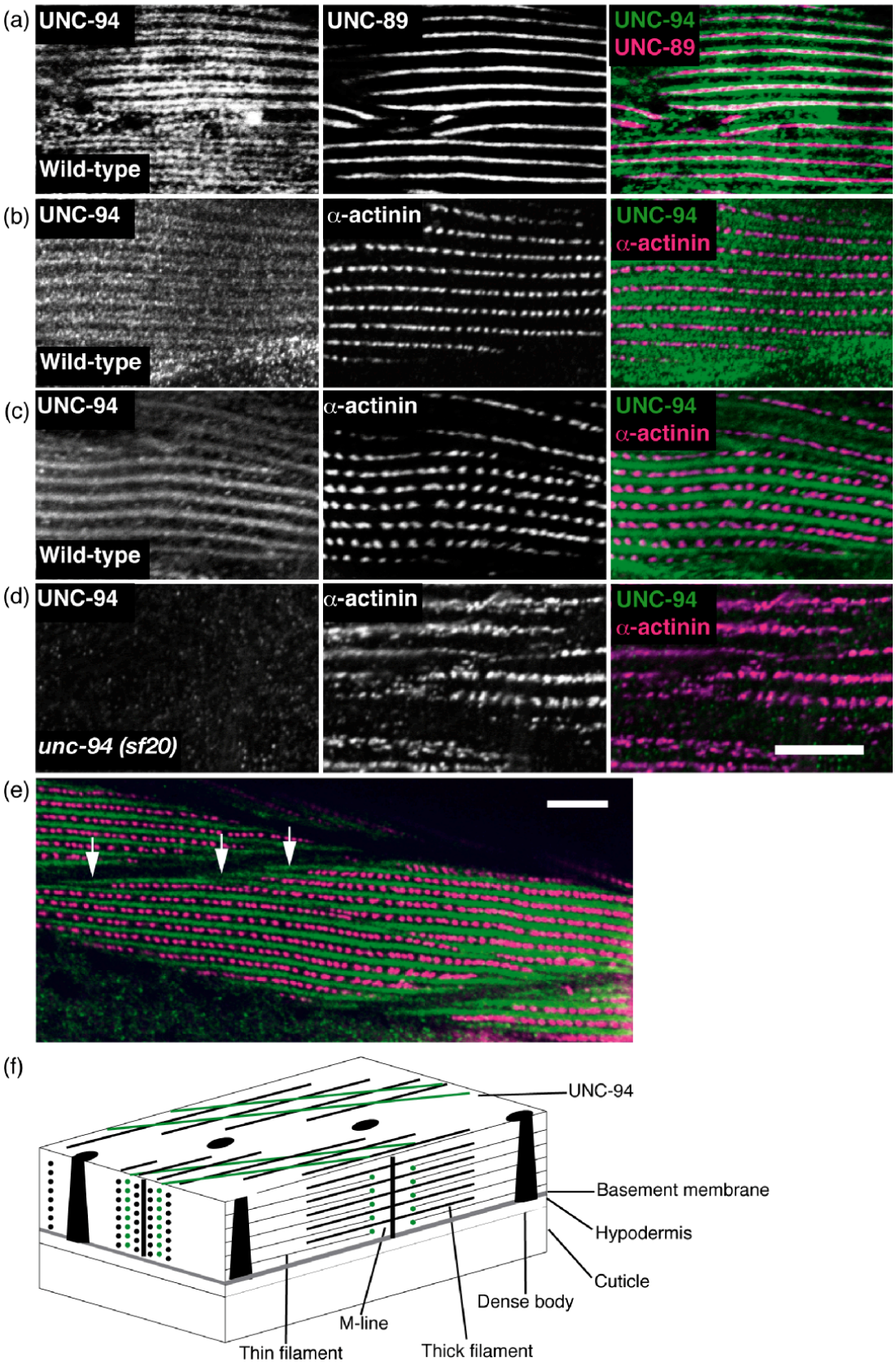
(a)
UNC-94
Wild-type
UNC-89
UNC-94
UNC-89
(b)
UNC-94
Wild-type
α-actinin
UNC-94
α-actinin
(c)
UNC-94
Wild-type
α-actinin
UNC-94
α-actinin
(d)
UNC-94
unc-94 (sf20)
α-actinin
UNC-94
α-actinin
(e)
(f)
UNC-94
Basement membrane
Hypodermis
Cuticle
Dense body
M-line
Thin filament
Thick filament

Figure 2.8 By immunofluorescence, UNC-94 localizes to the pointed ends of thin filaments and to muscle cell boundaries. (a and b) Adult wild type worms were fixed by the Nonet method and either co-incubated with anti-UNC-94 and anti-UNC-89 (M-line marker) as shown in (a), or anti-UNC-94 and anti-α-actinin (dense body marker), as shown in (b). UNC-94 is localized to two closely spaced parallel lines closely flanking the M-lines. (c) Adult wild type worms were fixed by the "constant spring" method[25] and co-incubated with anti-UNC-94 and anti-α-actinin. By this method, UNC-94 appears as a broad band, probably due to incomplete fixation. (d) Adult *unc-94(sf20)* worms (also fixed by the constant spring method) were co-incubated with anti-UNC-94 and anti-α-actinin. Note the absence of staining with anti-UNC-94: this suggests that the staining observed in wild type is due to reaction to UNC-94 and not cross reaction to the related protein, TMD-2. (e) The same animals as shown in (c), but at lower magnification. In this view, UNC-94 extends beyond the rows of dense bodies, likely at muscle cell/cell boundaries (white open arrows). (f) Drawing of *C. elegans* obliquely striated body-wall muscle with the localization of UNC-94 (green) to the pointed ends of thin filaments as indicated by this study. The scale bar represents 10μm.

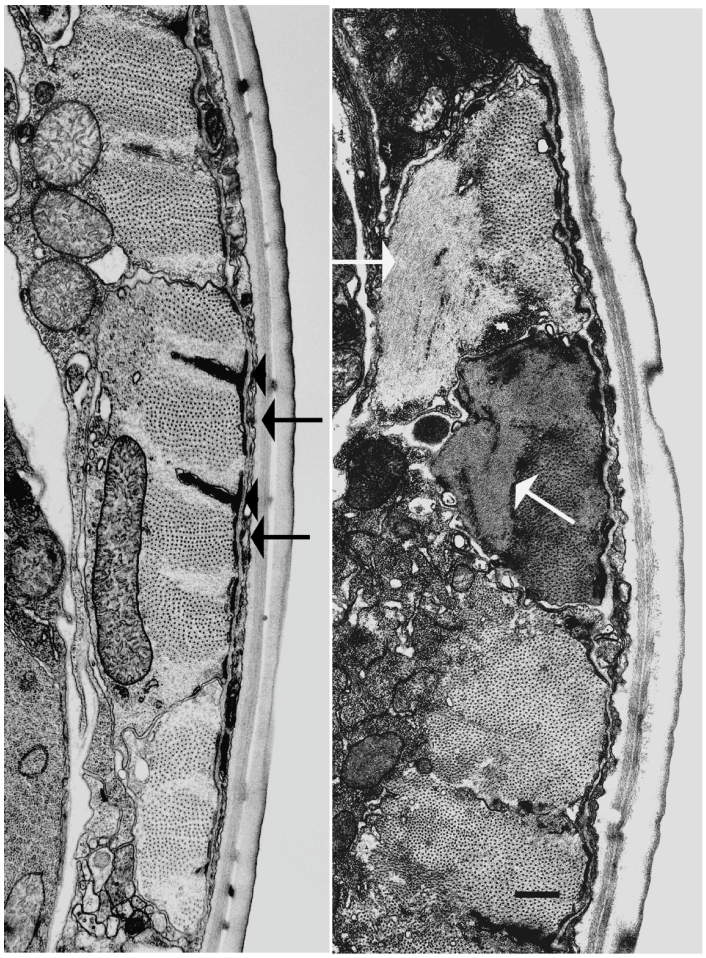

Supplementary Figure 2.1 (2.1S) Electron micrographs of body-wall muscle from wild type and from *unc-94(sf20)*. In these transverse sections, the filaments appear as dots. Arrowheads denote dense bodies and black arrows denote M-lines. In wild type highly ordered sarcomeres are present, with thin filaments in normal positions, either in I-bands, surrounding dense bodies, or in A-bands associated with thick filaments. Note that in *sf20*, there are large accumulations of what appear to be thin filaments without associated attachment structures or thick filaments, at the boundaries of two muscle cells (indicated with white arrows). Note also the presence of several nearly normal sarcomeres with dense bodies and M-lines. Scale bar, 500 nm.

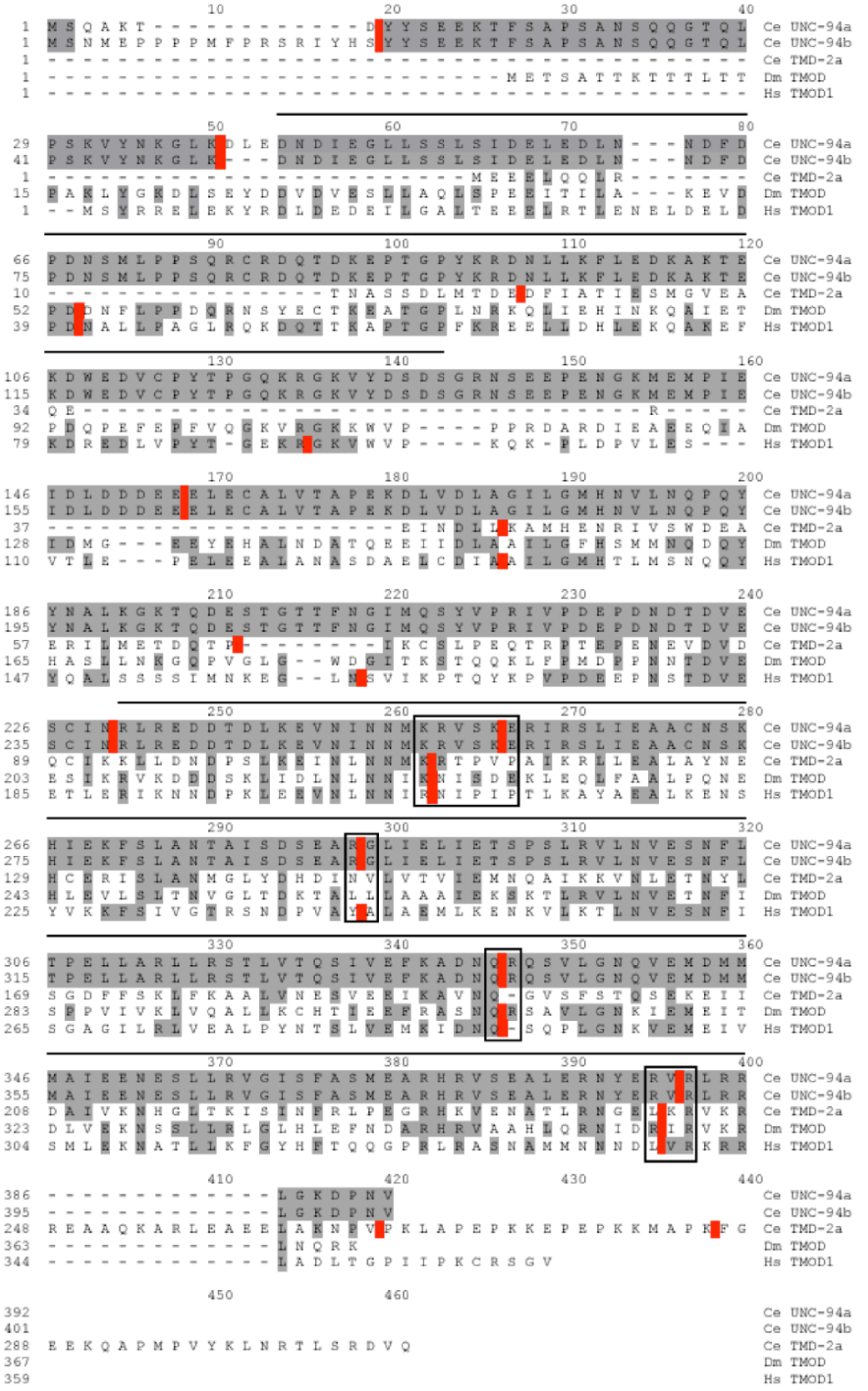
Ce UNC-94a
Ce UNC-94b
Ce TMD-2a
Dm TMOD
Hs TMOD1

Supplementary Figure 2.2 (2.2S) Comparison of tropomodulin sequences from worms, flies and humans. ClustalW alignment of three tropomodulins from *C. elegans* (Ce), and similar proteins from *Drosophila melanogaster* (Dm) and human (Hs). Gray shading indicate residues identical to those in UNC-94 proteins; the horizontal black lines indicate a tropomyosin-binding domain in the amino-terminal half of the alignment, and the actin-binding domain in the carboxy-terminal half of the alignment. Red bars indicate the position of introns in the gene sequences; boxes indicate introns whose positions are conserved.

Discussion

We have shown here that the mutationally identified gene *unc-94* corresponds with the sequence-predicted gene *tmd-1,* which encodes a tropomodulin. This discovery demonstrates yet another level of conservation in sarcomere components between *C. elegans* and mammals. Here we show that mutation in or RNAi against *unc-94* results in reduced organization of myofibrils, abnormal accumulation of F-actin near muscle cell-to-cell boundaries, reduced motility and brood size. In cultured chick cardiomyocytes, immunodepletion of tropomodulin results in abnormally long actin filament bundles and a reduction in the number of beating cells (Gregorio et al., 1995), while overexpression results in shortened actin filaments and myofibril degeneration (Littlefield et al., 2001). These complementary results are believed to be due to the fact that tropomodulin is a pointed end F-actin capping protein (Weber et al., 1994). Our immunofluorescent localization of UNC-94 to two closely spaced parallel lines closely flanking the M-line (Figure 2.8a), is consistent with UNC-94 being located, as expected, at the pointed ends of thin filaments in the middle of the sarcomere (Figure 2.8f). Consistent with our immunolocalization results, *C. elegans* TMD-1 has recently been shown to cap the pointed ends of tropomyosin coated F-actin *in vitro* (Cox et al., 2007). While our sequencing of UNC-94 reveals only 36% sequence identity to the C-terminal actin binding domain of chicken E-Tmod, an overlay of the two structures reveals striking conservation of three dimensional structure with a least squares fit in LSQMAN revealing a root-mean squared deviation between C_a atoms of 1.24 Å (Lu et al., 2004). Furthermore, a docking model of UNC-94 (TMD-1) to actin (Lu et al., 2004) reveals that the five

charged residues involved in charge-charge interaction between chicken E-Tmod and actin (Krieger et al., 2002) are not only conserved in *C. elegans*, but are also predicted to be involved in charge-charge interaction with actin.

In sum, the genetic, phenotypic, sequencing, protein localization and structural data suggest that UNC-94 acts as a pointed end capping protein in the striated muscles of *C. elegans*. Thus, we were surprised to observe that in *unc-94* mutants, including *sf20* which has no detectable UNC-94 proteins by immunoblot (Figure 2.7), there are still H zones, as revealed by phalloidin staining (Figure 2.2). This indicates that the thin filaments are not abnormally long in *unc-94* mutants, and thus although UNC-94 is a tropomodulin located at the pointed ends of thin filaments, it may not be required to regulate thin filament lengths. However, *sf20* may not be a null allele, and it may still produce sufficient UNC-94 proteins to regulate thin filament length. Several alternative explanations are also possible: (1) UNC-94 may be redundant to the second tropomodulin-like protein in *C. elegans* encoded by the separate gene, *tmd-2*. Consistent with this idea, *tmd-2* is expressed in body-wall muscle, based on both an mRNA tagging strategy (Roy et al., 2002) and SAGE data (McKay et al., 2003) in WormBase (http://www.wormbase.org). (2) Even in mammals, whether tropomodulins function to prevent abnormal elongation of thin filaments *in vivo*, is not certain. For example, Tmod1 is the only tropomodulin isoform expressed in heart muscle cells, and cardiomyocytes developing from Tmod1 null embryonic stem cells, have thin filaments of normal length (Ono et al., 2005). Moreover, in mammalian muscle, the giant protein nebulin which interacts with tropomodulin (McElhinny et al., 2001), also has a role in regulating thin filament lengths (McElhinny et al., 2005) Interestingly, *C. elegans* does not appear to

have a full length nebulin protein, but rather has one small protein with several nebulin-like repeats closely related to LASP, called Ce LASP (K. Wang, K. Mercer, G. Benian, unpublished data).

In addition to identifying UNC-94 as a *C. elegans* tropomodulin located at the pointed ends of muscle thin filaments, our data raise a new question about tropomodulin function. We have made two observations that suggest that tropomodulins may have a role in attaching sarcomeres to the muscle cell surface: (1) in *unc-94* mutant animals, there is an abnormal accumulation of actin filaments near muscle cell-to-cell boundaries (Figure 2.2 and Supplementary Figure 2.1), and (2) in wild type muscle, there is localization not only to the pointed ends of thin filaments, but also near muscle cell to cell boundaries (Figure 2.8e). In fact, using the same anti-UNC-94/TMD-1 antibodies, the protein has been shown recently to localize to the cell borders of nematode hypodermal cells, acting functionally with α-catenin (Cox et al., 2007). A role for tropomodulin at cell-cell contacts has previously been proposed for lens fiber cells (a type of epithelial cell) (Lee et al., 2000), and overexpression of Tmod1 in cardiac tissue causes dilated cardiomyopathy and disrupted intercalated disks (a type of intercellular junction) in TOT transgenic mice (Ehler et al., 2001). Tropomodulin may be involved in binding to a muscle attachment complex. A possible mechanism is suggested by the recent finding that tropomyosin is involved in erythrocyte membrane mechanical stability (An et al., 2007). Since, in the erythrocyte cytoskeleton, tropomyosin is bound to actin and tropomodulin, perhaps UNC-94 links actin to the cell membrane via tropomyosin in *C. elegans* muscle. Alternatively, it could be that at muscle cell-to-cell boundaries, in addition to usual roles in binding actin and tropomyosin, UNC-94 interacts with a

different protein with a low affinity. For example, Tmod4 has been shown to bind an intermediate filament protein in lens fiber cells, and this does not block its actin capping activity (Fischer et al., 2003).

By use of promoter-GFP experiments, we have shown that *unc-94* utilizes two promoters that express two very similar proteins in different sets of cells and tissues. Thus, as shown in Figure 2.5, *unc-94a* is expressed in body-wall, vulval and uterine muscle, while *unc-94b* is expressed in pharyngeal, vulval and anal depressor muscles, and the spermatheca and intestinal epithelial cells. Confirmation that native *unc-94a* is expressed in body-wall muscle and is functionally important in that tissue was provided by finding that *unc-94(su177),* which has a body-wall muscle phenotype and no UNC-94 immunostaining (data not shown), is a mutation in intron 1 that is specific for *unc-94a*. Although the differences between the two isoforms at the protein level are minimal, the use of two alternative promoters might have evolved to permit timing and levels of expression finely tuned for the requirements of particular sets of cells or tissues.

In addition to affecting muscle structure and motility, mutations in *unc-94* also affect the total number of progeny laid, (i.e., "brood size"). Both mutant alleles affect brood size. The mutation in *su177* affects only the *unc-94a* isoform, and because this isoform is expressed in vulval and uterine muscles, which are required for egg laying, the reduced brood size is expected. The mutation in *sf20* affects the expression of both isoforms and shows an even further reduction in brood size. This more severe brood size defect could be explained by noting that in addition to being expressed in vulval and uterine muscles, *unc-94b* is also expressed in the spermatheca, the site of fertilization and expulsion of the fertilized egg into the uterus. Alternatively, *sf20* might give a more

severe reduction in brood size because *sf20* is a more severe mutation molecularly than *su177* (premature stop vs. splice site mutation).

Interestingly, the alternative splicing pattern for *unc-94* is similar to that of the *Drosophila melanogaster* tropomodulin gene, which encodes two isoforms through two different promoters and use of two different first exons (Mardahl-Dumesnil and Fowler, 2001). Similar to nematode *unc-94*, the fly tropomodulin gene uses an upstream promoter to express a smaller isoform (367 residues; first exon encodes 2 residues), and a downstream promoter to express a larger isoform (402 residues; first exon encodes 36 residues). In contrast, all vertebrate Tmod genes studied to date do not show alternative splicing (Conley et al., 2001; Conley and Fowler, 2005) (C. Conley, unpublished data). A lack of alternative splicing has also been found for a newly-identified tropomodulin homologue from the hemichordate *Ciona intestinalis* (D. Hoffman and C. Conley, unpublished data).

Alignment of the UNC-94a protein sequence with sequences from the homologous proteins of *Drosophila* and humans (TMOD1) demonstrates that *C. elegans* UNC-94a is 35.2% identical to the *Drosophila* protein and 34.7 % identical to the human protein along the entire alignment (Supplementary Figure 2.2). The three proteins display two large regions of similarity that correspond to the amino-terminal tropomyosin-binding domain and the carboxy-terminal actin-binding domain of the vertebrate tropomodulins, respectively (Conley et al., 2001). The second *C. elegans* tropomodulin gene, *tmd-2*, uses alternative splicing of its 3'-most exons (confirmed by sequencing cDNAs), to encode two isoforms which differ only at their C-termini. The TMD-2a isoform is predicted to be 308 residues long with a 25 residue C-terminal tail,

whereas TMD-2b is 639 residues with a 354 residue C-terminal tail. UNC-94a is only 18.9% identical to TMD-2 (Supplementary Figure 2.2). TMD-2 seems to lack the amino-terminal tropomyosin binding domain and its amino terminal 35 residues are only weakly similar to the amino-terminal regions of the other tropomodulins. One possible reason for the lack of an obvious tropomyosin binding domain is that the N-terminal region of each TMD-2 isoform has not yet been defined. Alternatively, TMD-2 might indeed lack a tropomyosin binding region because it has a different function and localization in the sarcomere. This is suggested by the unusual sequence of the unique C-terminal 354 residues of TMD-2b: (1) It is enriched for the amino acids P, E, V, K and A (total of 55.4%). (2) PFAM predicts a PPAK motif (342-366), which is the 28 residue repeat that comprises the main elastic region of vertebrate titin called the "PEVK region" (Greaser, 2001; Bang et al., 2001; Gutierrez-Cruz et al., 2001). (3) The computer program Radar predicts two copies of another repeat (305-331 and 424-443). Thus, the amino acid composition and presence of short repeating elements, one of which is similar to vertebrate titin, suggest that this region of TMD-2b might be elastic.

Materials and Methods

Strains and Genetics

Two alleles of *unc-94* were employed in this study. The first allele, *su177*, was isolated and described by Zengel and Epstein using a motility and polarized light screen. When we obtained *unc-94* (*su177*) from the Caenorhabditis Genetics Center, it had only been outcrossed three times. These 3x outcrossed animals were used for polarized light, motility, and immunofluorescence experiments. We noticed the same polarized light phenotype in these animals as was reported by Zengel and Epstein. The motility of the animals was about 50% less than the motility of wild type animals and by immunofluorescence we noticed that the structure of all myofibrillar components tested for were compromised. After outcrossing these animals an additional two times (now 5x outcrossed), we repeated the motility assay, and noticed that the motility increased about 20%. The polarized light phenotype did not change; therefore immunofluorescence experiments were not repeated. We recovered the second *unc-94* allele, *sf20*, by using EMS mutagenesis and a polarized light F1 non-complementation screen. This allele was also outcrossed five times and previously mentioned experiments, in addition to brood size measurements, were performed using these animals. *unc-94* (*RNAi*) animals were created by feeding (Kamath and Ahringer, 2003) *rrf-3* animals (Simmer et al., 2002) (which are hypersensitive to RNAi) bacteria expressing double stranded RNA (dsRNA) for C06A5.7.

Polarized light microscopy, motility, brood size measurements, and electron microscopy

The procedures for polarized light microscopy and motility assays were performed as described in Mercer et al (2006). Brood size was determined by taking 10 L4 hermaphrodites (P0) of each allele (wt, *su177* and *sf20*) and putting these animals, individually, onto seeded agar plates. These animals were allowed 24 hours to mature and lay fertilized eggs. After this period, P0 animals were singly transferred to a new plate and were allowed 24 hours to lay more eggs. Laying and transferring were repeated until the P0 animals laid only unfertilized eggs (oocytes). After the P0 animals had been transferred from a plate, that plate, containing F1 larvae and eggs, was kept and the number of F1 progeny was scored by picking/counting individual worms as they were removed from the plate. Electron microscopy of wild type and *unc-94(sf20)* was performed using general methods described by Hall (1995), specifically the "conventional two step fixation" method described at http://www.wormatlas.org/anatmeth/anatmeth.htm.

During the first aldehyde fixation step, the worms were cut in half using a razor blade, to allow better penetration of fixative.

Immunofluorescent localization of antibodies to known myofibril components

The procedure used for immunofluorescent localization in adult muscle was described in Mercer et al (2003). The antibodies and the dilutions that were used for each were as follows: anti-MHC A, 1:400 (Miller et al., 1983); anti-UNC-89, 1:200 (Benian et al., 1996); and anti-α-actinin, 1:200 (Francis and Waterston, 1985). Phalloidin staining of thin filaments was carried out as described by Ono (2001). Images were obtained with a

Zeiss Axioskop microscope using Fuji Sensia 100 slide film and scanned and processed with Adobe Photoshop.

Genetic and physical mapping of *unc-94*, and determination of mutation sites

Zengel and Epstein used three-factor mapping to place *unc-94* between *dpy-5* and *unc-13* on chromosome I (Zengel and Epstein, 1980). To narrow down this 2MB region to a 500kb region (representing 12 overlapping cosmids), we used a combination of deficiency mapping and single nucleotide polymorphism (SNP) mapping (Hill et al., 2000). The Hawaiian strain of *C. elegans* was mated with the triple mutant, *dpy-5 unc-94 unc-13*, producing a number of recombinant animals. Sequencing SNPs of Dpy-5, Unc-94, non-Unc-13 individuals revealed that *unc-94* lies either within or to the left of cosmid F26B1, creating a left breakpoint. After sequencing SNPs of non-Dpy-5 Unc-94 Unc-13 individuals, we were able to create a right breakpoint that included the cosmid C06A5. After scanning the 500kb region for candidate predicted genes on WormBase, we thought a likely candidate for *unc-94* was C06A5.7, which encodes a tropomodulin, a known actin regulatory protein. Thus, the cosmid C06A5 was tested for its ability to rescue the Unc-94 phenotype in transgenic animals. (Cosmid DNA was prepared using a QIAGEN Plasmid Midiprep kit; QIAGEN, Valencia,CA). We were able to detect rescue of the mutant phenotype in five different lines. We performed RNAi, by feeding, in *rrf-3* animals using C06A5.7 (*tmd-1*) clones from the Ahringer library (available through GeneService, Cambridge, United Kingdom). Progeny from worms that were fed double stranded RNA- producing bacteria for C06A5.7 showed an Unc-94 phenotype by polarized light.

To determine mutation sites for both mutant alleles, we prepared genomic DNA from the mutant animals by means of phenol/chloroform extraction. Primers were then designed to amplify genomic regions of all C06A5.7 exons (for both isoforms) and ~100 base pairs of their flanking intronic sequences. For each exon/intron, the primers that were used for PCR amplification were also used for sequencing. Sequences were obtained from both strands.

Analysis of *unc-94*/*tmd-1* and *tmd-2* coding sequences

Plasmids containing cDNAs for the predicted transcripts *unc-94a/tmd-1a*, *unc-94b/tmd-1b*, *tmd-2a*, and *tmd-2b* were obtained from the Kohara lab (Kohara, 1996): yk1262e07, yk786f09, and yk618b4 for *unc-94a/tmd-1a*, yk1191a05, yk1009c10 and yk1056g10 for *unc-94b/tmd-1b*, yk724h2 for *tmd-2a*, and yk569e4 and yk416c2 for *tmd-2b*. Plasmid DNA was then prepared using a QIAGEN Plasmid Miniprep kit (QIAGEN, Valencia, CA) and sequenced (Certigen, Lubbock, Texas) using forward primer pME18F2: TCAGTGGATGTTGCCTTTAC and reverse primer ME-1250RV: TGTGGGAGGTTTTTTCTCTA. To sequence all cDNAs except y724h2 and yk1191a1 Certigen designed internal primers against sequenced portions of the cDNA; the sequence of these primers is available upon request from Certigen. Sequencing confirmed the predicted structure of *unc-94a/tmd-1a* and *unc-94b/tmd-1b,* but indicated that exons 5 and 6 of *tmd-2a* and *tmd-2 b* were shorter than initially predicted. The revised coding sequences of the *tmd-2* transcripts were submitted to www.wormbase.org and also confirmed by the *C. elegans* orfeome project (Reboul et al., 2003). yk262e07 (*unc-94a/tmd-1a*) was sent to the Southeast Collaboratory for Structural Genomics, which

independently confirmed the sequence and confirmed the protein sequence of the C-terminal, actin binding domain of TMD-1/UNC-94 by solving the crystal structure (Lu et al., 2004; Ding et al., 2003) Amino acid sequences were multiply-aligned using the ClustalW algorithm implemented on Lasergene. In addition, TMD-2 sequences were analyzed for protein domains by PFAM (Bateman et al., 1999) (version 21.0; www.sanger.ac.uk/Software/Pfam), and for repeating motifs using the program Radar (Heger and Holm, 2000) (www.ebi.ac.uk/Radar).

Generation of transgenic lines carrying *unc-94* promoter constructs

To obtain promoter sequences for *unc-94* isoforms a and b, we designed forward and reverse primers CATTCTGCAGATTTTTCAGGTGCCGAGAGTAACATTTTCAAAC and CATTGGATCCAGTTTTAGCCTGACTCATCGCTGATGG (respectively) for isoform a and designed forward and reverse primers CATTCTGCAGCTTATCTCTCACTGGTTCCAGAA-CAGGTGAC and CATTGGATCCATGATAAATTCGTGATCTAGGAAACATGGGTGG (respectively) for isoform b. These primers were used for PCR amplification using genomic DNA as template. In the case of isoform a, 3.8 kb of sequence upstream of the predicted start methionine plus the a-specific first exon were fused in-frame to GFP. For isoform b, 2.2 kb of sequence upstream plus b-specific first exon were fused to GFP. Both PCR products were then digested with PstI and BamHI. These fragments were ligated into the promotorless gfp vector pPD95.77 (provided by Andy Fire, Stanford University, Stanford, CA), which had been previously cut with the same two restriction enzymes. The ligation reactions were then used to transform *E. coli* strain XL1 Blue for plasmid amplification.

For each isoform, two clones were pooled and injected (25ng/µl) along with the reporter gene, *rol-6* (80ng/µl) into gravid N2 hermaphrodites. These injections resulted in the production of two transgenic lines for each isoform. GFP fluorescent images of different adult muscle structures were obtained as described in Mercer et al (2006).

Northern blot

Total RNA from mixed stage populations of wild type and the two *unc-94* mutant alleles was prepared using the TRIzol Reagent and a protocol provided by Invitrogen, Inc. A northern blot was prepared and hybridized using materials and methods described in the NorthernMax kit from Ambion, Inc. A 1.3% agarose formaldehyde MOPS buffer gel was used to separate the RNAs (18 µg per lane) and transferred to a nylon membrane. The 0.5—10 kb RNA Ladder from Invitrogen was used as a size marker. DNA probes were labeled with ^{32}P using the DECAprime II random primed labeling kit from Ambion, Inc. Three probes, produced by PCR from cDNA and gel-purified were used; (1) an *unc-94a*-specific probe containing the entire *unc-94a*-specific first exon generated by primers ATTTCGTCGTGGAAAGCCTGAG and CAGTTTTAGCCTGACTCATCGCTG; (2) a probe that recognizes both *unc-94a* and *unc-94b* transcripts containing most of exons 2 and 4 generated by primers CCTTCTCAGCACCGTCAGCG and CAGGGGCAGTTACAAGAGCAC; and (3) a probe that recognizes the 3' end of the *unc-15* (paramyosin) gene using primers CGCGGATCCGAGGAACAAGAACACTCGATG AND GCGGTCGACTTAATAATCGTCTTCCGTGAC.

Western blot and immunofluorescent localization of UNC-94/TMD-1

Extracts of Laemmli-soluble proteins from wild type, *su177*, *sf20*, worms fed *E. coli* harboring an empty RNAi vector, or *unc-94(RNAi)* worms were prepared by the method of Hannak et al (2002). The protein concentrations of these extracts were determined by the filter paper dye-binding method of Minamide and Bamburg (1990). After separation of 8 μgs of each extract on a 12% SDS-PAGE and transfer to nitrocellulose, the immunoblot was reacted with affinity-purified rabbit anti-TMD-1b (residues 144-401), the generation of which is described in Cox et al. (2007), at a 1:400 dilution and visualized by enhanced chemiluminescence (ECL) (Pierce, Inc.). To verify that equal amounts of total protein were loaded in each lane, the blot was washed and then incubated with anti-paramyosin (monoclonal 5-23), and visualized by chemiluminescence (Miller et al., 1983). The same affinity-purified anti-TMD-1b antibodies were used to localize UNC-94 in wild type and *sf20* adult muscle. Figure 8a and b show the results using the picric acid fixation method described in Nonet et al (1993). Anti-TMD-1 was used at 1:50 dilution, and anti-α-actinin (MH35) and anti-UNC-89 (MH42) were used at 1:200 dilutions. Figure 8 c, d and e show results using the standard paraformaldehyde/methanol fixation method described by Finney and Ruvkun (1990) and modified by Benian et al (1996). Anti-TMD-1 was used at 1:100 dilution, and anti-α-actinin (MH35) and anti-UNC-89 (MH42) were used at 1:200 dilutions. Rabbit antibodies were visualized by anti-rabbit antibodies conjugated with Alexa 488 (Molecular Probes, Inc.), and mouse antibodies were visualized by anti-mouse antibodies conjugated with Cy3 (Jackson Immunochemicals). Images were captured with a Carl Zeiss LSM 510 confocal microscopy system.

Chapter 3

Genetic and Molecular Characterization of *unc-100*, a Gene Required for Normal Myofibril Maintenance or Growth, but not Initial Assembly, in *C. elegans*

Introduction

In efforts to produce new "tools" to study myofibril assembly and function, Zengel and Epstein (1980) performed experiments in which they searched for new

mutants with altered body-wall muscle cell structure in *C. elegans*. Their screen involved EMS mutagenesis, enrichment for mutants with slow motility, and examination of myofilament lattice structures by polarized light. The polarized light screen resulted in 117 mutants and 102 of these contained alleles in one of ten previously described genes. The fifteen remaining genes represented seven new complementation groups. Of the seven new complementation groups, *unc-100* was the only one that was not mapped to a chromosome. As a result, Zengel and Epstein only reported *unc-100* mutants (*su115*, *su149* and *su170*) as having slow movement on agar plates and being slightly dumpy in appearance. Body wall muscle structure was not studied and therefore, not reported.

Many of the Unc mutants studied by our lab have shown a motility defect (compared to wild type animals) and after molecular cloning of the gene, have also been shown to encode proteins that are components of the myofilament lattice. For this reason, I decided to study *unc-100* to determine if this gene may also encode a protein that is a component of the myofilament lattice. After obtaining the *unc-100* mutants (*su115* and *su149*), my goals were to complete their phenotypic characterization by polarized light, EM, motility assays and immunofluorescent localization of known sarcomeric proteins. I then set out to determine the molecular identity of the *unc-100* gene.

Results and Discussion

To determine if *unc-100* displays a disorganized myofilament lattice, as most Unc mutants do, I examined the body-wall muscle cells of *su155* and *su149* adult animals by polarized light microscopy (Fig. 3.1). While wild type animals display a pattern of non-overlapping, parallel bright A-bands and dark I-bands, both *su155* and *su149* display disorganization. In these mutants, the A-bands appear to have areas of both increased and decreased birefringence, while the I-bands lack definition. To test for temperature sensitivity of these mutants, I allowed worms to grow at a higher than normal temperature (20ºC) of 25ºC and a lower temperature of 15ºC. The muscle phenotype of *su115* animals is suppressed at 15ºC in that the pattern of the A and I-bands in these animals resembles that of wild type. The muscle phenotype of *su149* animals could not be suppressed at 15ºC and neither allele showed suppression at 25ºC.

When viewed under the dissecting scope, both *unc-100* alleles are obviously less motile than wild type animals. In order to quantitate these differences in motility, I performed liquid motility or "swimming" assays (Fig. 3.2a) where I counted the number of times a single worm moved its head away from and back towards an imaginary starting position, during a period of one minute. Because the motility defect of many muscle Uncs is enhanced as adults, swimming assays were performed for both L4 and adult animals. While the motility of *su115* L4 animals is only decreased by 30% (compared to wild type), the motilities of *su115* adults and *su149* L4 and adult animals are decreased by 60-70%. Fig. 3.2b shows the results from brood size assays. These assays were performed because uterine and vulval myofibrils are composed of many of

the same components of body-wall muscle. In addition, many sarcomeric proteins are expressed in the myoepithelial cells of the somatic gonad, which is responsible for peristaltic movement of oocytes in the spermatheca for fertilization. I hypothesized that if the body-wall muscle of u*nc-100* mutants is disorganized, there may be some defect(s) in the egg-laying process of these animals as well. Brood size measurements show that both *su115* and *su149* lay about half as many eggs as wild type animals.

To further phenotypically characterize and analyze sarcomeric disorganization in the *unc-100* mutants, I used immunofluorescence microscopy to localize known sarcomeric proteins. The localized proteins included F-actin (marks thin filaments), MHC A (myosin heavy chain A marks thick filaments), UNC-89 (an M-line marker), and α-actinin (a dense body marker). As shown in Fig. 3.3, all four proteins are disorganized to some degree, with the most disorganization seen in MHC A, UNC-89 and α-actinin. These defects do not appear to be similar between the two alleles. *su149* clearly shows more disorganization of the aforementioned proteins than *su115*, which is consistent with *su149* L4s being ~50% slower than *su115* by motility assay.

To observe how proteins/structures in the myofilament lattice of *unc-100* mutants are disorganized from another point of view, I analyzed cross-sections of body-wall muscle by EM. Figure 3.4 shows side-by-side images of electron micrographs for wild type and the two mutant alleles. The cartoon on the left side of the figure shows the organization of sarcomeric structures in relation to the body-wall cavity and the cuticle of the worm: The dense bodies (pink) are surrounded by thin filaments (white spaces) and are attached to the muscle cell membrane (yellow). M-lines (blue) are surrounded by thick filaments (black dots) and are also attached to the muscle cell membrane. As noted

by the blue and pink arrows, the M-lines and dense bodies, respectively, are properly organized and attached in the wild type image. The two mutants display no obvious M-lines and broken dense bodies that are often detached from the cell membrane. Overall, *su115* and *su149* lack definition in the patterning of A band I-bands, which makes it extremely difficult to note where one sarcomere ends and where another begins.

Thus far, experimental results show the importance of UNC-100 in adult body-wall muscle structure, organization and function. To determine if UNC-100 is important for the initial assembly of myofibrils, I analyzed embryos of the stronger allele, *su149*, by immunofluorescent localization of the thick filament protein, MHCA. During embryonic development, at ~290 minutes after the first cell cleavage, muscle cells are born. At the same time, important structural proteins such as vinculin, integrins and myosins are diffusely distributed within the cells. At ~ 430 minutes after the first cell cleavage, attachment structures form and lattice components organize into sarcomeres (Hall and Altun, 2008). At this developmental time period the embryo is termed 2.5-fold stage. It is at this stage of development that we took images of wild type and *su149* embryos (Fig. 3.5). By simply analyzing the distribution pattern of MHC A in *su149* in comparison to wild type, it is clear that *su149* is not lacking in MHC A-thick filament organization. Therefore, I conclude that UNC-100 is necessary for normal myofibril assembly or maintenance in adult worms, but not necessarily for the initial assembly of myofibrils in early stage embryos.

After phenotypically characterizing the two *unc-100* mutants, I focused my efforts on cloning *unc-100*. Because *unc-100* had been previously mapped to the right arm of chromosome I (23.0 +/- 5.0cM) (Johnathan Hodgkn, personal communicaton), I checked

this region for deficiencies. There are four deficiency strains (*dxDf2*, *eDf3, eDf6*, and *eDf12*) which I mated with *unc-100 (su115)* males and looked for non-complementation in the F1 progeny. If a deficiency strain does not complement UNC-100, I expect to see a 50:50 ratio of wild type to Unc-100 animals in the F1 generation. Figure 3.6 show that 100% of F1 progeny for *eDf6* and *eDf12* and close to 100% for *dxDf2* and *eDf3* showed wild type organization of body-wall muscle. In other words, each deficiency complemented *unc-100*, which means that *unc-100* is not likely to reside in the deficient regions tested.

As a second method of mapping *unc-100* to the right arm of chromosome I, I decided to take the candidate gene mapping approach. I scanned the *C. elegans* genome for genes that were within the predicted area and that had been previously described as being Unc or slow by RNAi. I knocked down 13 genes, individually, in *rrf-3* (an RNAi hypersensitive strain) animals and scored the F1 progeny for an Unc-100 polarized light phenotype as well as other features that resemble *unc-100* animals (Table 3.1). Only F1 progeny from one gene, *tfg-1*, showed Unc-100-like phenotypes. After sequencing the exons and exon-intron boundaries of *tfg-1*, using both *su115* and *su149* genomic DNA, I did not find any mutations.

After having no luck in placing *unc-100* on the right arm of chromosome I, I decided to perform three-factor mapping of my own to determine if I had been investigating the correct area of the chromosome. I hypothesized that *unc-100* might not be on the right end of chromosome I, but could indeed be located somewhere in the middle or on the left end of the chromosome. I started mapping by using the double mutant *dyp-5 unc-101*; these markers are located at the left end (*dpy-5*, 0.0cM) and the

middle (*unc-101*, 13.2cM) of chromosome I. Results in Fig. 3.7 show that after analyzing recombinants from the *unc-100* x *dpy-5 unc-101* cross, I determined that there were fewer *dpy-5 unc-100* recombinants than there were *unc-100, ucn-101* recombinants. These data suggests that *unc-100* is between the two markers, but is probably closer to *dpy-5*. Next I decided to use the doubles *dpy-5 unc-13* and *dpy-5 unc-29* to mate with *unc-100* males as *unc-13*(2.13) and *unc-29* (3.31) are close to *dpy-5*. The data for recombinant animals from these two crosses, suggests that *unc-100* is between *dpy-5* and *unc-29* and probably very close to *unc-13*, due to the fact that I was not able to generate any *unc-13 unc-100* recombinants.

After determining that *unc-100* is more than likely between *dpy-5* and *unc-29*, I used both deficiency and SNP mapping to further locate a position for the gene. I inspected three deficiencies, namely *qDf16*, *ozDf5* and *nDf24*. When hermaphrodites containing these deficiencies were mated with *su115* males, all of the outcrossed F1 progeny displayed wild type body-wall muscle by polarized light (Fig. 3.11). Because the ends of these deficiencies are not very well defined and there were small gaps between the deficiencies, I categorized these data as inconclusive. There are no other deficiencies available for this region.

Next, I made a triple mutant consisting of *dpy-5* (*e61*) *unc-100 (*su115*) unc-29* (*e403*) (Bristol origin), which I mated with "Hawaiian" (strain CB4856) males for SNP mapping experiments. Because Hawaiian and Bristol strains of *C. elegans* have a different nucleotide every 800-900 bp (Wicks et al., 2001), the single nucleotide polymorphisms can be used to determine which portions of recombinant chromosomes were derived from Hawaiian and which ones came from Bristol. Since *unc-100* mutants

were generated in the Bristol strain, I only analyzed Bristol recombinants. From the 24 recombinant classes recovered (11-Dpy-5 Unc-100 non-Unc29, 13-non-Dpy-5 Unc-100 Unc-29), I PCR amplified 25 different SNP containing regions that were somewhat evenly scattered between *dpy-5* and *unc-29* (Table 3.2). Data from these recombinants allowed me to limit the position of *unc-100* to a ~500 kb region between (and including) cosmids F21C3 and T23G11, containing 17 overlapping cosmids (Fig. 3.7).

To determine if one or more of the 17 cosmids contain *unc-100*, I decided to perform transgenic rescue experiments where I divided the cosmids into four sets of three and one set of five for injecting *unc-100* mutants (Sets A,B,C,D and E) (Figure 3.9). I obtained these cosmids from the Sanger Centre, grew the bacterial strains and prepared cosmid DNA. Restriction digests verified that there were no obvious deletions of the cosmid inserts (In some cases, deletions were a problem, and those cosmids had to be re-grown or even re-ordered from the Sanger Centre). When beginning to inject worms by visualizing the gonad, the gonad seemed abnormal. Therefore, I decided to carefully image *unc-100* gonads by DIC. I found that the somatic gonads of *su149* animals are clearly abnormal (Fig. 3.8). Although the gonads of *su115* animals appear to be normal by DIC, there still may be other underlying reasons for why I was not able to obtain transgenic animals using these mutants. Since I could not use *unc-100* animals, I injected the cosmid sets (and individual cosmids) into wild type animals instead and performed steps for rescue as explained in the "Generation of Transgenic Lines and Rescue Experiments" section of Materials and Methods for this chapter. As shown in Fig. 3.9, I was only able to create transgenic lines for sets B and C.

Rescue data for set B shows that all of the green hermaphrodites (for both lines produced) screened after the final cross displayed mutant body-wall muscle. I expected that if a set did not rescue UNC-100, there would be a 50:50 ratio of wild type to Unc-100 green animals; for set B, this was obviously not the case. After scanning Worm Base for predicted genes on the three cosmids in set B, I found that *unc-15* (paramyosin) is contained in cosmid FO7A5. It is known that when *unc-15* is over-expressed, worms exhibit a mutant body-wall muscle phenotype (Kagawa, personal communication). Therefore, when I initially injected set B into wild type animals, the green F1 hermaphrodites that we selected and carried on to mate with *unc-100* males, already had disorganized body-wall muscle structure. It is for this reason that 100% of the green worms from the final mate were all mutant by polarized light. To be sure that *unc-100* alleles are not alleles of *unc-15*, I performed a complementation test with *unc-100 (su115)* and *unc-15 (e1215)*, which resulted in *unc-15* complementing *unc-100*. Mating experiments performed with a stronger allele of *unc-15*, *e1214*, were not successful being that the worms did not mate. Mating experiments were not performed using the stronger allele of *unc-100*, *su149*, due to the fact that *su149* animals are Dpy (Dpy males tend to have very low mating efficiencies, E1-E0). I also sequenced *unc-15* using genomic DNA from our lab N2 strain and both *unc-100* alleles. I found a mutation for paramyosin in *unc-100* mutants; there is an A to G transition for the first guanine of glutamate 842, which converts the glutamate to Lysine (Table 3.4). Neither this change nor any others were found for *su149* or N2. At that point, it was possible that *unc-15* and *unc-100* were the same gene. I hypothesized that maybe the reason I could not find a mutation in the coding sequence (and proximal intron sequences) for the more severe allele, *su149*, was

that *su149* had a mutation in its promoter which drastically reduced the level of paramyosin expression. To explore this idea, I performed a Western blot using extracts from wild type, *su115* and *su149* and reacted them against a monoclonal to paramyosin. No obvious difference in levels or sizes of paramyosin was found in *unc-100* mutants as compared to wild type (data not shown).

Rescue data for set C, shows that when screened by polarized light ~ 90% of the green hermaphrodites from the final cross had wild type body-wall muscle for line 2 and 100% had wild type body-wall muscle for line 3. After the three cosmids in set C were injected individually, cosmid C26C6 produced rescue data that made it seem a likely candidate for the cosmid containing *unc-100*. After checking Worm Base for genes on C26C6 that had reported "Unc" phenotypes by RNAi or mutations and/or SAGE or GFP-promoter data suggesting muscle expression, I found two candidates, *dcp-66* and *pbrm-1*. *dcp-66* (~ 4.3 kb) showed GFP-promoter expression in body-wall muscle and was reported as being a locomotion variant (Unc) and having slow growth by RNAi. *pbrm-1* (largest isoform ~ 8kb) showed muscle expression (by SAGE) and was also reported as being a locomotion variant and having slow growth, but was also reported as having reduced brood sizes (all by RNAi). With both *dcp-66* and *pbrm-1* animals being considered as "Unc" and also sharing other phenotypes associated with *unc-100* mutants, I decided to further investigate these genes as being possible *unc-100* candidates.

Although in my hands, RNAi for either *dcp-66* or *pbrm-1* did not yield disorganized myofibrils by polarized light, interestingly *dcp-66* (RNAi) clearly resulted in very slow moving animals. DNA sequencing of *dcp-66* or *pbrm-1* (exons and proximal intron regions) did not reveal any mutations for either *su115* or *su149*. For the sake of

exploring the other genes on the cosmid, I performed RNAi, sequenced, or performed both methods for four of the nine remaining genes (Fig. 3.10). Results show that none of the genes phenocopy Unc-100 when knocked down and that none of the sequenced genes have a mutation in either allele of *unc-100*.

Because RNAi and sequencing data suggest that *unc-100* may not be on cosmid C26C6, I decided to go back to the deficiency map to see exactly where the SNP mapping sets fall under the three deficiencies (Fig. 3.11). While sets B through E fall under *nDf24,* set A falls in the gap between *qDf16* and *ozDf5*. For this reason, I decided to perform candidate gene mapping by knocking down all the genes that lie on the cosmids in set A (Table 3.5). After performing RNAi for these genes (using *rrf-3* hermaphrodites), I scored the F1 progeny by polarized light and determined that F1s, for all 24 genes tested, had wild type body-wall muscle; none of the genes phenocopied Unc-100.

.

Figures

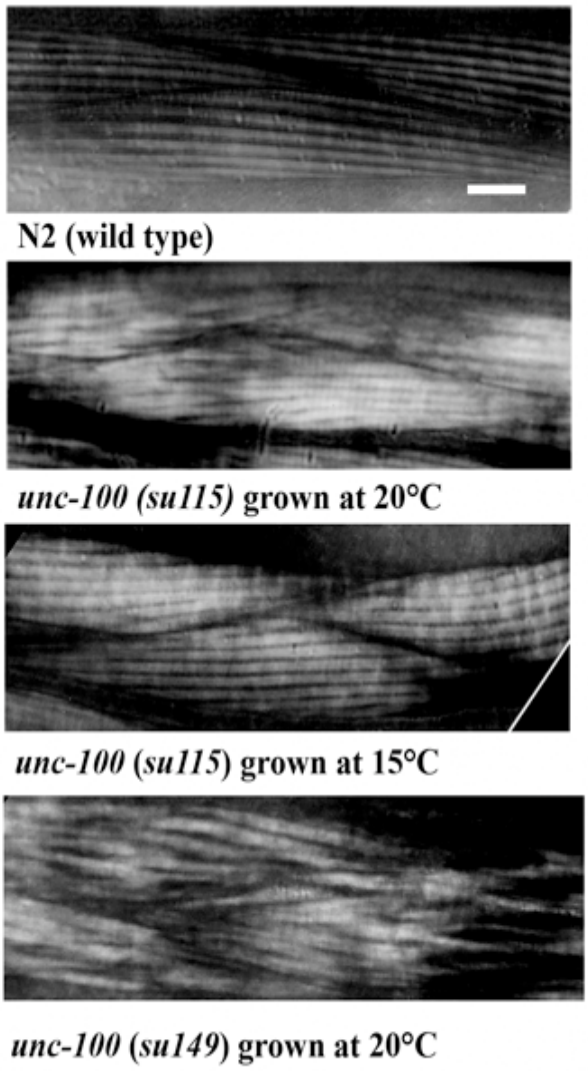

Figure 3.1 Polarized light microscopy of body-wall muscle from *unc-100* adults. In wild type muscle, there is a normal arrangement of alternating bright A-bands with dark I-bands. In *su115* animals, A-bands appear thicker and there are patchy areas of decreased birefringence. The phenotype of *su115* can be suppressed when the animals are

grown at a reduced temperature. *su149* has a similar polarized light phenotype, but is not suppressed at the lower temperature. The scale bar represents 10 μm.

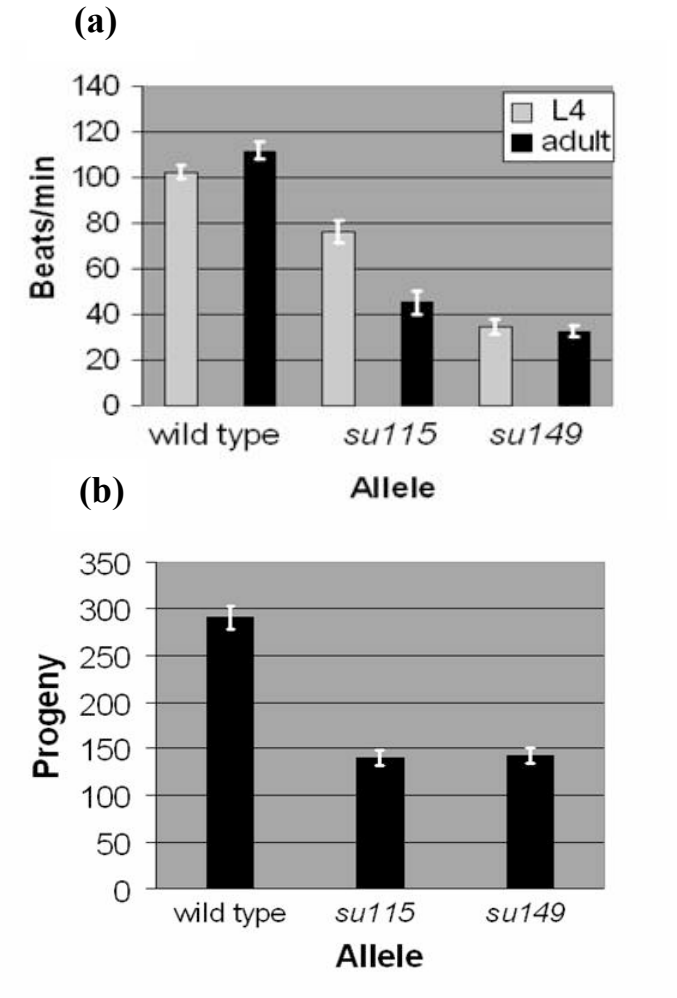

Figure 3.2 Liquid motility and brood size assays for *unc-100* animals. (a) Wild type and *unc-100* animals at the 4th larval (L4) and adult stages of development were subjected to a swimming asssay. Both mutants, for both stages, show a dramatic decrease in motility compared to wild type animals. *su149* animals are the most severe, being almost 70% slower than wild type. Data are shown as means and SEMs, with n=10. (b) Brood size assay comparing the number of eggs laid by wild type animals and the *unc-100* mutants. As shown, a wild type animal can lay between 200-300 eggs. Both *unc-100* mutants show a significant decrease in their brood sizes, with both laying about 50% fewer eggs than wild type animals.

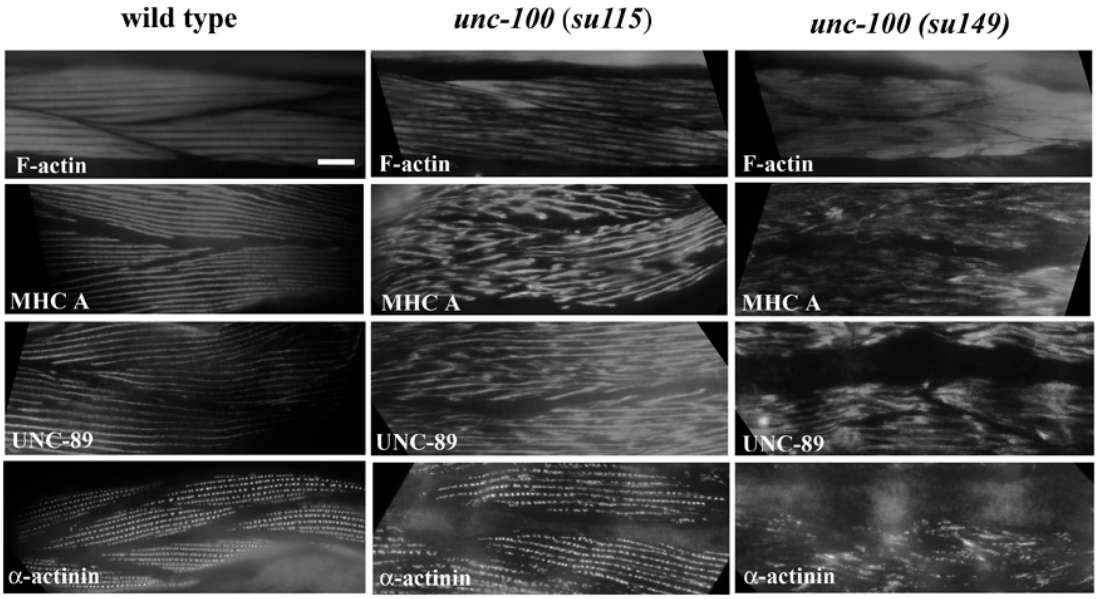

Figure 3.3 Immunofluorescent localization of several known sarcomeric proteins in wild type and *unc-100* adult body-wall muscle. Phalloidin was used to detect F-actin (thin filaments), and antibodies were used to detect MHC A (thick filaments), UNC-89 (M-lines), and α-actinin (dense bodies). Each of these structures shows disorganization, with the greatest effects on thick filaments, M-lines and dense bodies. *su149* has a more severe phenotype than *su115*.

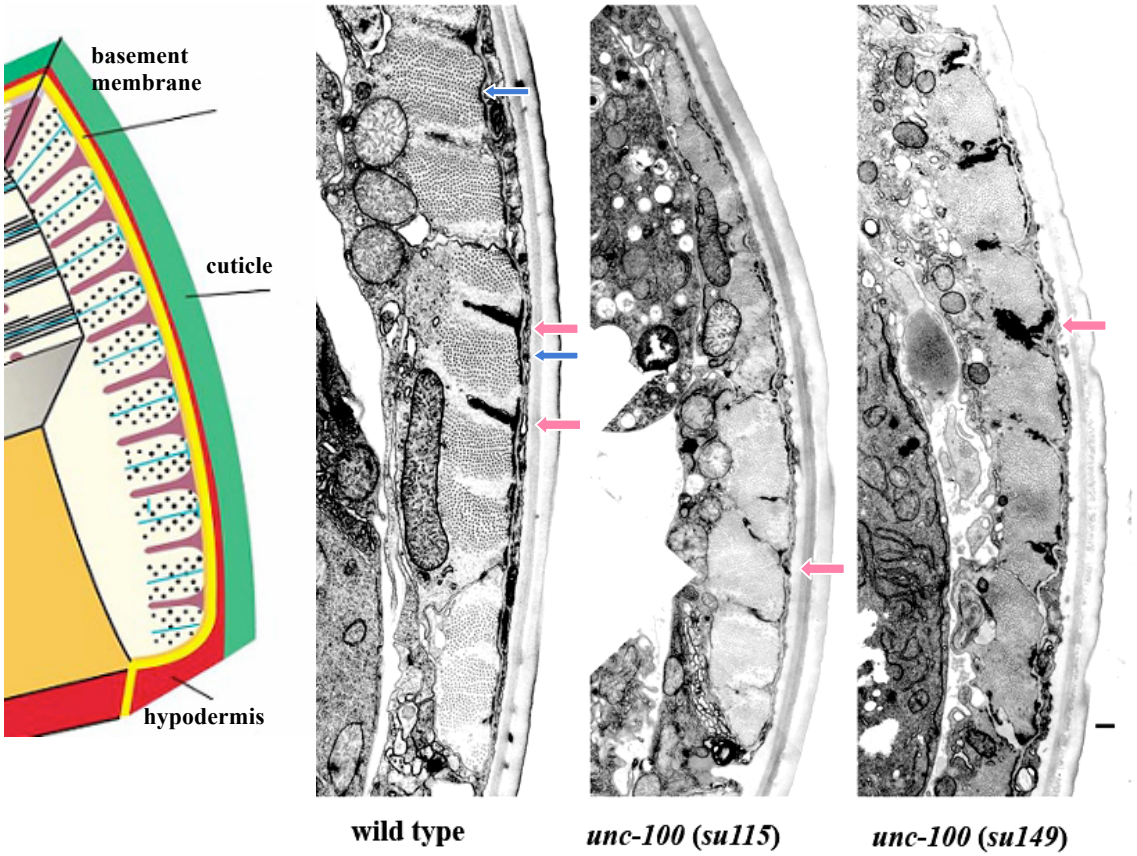

Figure 3.4 Electron micrographs of adult body-wall muscle from wild type and the two *unc-100* mutants. The cartoon shows the organization of sarcomeric structures from a cross-sectional plane when thin sections of C. elegans body-wall muscle are viewed by E.M. Dense bodies (pink) are attached to the basement membrane (yellow) and are surrounded by thin filaments (grey). M-lines (blue) bisect the dense bodies and are surrounded by thick filaments (black dots). Both micrographs of *unc-100*, show: 1. Missing M-lines, 2. Broken dense bodies that are often detached from the cell membrane and 3. Lack of defined A and I-bands. The scale bar represents 500 nm.

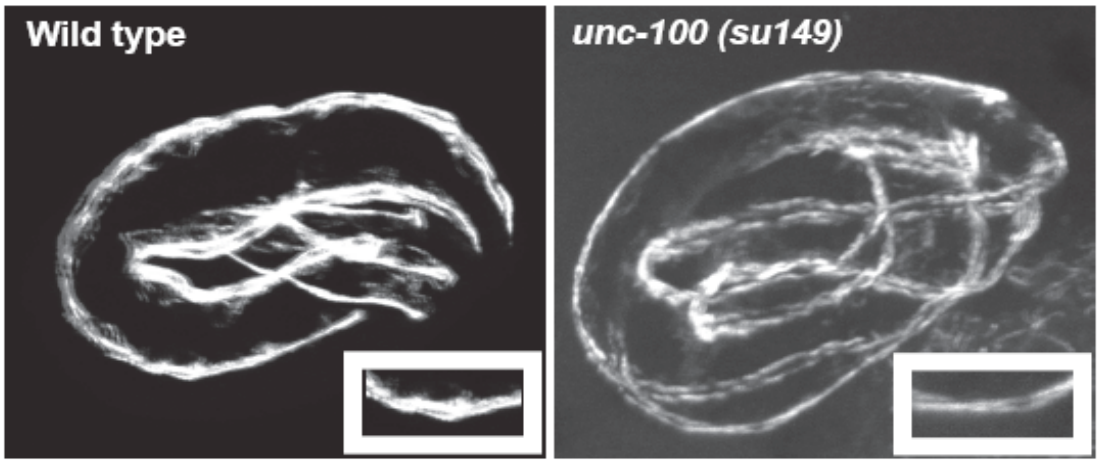

Figure 3.5 Immunofluorescent localization of MHC A in wild type and *unc-100* (*su149*) embryos. There appears to be a normal distribution of MHC A in the muscle of *su149* embryos compared to wild type. This result shows that *unc-100* is important for adult myofibril organization, but not for embryonic myofibril organization.

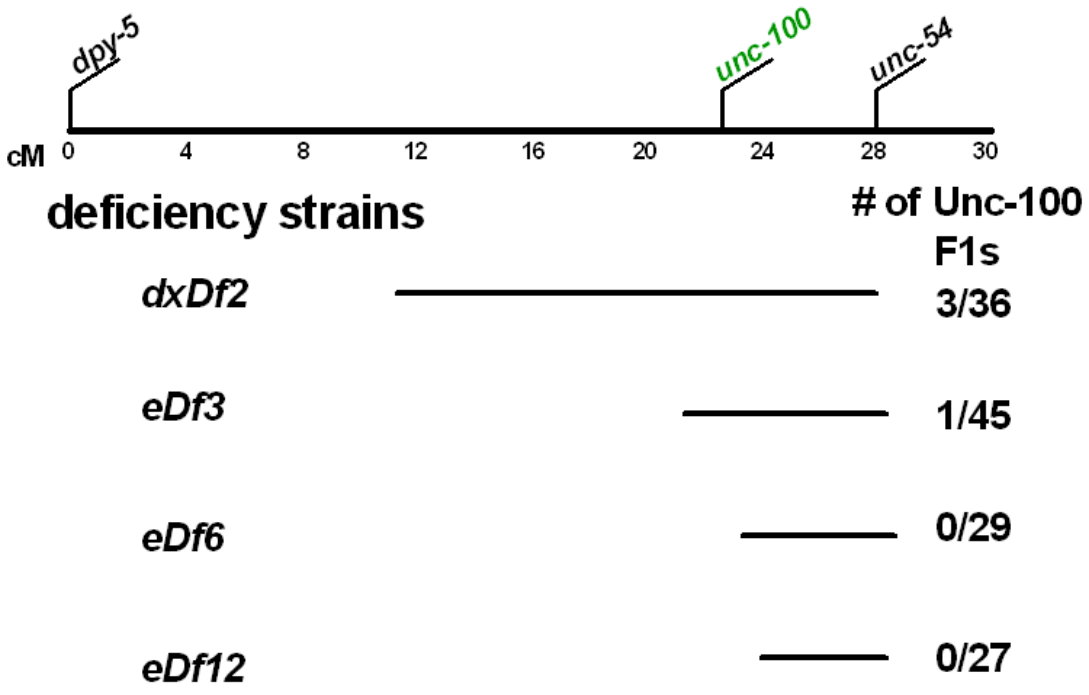

Figure 3.6 Deficiency mapping of *unc-100*. Strains carrying deficiencies for the regions of chromosome I, noted in the above figure, were individually mated with *unc-100* (*su115*) animals. F1 progeny from these individual mates were screened by polarized light for the presence of an Unc-100 phenotype.

Gene	RNAi phenotype of F1 progeny by polarized light
bath-35	**WT**
F22G12.4	**WT**
spf-3	**WT**
pad-1	**WT**
tag-183	**WT**
pfn-1	**WT**
F49B2.3	**WT**
pbs-5	**WT**
sur-2	**WT**
W04A8.4	**WT**
agef-1	**WT**
tfg-1	**Slight Unc-100 phenotype, Unc, Dpy, SG, EL, RBS**
let-49	**WT**

Table 3.1 Candidate gene mapping of *unc-100*. From two factor mapping data, the genetic position of *unc-100* was thought to be around 23.0 +/- 5.0 cM. After scanning the *C. elegans* genome for genes that lie within the predicted area and/or that have been previously describe as having Unc-100-like phenotypes (by RNAi), we performed RNAi of the genes (in *rrf-3* animals) and checked for a polarized light phenotype as well as other phenotypes that resemble Unc-100.

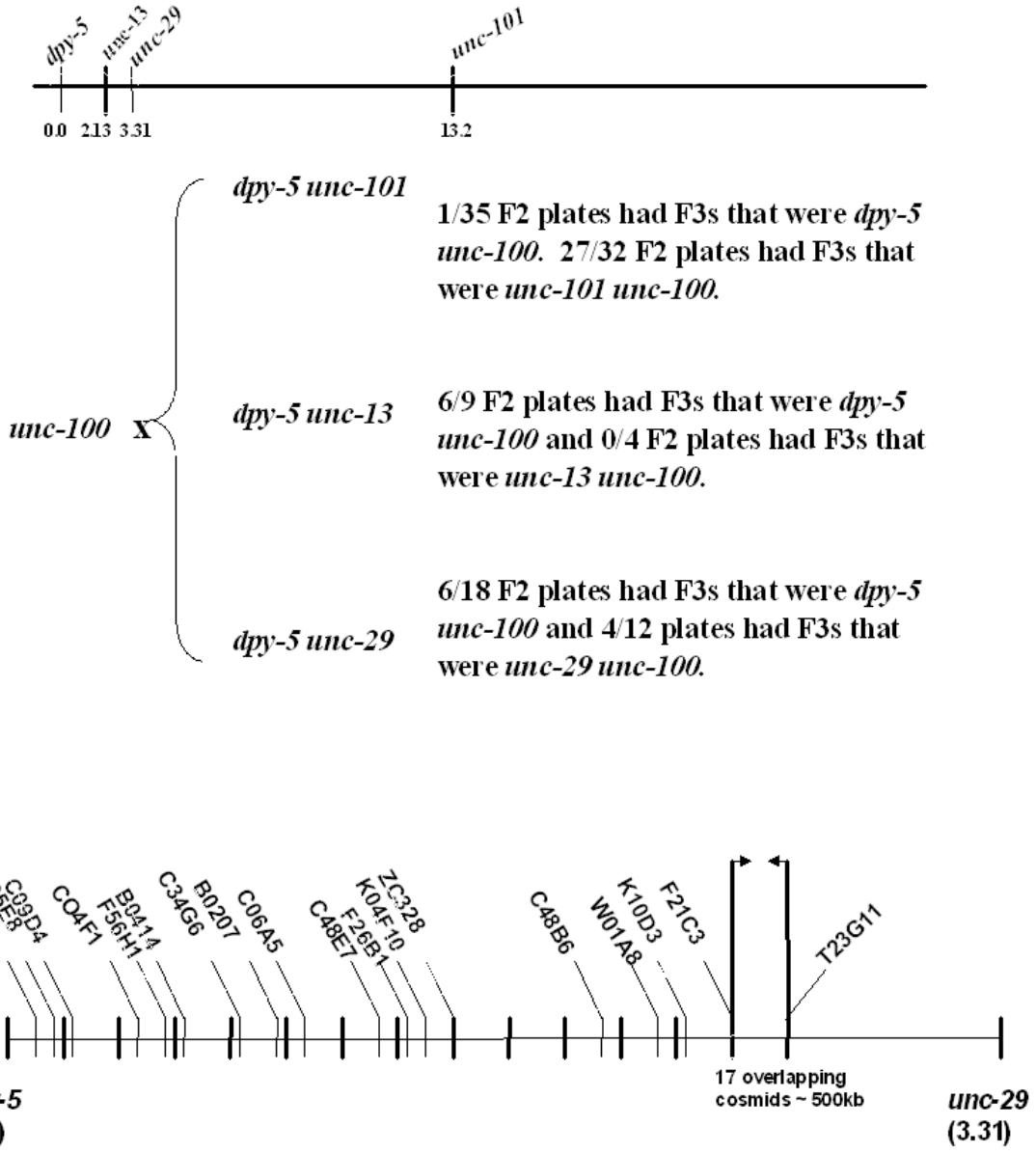

Figure 3.7 Mapping of *unc-100.* We used 3-factor mapping, followed by SNP mapping to narrow down the region where *unc-100* is located. Results from three-factor mapping allowed us to place *unc-100* on chromosome 1 between *dpy-5* and *unc-29.* SNP mapping allowed us to further limit the region between cosmids F21C3 and T23G11, a 500 kb segment that includes 17 overlapping cosmids.

											SNPs													
Recombinants	11	1	17	16	15	14	13	12	9	8	2	7	4	5	6	3	18	19	20	21	22	23	24	25	26
dpy-5 (#14) unc-100	B	B	B	B	B	B	B	B	B	B	B	B	B	B	B	B	B	B	B	B	B	H	H	H	H
dpy-5 (#21)unc-100	B	B	B	B	B	B	B	B	B	B	B	B	B	B	B	B	B	B	B	B	B	B	H	H	H
dpy-5 (#26) unc-100	B	B	B	B	B	B	B	B	B	B	B	B	B	B	B	B	B	B	B	B	B	H	H	H	H
dpy-5 (#31) unc-100	B	B	B	B	B	B	B	B	B	B	B	B	B	B	B	B	B	B	H	H	H	H	H	H	H
dpy-5 (#36) unc-100	B	B	B	B	B	B	B	B	B	B	B	B	B	B	B	B	B	B	B	B	B	B			
dpy-5 (#6) unc-100	B	B	B	B	B	B	B	B	B	B	B	B	B	B	B	B	B	B	B	B	?	H	H	H	H
dpy-5 (#37) unc-100	B	B	B	B	B	B	B	B	B	B	B	B	B	B	B	B	B	B	B	B	H	H	H	H	H
dpy-5 (#42) unc-100	B	B	B	B	B	B	B	B	B	B	B	B	B	B	B	B	B	B	B	H	H	H	H	H	H
dpy-5 (#44) unc-100	B	B	B	B	B	B	B	B	B	B	B	B	B	B	B	B	B	B	B	B	B	B			
dpy-5 (#45) unc-100	B	B	B	B	B	B	B	B	B	B	B	B	B	B	B	B	B	B	B	B	B	B			
dpy-5 (#50) unc-100	B	B	B	B	B	B	B	B	B	B	B	B	B	B	B	B	B	B	B	B	B	H	H	H	H
unc-29 (# 24) unc-100	H	H	H	H	H	H	H	H	H	H	H	H	B	B	B	B	B	B	B	B	B	B	B	B	B
unc-29 (#1) unc-100	H	H	B	B	B	B	B	B	B	B	B	B	B	B	B	B	B	B	B	B	B	B	B	B	B
unc-29 (#11) unc-100	H	H	H	H	H	H	H	H	H	H	H	H	B	B	B	B	B	B	B	B	B	B	B	B	B
unc-29 (#12) unc-100	H	H	H	H	H	B	B	B	B	B	B	B	B	B	B	B	B	B	B	B	B	B	B	B	B
unc-29 (#21) unc-100	H	H	H	H	H	H	H	H	H	H	H	H	B	B	B	B	B	B	B	B	B	B	B	B	B
unc-29 (#25) unc-100	H	H	H	H	H	H	H	H	H	H	H	H	B	B	B	B	B	B	B	B	B	B	B	B	B
unc-29 (#5) unc-100	H	H	B	B	B	B	B	B	B	B	B	B	B	B	B	B	B	B	B	B	B	B	B	B	B
unc-29#16 (unc-100)	H	H	H	H	H	H	H	H	H	H	H	H	B	B	B	B	B	B	B	B	B	B	B	B	B
unc-29 (#31) unc-100											B	B	B	B	B	B	B	B	B	B	B	B	B	B	B
unc-29 (#35) unc-100	H	H	H	H	H	H	H	H	H	H	H	H	H	H	H	B	B	B	B	B	B	B	B	B	B
unc-29 (#39) unc-100											B	B	B	B	B	B	B	B	B	B	B	B	B	B	B
unc-29 (#43) unc-100	H	H	H	H	H	H	H	H	H	H	H	H	H	H	H	H	B	B	B	B	B	B	B	B	B
unc-29 (#45) *unc-100*											B	B	B	B	B	B	B	B	B	B	B	B	B	B	B

B/H = sequenced SNPs

B/H = based on sequenced SNPs

? = SNP not determined

highlighted in blue/yellow are the most informative recombinants

Table 3.2 SNP mapping data for *dpy-5 unc-100* and *unc-29 unc-100* recombinants.

11 *dpy-5 unc-100* recombinants and 13 *unc-29 unc-100* recombinants were isolated (Numbers were assigned to each *dpy-5* and *unc-29* animal before they were screened for an Unc-100 phenotype by polarized light, i.e. *dpy-5* (#36) *unc-100*). Several SNPs were amplified using genomic DNA for each recombinant listed (SNPs are listed in order from left to right on chromosome I). If the sequencing data showed a Bristol nucleotide for a particular SNP, then the letter B was assigned. If the sequencing data revealed a Hawaiian nucleotide, then the letter H was assigned. See Table 3.3 for individual SNP information.

SNP #	Cosmid	Position	Type of Change	Bristol SNP	Hawaiian SNP
11	T05E8	23168	S	C	T
1	C09D4	3746	S	C	G
17	C04F1	3815	S	A	C
16	F56H1	28768	S	A	T
15	B0414	29886	S	A	G
14	C34G6	15466	S	C	T
13	B0207	42122	S	A	T
12	C06A5	19725	S	C	T
9	C48E7	24585	S	C	T
8	F26B1	23911	I1		T
2	K04F10	19618	S	A	T
7	ZC328	9784	S	C	T
4	C48B6	10952	D1	A	
5	W01A8	2242	S	A	C
6	K10D3	27932	D1	A	
3	F21C3	18337	S	G	T
18	ZK524	1111	S	C	T
19	H15M21	5760	S	C	G
20	T23G11	9064	S	A	G
21	D2005	31734	S	A	G
22	F18C12	23323	S	T	G
23	K02B12	15218	S	T	C
24	VF39H2L	3079	S	G	A
25	K07A12	17992	S	G	A
26	C36B1	29243	D7	AATACAA	

S = substitution
I = insertion, I1 = insertion of 1 base in Hawaiian sequence
D = deletion, D1 = deletion of 1 base in Hawaiian sequence

Table 3.3 Individual SNP data. 25 SNPs for Bristol and Hawaiian, wild type *C. elegans* strains, were used to determine the map position of *unc-100*. After sequencing SNP regions using genomic DNA from recombinants listed in Table 3.2, sequence changes were noted as substitutions, insertions, or deletions. Each SNP is located at the position listed for its respective cosmid. Information for these SNPs can also be found at the website: http://genomeold.wustl.edu/genome/celegans/celegans_snp.cgi.

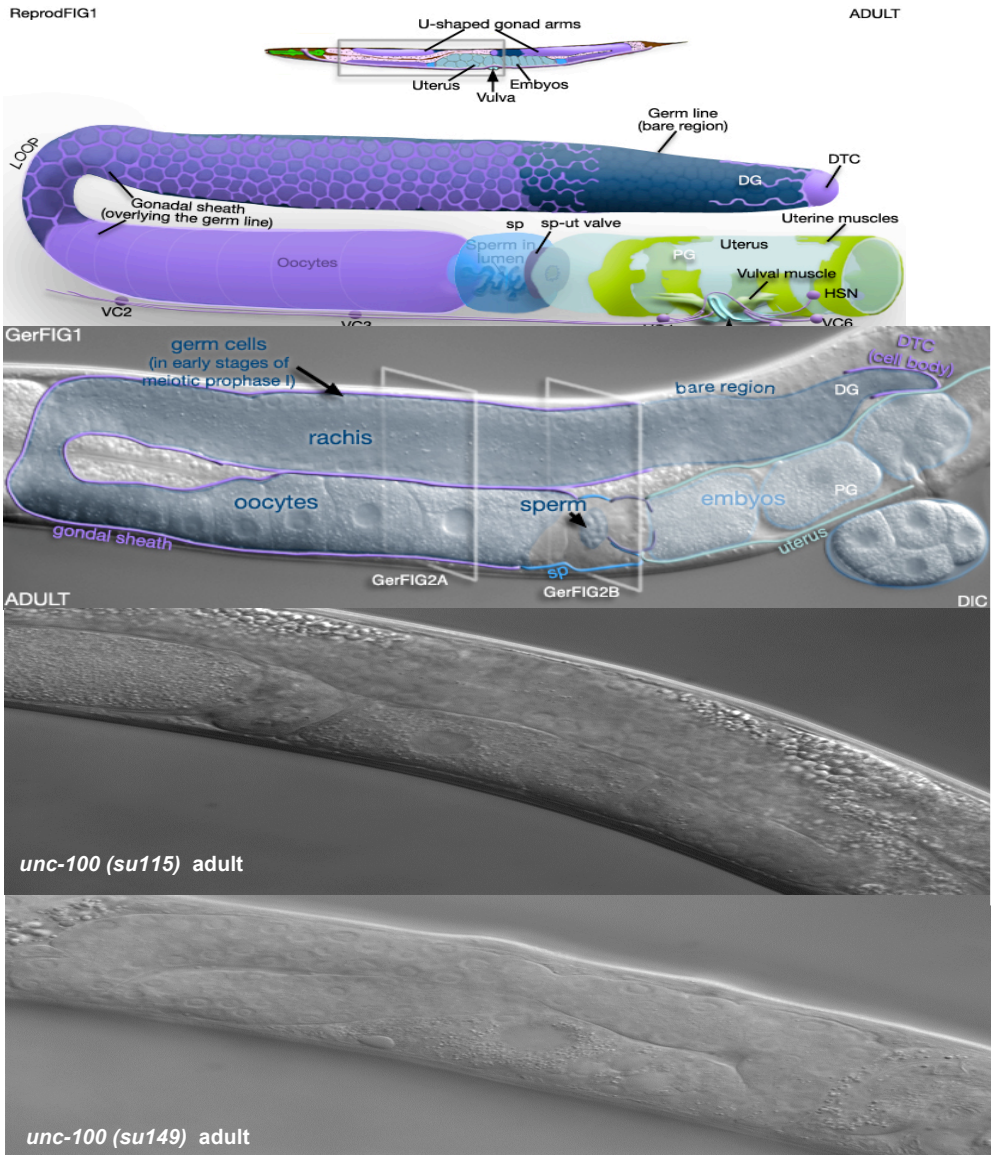

Figure 3.8 Nomarski images of the gonad of *su115* and *su149* adult animals. *su115* animals look normal at all stages of development and have normal gonads as adults. As larvae, *su149* animals look normal. As adults, the somatic gonad has a clearly abnormal structure. (Image from Worm Atlas 2008)

17 overlapping cosmids (L → R):

		# of transgenic lines	rescue data (green♂)
F21C3 F13G3 F52A8	A	0	N/A
F07A5 C15A11 C44E1	B	2	line 1: 0/8 wt; line 2: 0/5 wt
ZK524 T28F4 C26C6	C	3	line 2: 12/13 wt; line 3: 12/12
H15M2 T25G3 D2030	D	0	N/A
F57A5 F29D11 F26A3 T24B1 T23G11	E	0	N/A

Group "C" 3 overlapping cosmids (L → R) :

	# of transgenic lines	rescue data (green ♂)
ZK524	1	12/22 wt
T28F4	1	N/A
C26C6	3	line 1: 17/21wt, 16/20 wt line 3: 3/4 wt

Figure 3.9 Transgenic Rescue of *unc-100*. It was determined that a set of 3 cosmids ("C") rescues the Unc-100 phenotype by polarized light. After injecting single cosmids, we determined that *unc-100* might reside on C26C6.

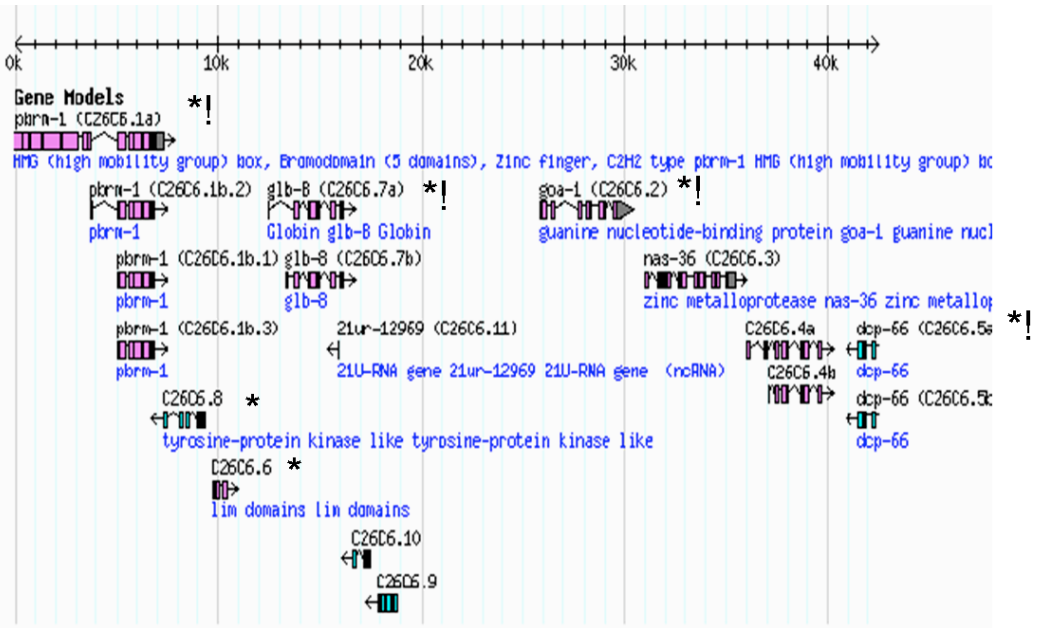

Figure 3.10 Predicted genes on cosmid C26C6. We performed RNAi and/or sequencing of marked genes (*=RNAi, ! =sequenced).

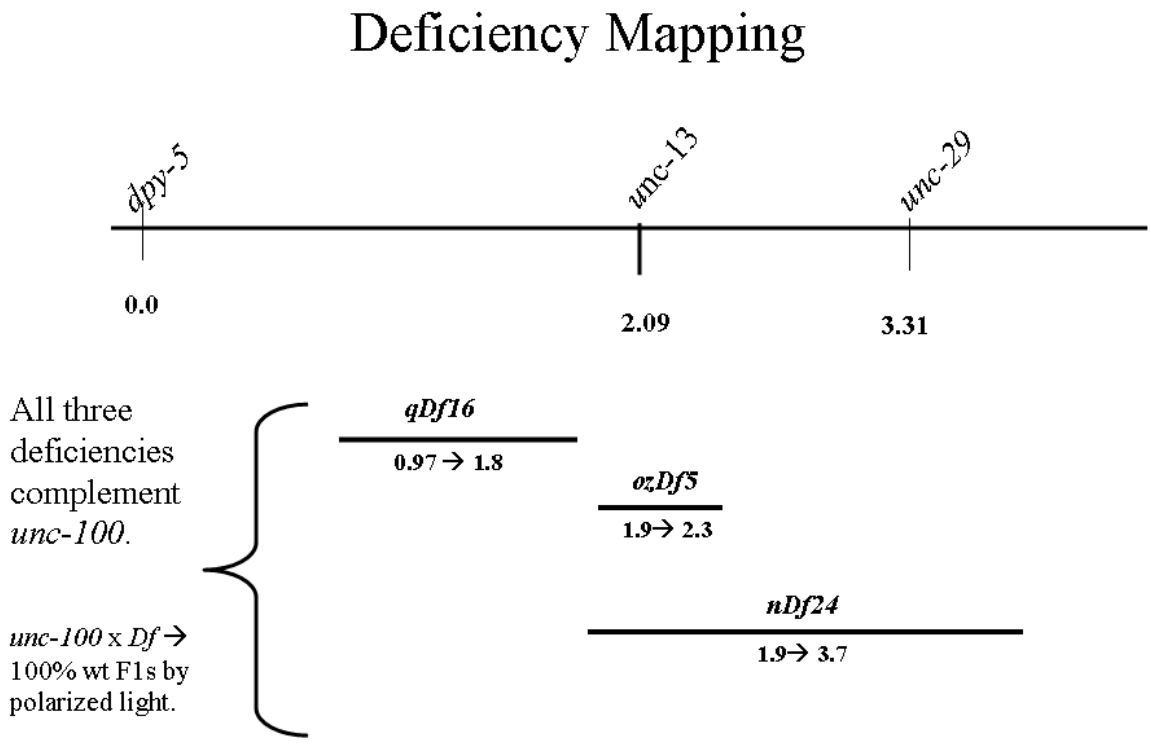

Figure 3.11 Deficiency mapping of *unc-100*. Deficiencies *qDf16, ozDf5* and *nDf24* all complement *unc-100* when F1 progeny from matings are scored by polarized light. Cosmid sets B through E are covered by *ozDf5* and *nDf24*, while set A lies in the gap between *qDf16* and *ozDf5*.

	unc-15	*dcp-66*
Worm Base	**GAG=E**	**No insertion**
Lab N2	**GAG=E**	**G insertion, exon 8**
unc-100 (su115)	**AAG=K**	**G insertion, exon 8**
unc-100(su149)	**GAG=E**	**G insertion, exon 8**

Table 3.4 *unc-15* and *dcp-66* sequence comparison. After sequencing *unc-15* using genomic DNA from N2, *su115* and *su149*, it was determined that for *su115* there is an G→A transition for the first guanine of glutamate 842, which converts the glutamate to lysine (E→K) in UNC-15 (paramyosin). Sequence data for *dcp-66* reveals a G insertion in the 8th exon for our lab N2 strain, *su115* and *su149*, which suggests that this insertion is likely a polymorphism.

Gene	RNAi phenotype of F1 progeny by polarized light
tyr-1	**WT**
rde-2	**WT**
twk-1	**WT**
hint-1	**WT**
pfd-6	**WT**
F21C3.6	**WT**
F21C3.t1	**WT**
F21C3.7	**WT**
21ur-12937	**N/A**
21ur-14201	**N/A**
eat-5	**WT**
ztf-2	**WT**
ttx-7	**WT**
dylt-1	**WT**
F13G3.7	**WT**
mif-3	**WT**
F13G3.10	**WT**
F13G3.3	**WT**
srd-53	**WT**
F13G3.6	**WT**
F13G3.11	**N/A**
F13G3.12	**N/A**
gpb-2	**WT**
glb-18	**WT**
F52A8.1	**WT**
F52A8.3	**WT**
F52A8.5	**WT**
F52A8.6	**WT**
21ur-13600	**N/A**

Table 3.5 RNAi (by feeding) of predicted genes on cosmids in set A (Candidate gene mapping of *unc-100*). 24/29 genes in set A were knocked down in *rrf-3* animals (P0). The progeny from these worms (F1) were scored by polarized light for either a wild type (WT) or Unc-100 muscle phenotype. F1s for all 24 genes were wild type by polarized light. N/A= RNAi was not performed.

.

Materials and Methods

C. elegans strains and genetics

Using a motility and polarized light screen for new muscle "Uncs", Zengel and Epstein isolated three alleles of *unc-100*: *su115*, *su149*, and *su170*. However, only *su115* and *su149* were employed in this study. Because Zengel and Epstein (1980) did not assign these mutants to a chromosome, they did not report any information regarding muscle phenotype for these animals. After obtaining *su115* and *su149* mutants from Pamela Hoppe (Western Michigan University), these animals were outcrossed three times, using *him-5* males, and used in subsequent polarized light, liquid motility, brood size, and immunofluorescence experiments. Each allele was then outcrossed an additional two times (for a total of five times outcrossed). The polarized light phenotype for both alleles did not change after being outcrossed an additional two times; therefore, previously mentioned experiments were not repeated. For deficiency mapping, hermaphrodites of the following strains were used to perform complementation tests with homozygous *unc-100; him-5* males: SL536: *dxDf2*/*spe-9*(*eb19*) *unc-101*(*m1*), CB2769: (eDf3), CB2772 (eDf6), CB2778: *eDf12*/*eDf24*, JK1726: *qDf16*/*dpy-5*(*e61*) *unc-15*(*e1402*), BS585: *unc-13*(*e51*) *ozDf5* I; *nDp4*(I;V)/+ and MT2181: *nDf24*/*unc-13*(*e1091*) *lin-11*(*n566*). Double mutant strains DR293 (*dpy-5* (*e61*) *unc-101*(*m1*))*;* DR102 (*dpy-5* (*e61*) *unc-29* (*e403*)) and *dpy-5* (*e61*) *unc-13* (*e51*) were used in three-factor mapping experiments. Double mutant strains *unc-29* (*e403*)*; him-5* (*e1490*) and *dpy-5* (*e61*) *unc-100* (*su115*) were mated to produce the triple mutant *dpy-5* (*e61*) *unc-100* (*su115*) *unc-29* (*e403*), which was used to mate with the N2 CB4856 (Hawaiian) strain for SNP mapping.

Polarized light microscopy, motility, brood size measurements and electron microscopy

The procedures for polarized light microscopy and motility assays were performed as described in Mercer et al., (2006). Brood size assays were performed as described in Stevenson et al., (2007). Electron microscopy was performed using methods described by Hall (1995); in particular, the "conventional two-step fixation" method which is described at http://www.wormatlas.org/anatmeth/anatmeth.htm. To allow better penetration of the fixative during the first aldehyde fixation step, the worms were cut in half with a razor blade.

Immunofluorescent localization of antibodies to known myofibril components

Immunofluorescent localization in adult muscle and imaging of adult muscle was performed as described in Stevenson et al., (2007). The procedure for phalloidin staining of thin filaments was performed as described by Ono (2001). Embryo immunostaining and imaging was performed as described in Soto et al., (2002).

Western blot of UNC-15 (paramyosin)

Extracts of Laemmli-soluble proteins from wild type*, su115* and *su149* worms were prepared as previously described (Hannak et al., 2002). To determine equal loading of protein, 5 µl of each protein was loaded and separated on a 10% SDS-PAGE, incubated in Coomasie stain overnight and de-stained the next morning. The de-stained gel showed that N2 and *su149* were similar in the amount of total protein loaded and that there was about half of that amount for *su115*; therefore, 5 µl of protein extract for N2 and *su115* and 10µl for *su149* were subsequently used. After the extracts were separated

on a 12% SDS-PAGE and transferred to nitrocellulose, the immunoblot was reacted with anti-paramyosin (mouse monoclonal 5-23; Miller et al., 1983) at a 1:2,000 dilution and was visualized by enhanced chemiluminescence (Pierce, Inc). To verify that equal amounts of total protein were loaded for each protein extract, the blot was washed and incubated with anti-actin (mouse monoclonal C4, Chemicon/Millipore) at a dilution of 1:12,000 and visualized by chemiluminescence.

Deficiency Mapping

Hermaphrodites of the strains that were mentioned in the "*C. elegans* strains and genetics" section were mated with homozygous *unc-100 (su115); him-5 ()* males. The F1 progeny from each mating experiment were examined by polarized light. The progeny from each experiment was scored for having wild type body-wall muscle or an Unc-100 phenotype.

Three-Factor Mapping

***dpy-5 (e61) unc-101 (m1)*:**

At a ratio of 12:3 *unc-100* (*su115*)*; him-5* (*e1490*) males were mated with *dpy-5* (*e61*) *unc-101* (*m1*) hermaphrodites, respectively. From the F1 generation, five non-Dpy-5 L4 hermaphrodites were picked to individual plates and allowed to self-fertilize. From these plates, F2 animals that had a Dpy-5, non-Unc-101 phenotype or an Unc-101, non-Dpy-5 phenotype were transferred to new individual plates. To allow for propagation of animals that might contain recombinant alleles, the F2 animals were then allowed to self-fertilize, to produce F3 generations. Approximately 10-12 F3 animals from each F2 were

screened by polarized light for an Unc-100 body-wall muscle phenotype. For both categories (Dpy-5, non-Unc-101 and Unc-101, non-Dpy-5), ratios were determined for the number of F2 plates that contained F3 progeny with an Unc-100 phenotype). These ratios were used to determine which gene (*dpy-5* or *unc-101*) *unc-100* may be closer to.

***dpy-5* (*e61*) *unc-29* (*e403*):**

The same experimental procedure was used as mentioned above; in the first step *unc-100* (*su115*)*; him-5* (*e1490*) males and *dpy-5* (*e61*) *unc-29*(*e403*) hermaphrodites were mated. The F2 animals picked to individual plates for this experiment were either Dpy-5, non-Unc-29 or Unc-29, non-Dpy-5.

***dpy-5* (*e61*) *unc-13* (*e51*):**

The same experimental procedure was used as mentioned above; in the first step, *unc-100* (*su115*); *him-5* (*e1490*) males and *dpy-5* (*e61*) *unc-13*(*e51*) hermaphrodites were mated. The F2 animals picked to individual plates for this experiment were either Dpy-5, non-Unc-13 or Unc-13, non-Dpy-5.

SNP Mapping

At a ratio of 12:3, Hawaiian males were mated with Bristol (*dpy-5*(*e61*) *unc-100* (*su115*) *unc-29* (*e403*)) hermaphrodites. From the F1 generation, five non-Dpy-5 L4 hermaphrodites were picked to individual plates and were allowed to self-fertilize. From the F2 generation, Bristol recombinants that were either Dpy-5*,* non-Unc-29 or Unc-29, non-Dpy-5 were selected and placed onto individual plates. These animals were then allowed to self-fertilize to produce an F3 generation that contained animals that were homozygous for recombinant alleles. Between eight and twelve F3 hermaphrodites were

picked to individual plates and were allowed to self-fertilize. After the second day of egg laying, each F3 animal was examined by polarized light for an Unc-100 body-wall muscle phenotype. The F4 generations were then examined for uniformity in phenotype to determine if the F3 animal was truly homozygous (Only heterozygous F3 animals produce a non-uniform population of F4 animals). Only F4 plates that contained 100% of worms with homozygous recombinant alleles were used to make frozen stocks and used for SNP analysis. Between the two markers *dpy-5* and *unc-29*, 25 SNPs (obtained from Washington University's C. elegans SNP Site) were selected (based on having a Psnp value greater than 80%) for PCR amplification; therefore 25 animals from each recombinant class were used to perform whole worm PCR experiments. After the regions containing each SNP had been amplified for each recombinant class, the DNA was PCR purified and sequenced to determine if the SNP was of Hawaiian or Bristol origin (For recombinants classes that contained *unc-100*, regions where Hawaiian SNPs were found were not likely regions to place *unc-100* since *unc-100* was created in a Bristol background). These experiments were repeated an additional three times to obtain enough recombinant classes to further narrow down the region of *unc-100* to one of ~500 kB (consisting of 17 overlapping cosmids).

Generation of Transgenic Line and Rescue Experiments

Due to gonad defects in *unc-100* animals, conventional methods for creating transgenic animals, which involves directly injecting DNA into the gonad of the *unc-100* mutant animal, could not be done. Therefore, the following methods were used: First, an injection mix consisting of cosmid DNA (set A, B, C, D or E; 30 ng/µl) and pTG96 (sur-

5::NLS::GFP, a transformation marker that is expressed in nearly all somatic cells) (100 ng/µl) was prepared (Yochem et al., 1998). Next, the DNA mixture was injected into the gonads of 10-20 young adult hermaphrodites. After allowing these animals to self-fertilize, the progeny was screened for a GFP signal. The green hermaphrodites were selected and mated with homozygous *unc-100 (su115)* males. Green males which resulted from that cross, which were *unc-100* heterozygotes, were selected and mated with homozygous *unc-100 (su115)* hermaphrodites. Finally, the green hermaphrodites which resulted from that cross were screened by polarized light.

If a cosmid(s) in a particular set rescues the UNC-100 phenotype, then 100% of the green hermaphrodites that resulted from the final cross should have wild type body-wall muscle. If the cosmid set does not rescue, then there should be a 50:50 ratio of wild type to mutant animals.

The same procedure was performed for creating transgenic animals with single cosmids, which were injected at a concentration of 10 ng/µl.

Chapter 4

Conclusions & Future Directions

With my discovery of *unc-94* encoding the tropomodulin, TMD-1, I have demonstrated yet another instance of how sarcomeric proteins are conserved between *C. elegans* and mammals. In accordance with previous studies of tropomodulin in vertebrate muscle, my immunofluorescent localization of UNC-94 is consistent with it being a pointed end capping protein. This biochemical activity has been confirmed recently by Yamashiro et al. (2008). In addition, my finding that *unc-94* mutants have disorganized myofibrils and abnormal accumulations of F-actin, suggests for the first time that tropomodulins have a role in myofibril assembly and/or maintenance, and in actin filament dynamics. Although UNC-94 is a tropomodulin with pointed end capping activity, I have found that in *unc*-94 mutants, including the allele *sf20*, which has no detectable UNC-94 proteins by immunoblot, H zones are still present. This suggests that the thin filaments in *sf20* are not abnormally long, and thus UNC-94 may not be required to regulate thin filament length. However, *sf20* may not be a null allele, and it may still produce sufficient UNC-94 to regulate thin filament length. One possibility is that UNC-94 may be redundant to the second tropomodulin in *C. elegans* encoded by the separate gene, *tmd-2*. Consistent with this idea, *tmd-2* is expressed in body wall muscle (based on SAGE data available on WormBase). I have also proposed a new function for tropomodulin in muscle from my results, which suggest that UNC-94 has a role at or near the muscle cell membrane. A role for tropomodulin at cell to cell contacts has previously been proposed for lens fiber cells (a type of epithelial cell)(Lee et al. 2000), and over-expression of Tmod1 in cardiac tissue results in dilated cardiomyopathy and disrupted intercalated disks, a type of intercellular junction (Ehler et al. 2001).

To help increase our understanding of the role of UNC-94 in sarcomere organization and assembly, Yamashiro et al., (2008) performed studies in which they investigated the functional relationship between UNC-94 and known enhancers of actin filament dynamics. By assessing the phenotypes of animals (by motility or phalloidin staining) that were depleted of UNC-94 along with either enhancer (ADF/cofilin, AIPI or profilin), Yamashiro et al., (2008) concluded that UNC-94 synergistically functions with all three enhancers to regulate elongation and shortening at the pointed ends of actin thin filaments. More importantly they propose a model for how such regulation is achieved (Fig 4.1).

I have shown that *unc-100* is required for normal myofibril maintenance and growth in adult animals. In particular, I have demonstrated the importance of *unc-100* for M-line, thick filament, and dense body organization. After use of several mapping strategies I have found a region in which *unc-100* resides, but have yet to determine an exact location. After having performed RNAi and/or having sequenced several potential candidates, I also have not determined the molecular identity of *unc-100*. Therefore, it is critical that future work for *unc-100* begin with the determination of its molecular identity.

Mapping experiments should be continued by performing transgenic rescue through the use of cosmid injections (as described in Chapter 3). In particular, cosmid sets or individual cosmids that we have not yet successfully injected should be of first priority (cosmid sets A, D and E and the individual cosmid T28F4). Mapping experiments may also include performing more SNP mapping (to obtain new informative recombinants) to further narrow down the 500 kb region. Once *unc-100* has been

precisely mapped and its molecular identity has been determined, one can then proceed with experiments to determine its localization in the sarcomere, using GFP-promoter fusions and anti-UNC-100 antibodies. Based on the strong effect of *unc-100* on the structure of M-lines, dense bodies and A-bands, we would expect that UNC-100 is a component of one or several of these structures. In the future, the Benian lab will use UNC-100 to screen yeast-2-hybrid libraries and restricted "bookshelves" to find interacting proteins. For example, the Benian lab has a 2-hybrid bookshelf collection of 25 known components of M-lines and dense bodies. Over the past seven years, the lab (through the expertise of Hiroshi Qadota) has defined protein interactions matrices for both the M-line and dense body (Fig 1.12). These were defined by taking cloned genes, screening libraries and bookshelves, confirming interactions by biochemical assays and localizing new proteins by antibodies and GFP fusions. It will be interesting to find out if and how UNC-100 might fit into these matrices.

Like *unc-100*, all of the other known muscle mutants, be it "Unc" or "Pat", were discovered using traditional genetic screens (Waterston et al., 1980; Zengel and Epstein, 1980; Williams and Waterston, 1994). From these discoveries and a few others, about 40 Unc genes and about 16 Pat genes have been found. Among the muscle Unc genes, the only gene yet to be identified at the molecular level is *unc-100*. Also, there are no reports on the molecular cloning of three Pat genes (*pat-9*, *pat-11*, and *pat-12*). It will be interesting to learn the molecular nature of the encoded proteins for these genes, and whether the proteins are localized to M-line, dense bodies or both. Additionally, the lab will determine with which existing proteins of the M-line and dense body interacting network these proteins interact.

Our lab has found that two M-line proteins, SCPL-1 and LIM-9, interact with the C-terminal portion of the giant protein UNC-89 (obscurin) (Qadota et al., 2008; Xiong et al., 2009). Efforts are underway to search for additional binding partners for this giant protein, and this is likely to identify new M-line proteins. Most recently, Meissner et al. (2009) used a bioinformatics approach to identify ~ 3500 muscle expressed genes; they used RNAi to determine how many of these genes had either Pat phenotypes or affected the organization of myosin in adult muscle. From these two screens, they identified four new Pat genes and 104 new genes that are important for the organization of the myofilament lattice. It will be interesting to determine how many of these new genes encode proteins that are located at M-lines and/or dense bodies. It will then be interesting to determine how they interact with previously described and new components of these structures, to obtain a more complete picture of sarcomere assembly.

Overall, my studies of two genes, initially identified by mutant hunts, are a contribution to the quest to identify every protein component of the sarcomere. Such mutant hunts in *C. elegans* have identified at least 60 genes required for sarcomere organization and/or initial assembly, the 40 Unc and 20 Pat genes. The recent RNAi screen by Meissner et al. (2009) identified 104 new genes required for sarcomere organization. Yeast 2-hybrid screens, primarily from our laboratory, have identified at least a dozen more proteins. Finally, homology to proteins originally identified in vertebrate muscle adds at least another 24 proteins. Thus, at this point, at least for *C. elegans,* approximately 200 different proteins are required for sarcomere assembly/maintenance and organization. Because the sarcomere is highly conserved across evolution, it is reasonable to expect that human muscle sarcomeres are at least as

complex. By further understanding the individual functions and interactions of these proteins, and others yet to be discovered, we will eventually learn how this complex "micro-machine" is assembled and maintained. These discoveries will have important implications for learning general principles of organelle assembly and learning the role(s) of these proteins in human muscular diseases.

.

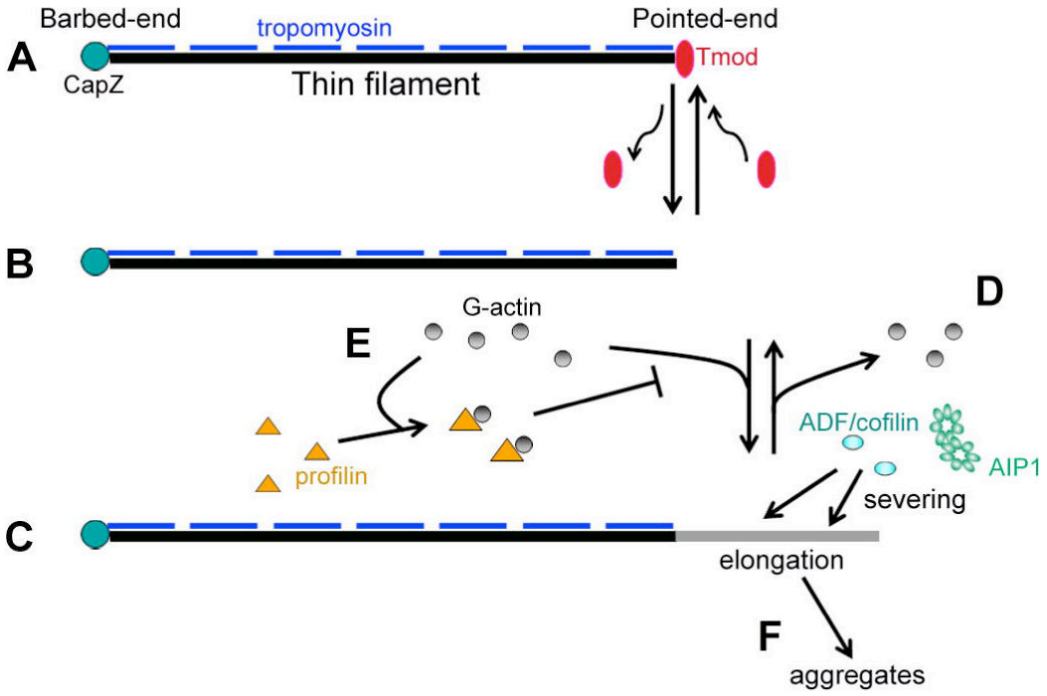

Figure 4.1 A model of synergistic regulation of sarcomeric actin organization by Tmod, ADF/cofilin, AIP1, and profilin. A stable thin filament has CapZ at the barbed end, Tmod at the pointed end, and tropomyosin on the side (A). Dynamic behavior of Tmod at the pointed end transiently generates a free pointed end (B) and allows elongation (C). This tropomyosin-free region of the filament is subjected to severing by ADF/cofilin and AIP1 (D), and depolymerized actin is captured by profilin, which prevents elongation from the pointed end (E). When this machinery is impaired, excessively elongated filaments may become unstable and form aggregates (F).

Literature Cited

Alberts, Bruce, et al. *Molecular Biology of the Cell.* 4th edition. New York, N.Y.; Garland Science, 2002.

An, X., Salomao, M., Guo, X., Gratzer, W. & Mohandas, N. (2007). Tropomyosin modulates erythrocyte membrane stability. *Blood* **109**, 1284-1288.

Bang, M.-L., Centner, T., Fornoff, F., Geach, A.J., Gotthardt, M., McNabb, M., Witt, C.C., Labeit, D., Gregorio, C.C., Granzier, H. & Labeit, S. (2001). The complete gene sequence of titin, expression of an unusual 700-kDa titin isoform, and its interaction with obscurin identify a novel Z-line to I-band linking system. *Circ. Res*. **89**, 1065 – 1072.

Barral, J.M., Bauer, C.C., Ortiz I. & Epstein H.F. (1998). *unc-45* mutations in *Caenorhabditis elegans* implicate a CRO1/She4p-like domain in myosin assembly. *J. Cell. Biol.* **143**, 1215-1225.

Barral, J.M., Hutagalung, A.H., Brinker, A., Hartl, F.U. & Epstein, H.F. (2002). Role of the myosin assembly protein UNC-45 as a molecular chaperone for myosin. *Science*. **295**, 669-671.

Barstead, R.J., Kleiman, L. & Waterston, R.H. (1991). Cloning, sequencing and mapping of an alpha-actinin gene from the nematode *Caenorhabditis elegans*. *Cell Motil Cytoskel*. **20**, 69-78.

Bateman, A., Birney, E., Durbin, R., Eddy, S.R., Finn, R.D. & Sonnhammer, E.L.L. (1999). Pfam 3.1: 1313 multiple alignments match the majority of proteins. *Nucl. Acids Res*. **27**, 260-262.

Benian, G.M., Kiff, J.E., Neckelmann, N., Moreman, D.G., & Waterston, R.H. (1989). The sequence of twitchin: an unusually large protein implicated in regulation of myosin activity in *C. elegans*. *Nature*. **342**, 45-50.

Benian, G.M., L'Hernault, S.W. & Morris, M.E. (1993). Additional sequence complexity in the muscle gene *unc-22*, and its encoded protein, twitchin, of *C. elegans*. *Genetics*. **134**, 1097-1104.

Benian, G.M., Tinley, T.L., Tang, X. & Borodovsky, M. (1996). The *C. elegans* gene *unc-89*, required for muscle M-line assembly, encodes a giant modular protein composed of immunoglobulin and signal transduction domains. *J. Cell Biol*. **132**, 835-848.

Brenner, S. (1974). The Genetics of *Caenorhabditis elegans*. *Genetics*. **77,** 71-94.

Broday, L., Kolotuev, I., Didier, C., Bhoumik, A., Podbilewicz, B., Ronai, Z. (2004). The LIM domain protein UNC-95 is required for the assembly of muscle attachment structures and is regulated by the RING finger protein RNF-5 in *C. elegans. J. Cell. Biol.* **165**, 857-867.

Brown, S.S. & Spudich, J.A. (1979). Nucleation of polar actin filament assembly by a positively charged surface. *J. Cell. Biol.* **80**, 499-504.

Bodine, S.C., Latres, E., Baumhueter, S. et al., (2001). Identification of ubiquitin ligases required for skeletal muscle atrophy. *Science*. **294,** 1704-1708.

Cox, E.A., Yamashiro, S., Ono, S. and Hardin, J. (2007). TMD-1/tropomodulin acts with HMP-1/α-catenin to reinforce adherens junctions under stress during morphogenesis. Submitted.

Conley, C.A., Fritz-Six, K.L, Almenar-Queralt, A. & Fowler, V.M. (2001). Leiomodins: larger members of the tropomodulin (Tmod) gene family. *Genomics*. **73**, 27-139.

Conley, C.A. & Fowler, V.M. (2005). Tropomodulin genes in *Gallus domesticus* and in mammals: gene structure, protein homologies and tissue distribution. *Cytogen. & Gen. Res*. **109**, 457-459.

Constantin, L. L. (1970). The role of sodium current in the radial spread of contraction in frog muscle fibres. *J. gen. Physiol*. **55**, 703–715.

Didier, C., Broday, L., Bhoumik, A. et al., (2003). RNF5, a RING finger protein that regulates cellmotility by targeting paxillin ubiquitination and altered localization. *Mol Cell Bio*l. **23,** 5331-5345.

Didry, D., Carlier, M.F. & Pantaloni, D. (1998). Synergy between actin depolymerizing factor/cofilin and profilin in increasing actin filament turnover. *J. Biol. Chem.* **273**, 25602-25611.

Ding, H., Qiu, S., Bunzel, R.J., Luo, D., Arabashi, A., Lu, S., Symersky, J., Nagy, L.A., DeLucas, L.J., Li, S. & Luo, M. (2003). Purification, nanocrystallization and preliminary X-ray analysis of a C-terminal part of tropomodulin protein 1, isoform A, from *Caenorhabditis elegans*. *Acta Crystallogr. D Biol. Crystallogr*. **59**, 1106-1108.

Duband J.L., Nuckolls, G.H., Ishihara, A., Hasegawa, T., Yamada, K.M., Thiery, J.P., & Jacobson, K. (1988). Fibronectin receptor exhibits high lateral mobility in embryonic locomoting cells but is immobile in focal contacts and fibrillar streaks in stationary cells. *J. Cell. Biol.* **107**, 1385-1396.

Ebashi, S., Endo, M. & Ohtsuki, I. Q. (1969). Control of muscle contraction.*Rev. Biophys.* **2**, 351–384.

Ehler, E., Horowits, R., Zuppinger, C., Price, R.L., Perriard, E.,Leu, M., Caroni, P., Sussman, M., Eppenberger, H.M. & Perriard, J.-C. (2001). Alterations at the intercalated disk associated with the absence of muscle LIM protein. *J. Cell. Biol*. **153**, 763-772.

Ervasti, J.M. (2003). Costameres: The Achilles' heel of Herculean muscle. *J Biol Chem.* **278**, 13591–13594.

Ferrara, T.M., Flaherty, D.B., & Benian, G.M. (2005). Titin/connectin-related proteins in *C. elegans*: a review and new findings, *J. Muscle Res. Cell Motil.* **26**, 435–447.

Finney, M. & Ruvkun, G. (1990). The *unc-86* gene product couples cell lineage and cell identity in *C. elegans*. *Cell* **63**, 895-905.

Fischer, R.S., Quinlan, R.A. & Fowler, V.M. (2003). Tropomodulin binds to filensin intermediate filaments. *FEBS Lett*. **547**, 228-232.

Fowler, V.M., Sussmann, M.A., Miller, P.G., Flucher, B.E. & Daniels, M.P. (1993). Tropomodulin is associated with the free (pointed) ends of the thin filaments in rat skeletal muscle. *J. Cell. Biol.* **120**, 411-420.

Francis, G.R. & Waterston, R.H. (1985). Muscle organization in *Caenorhabditis elegans*: localization of proteins implicated in thin filament attachment and I-band organization. *J. Cell Biol.* **101**, 1532-1549.

Franzini-Armstrong, C.J. (1971). Studies of the triad II. Penetration of tracers into the junctional gap. *J. Cell Biol*. **49**, 196–203.

Franzini-Armstrong, C. J. (1975). Membrane particles and transmission at the triad. *Fedn Proc*. **34**, 1382–1389.

Fritz-Six K.L., Cox, P.R., Fischer, R.S., Xu, B., Gregorio, C.C., Zoghbi, H.Y. & Fowler V.M. (2003). Aberrant myofibril assembly in tropomodulin1 null mice leads to aborted heart development and embryonic lethality. *J. Cel.l Biol*. **163**, 1033-1044.

Gautel, M. (2008). The sarcomere and the nucleus: functional links to hypertrophy, atrophy and sarcopenia. In: The Sarcomere and Skeletal Muscle Disease, ed. N. G. Laing, pp. 176-191, Landes Bioscience and Springer Science + Business Media.

Gomes, M.D., Lecker, S.H., Jagoe, R.T., Navon, A. & Goldberg, A.L. (2001). Atrogin-1, a muscle-specific F-box protein highly expressed during muscle atrophy. *Proc Natl Acad Sci U S A*. **98**, 14440-14445.

Goetinck, S. & Waterston R.H. (1994). The *Caenorhabditis elegans* muscle-affecting gene *unc-87* encodes a novel thin filament-associated protein. *J. Cell. Biol.* **127**, 79-93.

Greaser, M. (2001). Identification of new repeating motifs in titin. Proteins: *Struct. Funct. Genet*. **43**, 145-149.

Gregorio, C.C., Weber, A., Bondad, M., Pennise, C.R. & Fowler, V.M. (1995). Requirement of pointed-end capping by tropomodulin to maintain actin filament length in embryonic chick cardiac myocytes. *Nature*. **377**, 83-86.

Gutierrez-Cruz, G., Van Heerden, A. & Wang, K. (2001). Modular motif, structural folds and affinity profiles of PEVK segment of human fetal skeletal muscle titin. *J. Biol. Chem*. **276**, 7442-7449.

Hall, D.H. (1995). Electron microscopy and three-dimensional image reconstruction. In *Caenorhabditis elegans*: modern biological analysis of an organism (Epstein, H.F. & Shakes, D.C., eds), pp. 396-436, Academic Press, San Diego.

Hannak, E., Oegema, K., Kirkham, M., Gonczy, P., Habermann, B. & Hyman, A.A. (2002). The kinetically dominant assembly pathway for centrosomal asters in *C. elegans* is γ-tubulin dependent. *J. Cell. Biol*. **157**, 591-602.

Heger, A. & Holm, L. (2000). Rapid automatic detection and alignment of repeats in protein sequences. *Proteins: Struct. Funct. Genet*. **41**, 224-237.

Heiss, S.G. & Cooper, J.A. (1991). Regulation of CapZ, an actin capping protein of chicken muscle, by anionic phospholipids. *Biochemistry*. **30,** 8753-8758.

Hikita, T., Qadota, H., Tsuboi, D., Taya, S., Moerman, D.G. & Kaibuchi, K. (2005). Identification of a novel Cdc42 GEF that is localized to the PAT-3-mediated adhesive structure. *Biochem. Biophys. Res*. **335**, 139-145.

Hill, K., Harfe, B.D., Dobbins, C.A. & L'Hernault, S.W. (2000). *dpy-18* encodes an alpha-subunit of prolyl-4-hydroxylase in *C. elegans*. *Genetics*. **155**, 1139-1148.

Hobert, O., Moerman, D.G., Clark, K.A., Beckerle, M.C. & Ruvkun, G. (1999). A conserved LIM protein that affects muscular adherens junction integrity and mechanosensory function in *Caenorhabditis elegans*. *J. Cell Biol*. **144**, 45-57.

Hresko, M.C., Williams, B.D. & Waterston, R.H.. (1994). Assembly of body wall muscle and muscle cell attachment structures in *C. elegans*. *J Cell Biol*. **124**, 491-506.

Hueston, J.L., & Suprenant, K.A. (2009). Loss of dystrophin and the microtubule-binding proteinELP-1 causes progressive paralysis and death of adult *C. elegans*. *Dev Dyn*. **238**, 1878-1886.

Hug, C., Miller, T.M., Torres, M.A., Casella, J.F. & Cooper, J.A. (1992). Identification and characterization of an actin-binding site of CapZ. *J. Cell. Biol.* **116,** 923-931.

Huxley, H.E. (1969). The mechanism of muscle contraction. *Science*. **164**, 1356-1366.

Huxley, H.E. & Hansen, J. (1954). Changes in the cross striations of muscle during contraction and stretch and their structural interpretation. *Nature.* **173**, 973-976.

Jöbsis, F. F. & O'Connor, M. J. (1966). Calcium release and reabsorption in the satorius muscle of the toad. *Biochem. biophys. Res. Commun.* **25**, 246–252.

Kamath, R.S. & Ahringer, J. (2003). Genome-wide RNAi screening in *Caenorhabditis elegans*. *Methods*. **30**, 313-321.

Kohara, Y. (1996). Large scale analysis of *C. elegans* cDNA. *Tanpakushitsu Kakusan Koso*. **41**, 715-720.

Korn, E. (1982). Actin polymerization and its regulation by proteins from nonmuscle cells . *Physiol. Rev*. **62,** 672-737.

Kostyukova, A.S., Choy, A. & Rapp, B.A. (2006). Tropomodulin binds two tropomyosins: a novel model for actin filament capping. *Biochemistry.* **45**, 12068-12075.

Krieger, I., Kostyukova, A., Yamashita, A., Nitanai, Y. & Maeda, Y. (2002). Crystal structure of the C-terminal half of tropomodulin and structural basis of actin filament pointed-end capping. *Biophys. J*. **83**, 2716-2725.

Kruger, M., Wright, J. & Wang, K. (1991). Nebulin as a length regulator of thin filaments of vertebrate skeletal muscles: correlation of thin filament length, nebulin size, and epitope profile. *J. Cell Biol*. **115,** 97-107.

Lange, S., Ehler, E. & Gautel, M. (2006). From A to Z and back? Multicompartment proteins in the sarcomere. *Trends Cell Biol*. **16**, 11-18.

Lecroisey, C., Segalat. L. & Gieseler, K. (2007). The *C. elegans* dense body: anchoring and signaling structure of the muscle. *J Muscle Res Cell Motil*. **28**, 79-87.

Lecroisey, C., Martin, E., Mariol, M.C., Granger, L., Schwab, Y., Labouesse, M., Segalat, L. & Gieseler, K. (2008). DYC-1, a protein functionally linked to dystrophin in *Caenorhabditis elegans* is associated with the dense body, where it interacts with the muscle LIM domain protein ZYX-1. *Mol Biol Cell*. **19**, 785-796.

Lee, A., Fischer, R.S. & Fowler, V.M. (2000). Stabilization and remodeling of the membrane skeleton during lens fiber cell differentiation and maturation. *Dev. Dyn*. **217**, 257-270.

Littlefield, R., Almenar-Queralt, A. & Fowler, V.M. (2001). Actin dynamics at pointed ends regulates thin filament length in striated muscle. *Nat. Cell Biol*. **3**, 544-551.

Lu, S., Symersky, J., Li, S., Carson, M., Chen, L., Meehan, E. & Luo, M. (2004). Structural genomics of *Caenorhabditis elegans*: crystal structure of the tropomodulin C-terminal domain. *Proteins*. **56**, 384-386.

Lymn, R.W., & Taylor, E.W. (1971). Mechanism of adenosine triphosphate hydrolysis by actomyosin. *Biochemistry*. **10,** 4617–4624.

Maduro, M.F., Gordon, M., Jacobs, R. & Pilgrim, D.B. (2000). The UNC-119 family of neural proteins is functionally conserved between humans, *Drosophila* and *C. elegans*. *J. Neurogenet.* **13,** 191-212.

Mardahl-Dumesnil, M. & Fowler, V.M. (2001). Thin filaments elongate from their pointed ends during myofibril assembly in Drosophila indirect flight muscle. *J. Cell Biol*. **155**, 1043-1053.

McDonald, K.A., Lakonishok, M. & Horwitz, A.F. (1995). Alpha v and alpha 3 integrin subunits are associated with myofibrils during myofibrillogenesis. *J Cell Sci*. **108** (Pt 7), 2573-81.

McElhinny, A.S., Kolmerer, B., Fowler, V.M., Labeit, S. & Gregorio, C.C. (2001). The N-terminal end of nebulin interacts with tropomodulin at the pointed ends of the thin filaments. *J. Biol. Chem.* **276**, 583-592.

McElhinny, A.S., Schwach, C., Valichnac, M., Mount-Patrick, S. & Gregorio, C.C. (2005). Nebulin regulates the assembly and lengths of the thin filaments in striated muscle. *J. Cell Biol.* **170**, 947-957.

McKay, S.J., Johnsen, R., Khattra, J., Asano, J., Baillie, D.L. et al. (2003). Gene expression profiling of cells, tissues, and developmental stages of the nematode *C. elegans. Cold Spring Harb. Symp. Quant. Biol*. **68**, 159-169.

McKeown, C.R., Han, H.-F. & and Beckerle, M.C. (2006). Molecular characterization of the *Caenorhabditis elegans* ALP/Enigma gene *alp-1*. *Dev Dyn*. **235**, 530-538.

Meissner, B., Warner, A., Wong, K., Dube, N., Lorch, A., McKay, S.J., Khattra, J., Rogalski, T., Somasiri, A., Chaudhry, I., Fox, R.M., Miller, D.M. 3rd, Baillie, D.L., Holt, R.A., Jones, S.J., Marra, M.A., Moerman, D.G. (2009). An integrated strategy to study muscle development and myofilament lattice structure in *Caenorhabditis elegans*. *PLoS Genet.* 5(6):e1000537.

McKim, K.S., Matheson, C., Marra, M.A., Wakarchuk, M.F., Baillie, D.L. (1994). The *Caenorhabditis elegans unc-60* gene encodes proteins homologous to a family of actin-binding proteins. *Mol. Gen. Genet.* **242**, 346-357.

Mercer, K.B., Flaherty, D.B., Miller, R.K., Qadota, H., Tinley, T.L., Moerman, D.G. & Benian, G.M. (2003). *Caenorhabditis elegans* UNC-98, a C2H2 Zn finger protein, is a novel partner of UNC-97/PINCH in muscle adhesion complexes. *Mol. Biol. Cell* **14**, 2492-2507.

Mercer, K.B., Miller, R.K., Tinley, T.L., Sheth, S., Qadota, H. & Benian, G.M. (2006). *Caenorhabditis elegans* UNC-96 is a new component of M-lines that interacts with UNC-98 and paramyosin and is required in adult muscle for assembly and/or maintenance of thick filaments. *Mol. Biol. Cell*. **17,** 3832-3847.

Moerman, D.G. & Fire, A. (1997). Muscle: structure, function and development. In *C. elegans II*. (D.L. Riddle, T. Blumenthal, B.J. Meyer & J.R. Priess., eds.), pp.417-470 Cold Spring Harbor Laboratory Press, Cold Spring Harbor, New York.

Moerman, D. G. and Williams, B. D. Sarcomere assembly in *C. elegans* muscle (January 16, 2006), WormBook, ed. The *C. elegans* Research Community, WormBook, doi/10.1895/wormbook.1.81.1, http://www.wormbook.org.

Miller, D.M., Ortiz, Il, Berliner, G.C. & Epstein, H.F. (1983). Differential localization of two myosins within nematode thick filaments. *Cell*. **34**, 477-490.

Miller, R.K., Qadota, H., Landsverk, M.L., Mercer, K.B., Epstein, H.F. & Benian, G.M. (2006). UNC-98 links an integrin-associated complex to thick filaments in *C. elegans* muscle. *J. Cell. Biol*. **175**, 853-859.

Miller R.K., Qadota H., Stark T.J., Mercer K.B., Wortham T.S., Anyanful A., Benian G.M. (2009). CSN-5, a component of the COP9 signalosome complex, regulates the levels of UNC-96 and UNC-98, two components of M-lines in *Caenorhabditis elegans* muscle. *Mol. Biol. Cell.* **20**, 3608-3616.

Minamide, L.S. & Bamburg, J.R. (1990). A filter paper dye-binding assay for quantitative determination of protein without interference from reducing agents or detergents. *Anal. Biochem*. **190**, 66-70.

Moerman, D.G., Benian, G.M., Barstead, R.J., Schreifer, L., & Waterston, R.H. (1988). Identification and intracellular localization of the *unc-22* gene product of *C. elegans*. *Genes Devel*. **2**, 93-105.

Mohri, K. & Ono, S. (2003). Actin filament disassemblying activity of *Caenorhabditis elegans* actin-interacting protein1 (UNC-78) is dependent on filament binding by a specific ADF/cofilin isoform. *J. Cell Sci*. **116,** 4107-4118.

McKim, K.S., Matheson, C., Marra, M.A., Wakarchuk, M.F. & Baillie, D.L. (1994). The *Caenorhabditis elegans unc-60* gene encodes proteins homologous to a family of actin-binding proteins. *Mol Gen. Genet.* **242**, 346-357.

Norman, K.R., Cordes, S., Qadota, H., Rahmani, P. & Moerman, D.G. (2007). UNC-97 / PINCH is involved in the assembly of integrin cell adhesion complexes in *Caenorhabditis elegans* body wall muscle. *Dev Biol*.. **309**, 45-55.

Nonet, M.L., Grundahl, K., Meyer, B.J. & Rand, J.B. (1993). Synaptic function is impaired but not eliminated in *C. elegans* mutants lacking synaptotagmin. *Cell*. **73**, 1291-1305.

Ono, S., Baillie, D.L. & Benian, G.M. (1999). UNC-60B, an ADF/cofilin family protein, is required for proper assembly of actin into myofibrils in *Caenorhabditis elegans* body wall muscle. *J. Cell Biol*. **145**, 491-502.

Ono, S. (2001). The *Caenorhabditis elegans unc-78* gene encodes a homologue of actin-interacting protein 1 required for organized assembly of muscle actin filaments. *J. Cell Biol*. **152**, 1313-1319.

Ono S. & Ono K. (2002). Tropomyosin inhibits ADF/cofilin-dependent actin filament dynamics. *J. Cell. Biol.* **156**, 1065-1076.

Ono, Y., Schwach, C., Antin, P.B. & Gregorio, C.C. (2005). Disruption in the tropomodulin1 (Tmod1) gene compromises cardiomyocyte development in murine embryonic stem cells by arresting myofibril maturation. *Devel. Biol*. **282**, 336-348.

Phillips, G.N., Fillers, J.P. & Cohen, C. (1986). Tropomyosin crystal structure and muscle regulation. *J. Mol. Biol.* **192**, 111-131.

Pirani, A., Vinogradova, M.V., Curmi, P.M., King, W.A., Fletterick, R.J., Craig, R., Tobacman, L.S., Xu, C., Hatch, V. & Lehman, W. (2006). An atomic model of the thin filament in the relaxed and Ca2+-activated states. *J. Mol. Biol.* **357**, 707-717.

Pope, B., Way, M., Matsudaira, P.T. & Weeds, A. (1994). Characterisation of the F-actin binding domains of villin: classification of F-actin binding proteins into two groups according to their binding sites on actin. *FEBS Lett.* **338**, 58-62.

Pulak, R. & Anderson, P. (1993). mRNA surveillance by the *Caenorhabditis elegans smg* genes. *Genes Dev*. **7**, 1885-1897.

Qadota, H., Mercer, K.B., Miller, R.K., Kaibuchi, K. & Benian, G.M. (2007). Two LIM domain proteins and UNC-96 link UNC-97 / PINCH to myosin thick filaments in *Caenorhabditis elegans* muscle. *Mol. Biol. Cell*. **18,** 4317-4326.

Qadota, H., McGaha, L.A., Mercer, K.B., Stark, T.J., Ferrara, T.M. & Benian, G.M. (2008). A novel protein phosphatase is a binding partner for the protein kinase domains of UNC-89 (obscurin) in *Caenorhabditis elegans*. *Mol Biol Cell*. **19**, 2424-2432.

Quinzii, C.M., Vu, T.H., Min, K.C., Tanji, K., Barral, S., Grewal, R.P., Kattah, A., Camaño, P., Otaegui, D., Kunimatsu, T., Blake, D.M., Wilhelmsen, K.C., Rowland, L.P., Hays, A.P., Bonilla, E., Hirano, M. (2008). X-linked dominant scapuloperoneal myopathy is due to a mutation in the gene encoding four-and-a-half-LIM protein 1. *Am. J. Hum. Genet.* **82**, 208-213.

Reboul, J., Vaglio, P., Rual, J.F., Lamesch, P., Martinez, M., Armstrong, C.M., Li, S., Jacotot, L., Bertin, N., Janky, R., Moore, T., Hudson, J.R., Jr., Hartley, J.L., Brasch, M.A., Vandenhaute, J., Boulton, S., Endress, G.A., Jenna, S., Chevet, E., Papasotiropoulos, V., Tolias, P.P., Ptacek, J., Snyder, M., Huang, R., Chance, M.R., Lee, H., Doucette-Stamm, L., Hill, D.E. and Vidal, M. (2003). *C. elegans* ORFeome version 1.1: experimental verification of the genome annotation and resource for proteome-scale protein expression. *Nat. Genet*. **34**, 35-41.

Rogalski, T.M., Mullen, G.P., Gilbert, M.M., Williams, B.D. & Moerman, D.G. (2000). The *unc-112* gene in *Caenhorhabditis elegans* encodes a novel component of cell-matrix adhesion structures required for integrin localization in the muscle cell membrane. *J. Cell Biol*. **150**, 253-264.

Roy, P.J., Stuart, J.M., Lund, J. and Kim, S.K. (2002). Chromosomal sluctering of muscle-espressed genes in *Caenorhabditis elegans*. *Nature.* **418**, 975-979.

Satoko, H., Sachiko, E. & Saigo, K. (2000). Requirements of kettin, a giant muscle protein highly conserved in overall structure in evolution, for normal muscle function, viability, and flight activity of *Drosophila*. *J. Cell. Biol*. **148**, 101-114.

Schneider, M. F. & Chandler, W. K. (1973). Voltage dependent charge movement in skeletal muscle: a possible step in excitation-contraction coupling. *Nature*. **242**, 244–246.

Schwock, J., Dhani, N., Hedley, D.W. (2010). Targeting focal adhesion kinase signaling in tumor growth and metastasis. *Expert Opin Ther Targets*. **14**, 77-94.

Seymour, J. & O'Brien, E.J. (1980). The position of tropomyosin in muscle thin filaments. *Nature*. **283**, 680-682.

Simmer, F., Tijsterman, M., Parrish, S., Koushika, S.P., Nonet, M.L., Fire, A., Ahringer, J. & Plasterk, R.H.A. (2002). Loss of the putative RNA-directed RNA polymerase RRF-3 makes *C. elegans* hypersensitive to RNAi. *Curr. Biol*. **12**, 1317-1319.

Singer, I.I. (1979). Fibronectin receptor exhibits high lateral mobility in embryonic locomoting cells but is immobile in focal contacts and fibrillar streaks in stationary cells. *Cell.* **16**, 675 – 685.

Small, T.M., Gernert, K.M., Flaherty, D.B., Mercer, K.B., Borodovsky, M., & Benian, G.M. (2004). Three new isoforms of *Caenorhabditis elegans* UNC-89 containing MLCK-like protein kinase domains, *J. Mol. Biol.* **342**, 91–108.

Sussman, M.A., Welch, S., Cambon, N., Klevitsky, R., Hewett, T.E., Price, R., Witt, S.A. & Kimball, T.R. (1998). Myofibril degeneration caused by tropomodulin overexpression leads to dilated cardiomyopathy in juvenile mice. *J. Clin. Invest.* **101**, 51-61.

Taylor, S. R., Rüdell, R. & Blinks, J. R. (1975). Calcium transients in amphibian muscle. *Fedn Proc.* **34,** 1379–1381.

Tuxworth, R.I. & Titus, M.A. (2000). Unconventional myosins: anchors in the membrane traffic relay, *Traffic* **1**, 11–18.

Warrick, H.M. & Spudich, J.A. (1987). Myosin structure and function in cell motility. *Annu Rev Cell Biol.* **3**, 379-421.

Waterston, R.H., Thomson, J.N. & Brenner, S. (1980). Mutants with altered muscle structure in *C. elegans. Dev Biol.* **77**, 271-302.

Waterston,R.H. (1988). Muscle. In *The Nematode Caenorhabditis elegans*. (W.B. Wood, editor), pp.281-335, Cold Spring Harbor Laboratory Press, Cold Spring Harbor, New York.

Weber, A., Pennise, C.R., Babcock, G.G. & Fowler, V.M. (1994). Tropomodulin caps the pointed ends of actin filaments. *J. Cell Biol*. **127**, 1627-1635.

Wicks, S.R., Yeh, R.T., Gish, W.R., Waterston R.H., Plasterk, R.H. (2001). Rapid gene mapping in *Caenorhabditis elegans* using a high density polymorphism malp. *Nat. Genet.* **28**, 160-164.

Williams, B.D. & Waterston R,.H. (1994). Genes critical for muscle development and function in *Caenorhabditis elegans* identified through lethal mutations. *J. Cell Biol.* **124**, 491-506.

Windpassinger C., Schoser, B., Straub, V., Hochmeister, S., Noor, A., Lohberge,r B., Farra, N., Petek, E., Schwarzbraun, T., Ofner, L., Löscher, W.N., Wagner, K., Lochmüller, H., Vincent, J.B., Quasthoff, S. (2008). An X-linked myopathy with postural muscle atrophy and generalized hypertrophy, termed XMPMA, is caused by mutations in FHL1. *Am. J. Hum. Genet*. **82**, 88-99.

Xiong, G., Qadota, H., Mercer, K.B., McGaha, L.A., Oberhauser, A.F., Benian, G.M. (2009). A LIM-9 (FHL)/SCPL-1 (SCP) complex interacts with the C-terminal protein kinase regions of UNC-89 (obscurin) in *Caenorhabditis elegans* muscle. *J. Mol. Biol.* **386**, 976-988.

Yamashiro, S., Cox, E.A., Baillie, D.L., Hardin, J.D., & Ono, S. (2008). Sarcomeric actin organization is synergistically promoted by tropomodulin, ADF/cofilin, AIP1, and profilin in *C. elegans*. *J. Cell. Sci.* **121**, 3867-3877.

Zengel, J.M. & Epstein, H.F. (1980). Identification of genetic elements associated with muscle structure in the nematode *Caenorhabditis elegans*. *Cell Motil.* **1,** 73-97.